Spectroscopic Study of Meteors and Persistent Trains

A Dissertation Submitted to the Faculty of the

Department of Astronomical Science,
School of Mathematical and Physical Science

In Partial Fulfillment of the Requirements
For the Degree of

Doctor of Philosophy (Science)

in

The Graduate University for Advanced Studies

2000

by

Shinsuke Abe

学位論文

Spectroscopic Study of Meteors and Persistent Trains

流星と永続痕の分光学的研究

2000年度 博士（理学）

総合研究大学院大学 数物科学研究科
天文科学専攻

阿部 新助

ACKNOWLEDGMENTS

First of all, I would like to express my deepest gratitude to Prof. Jun-ich Watanabe, my supervisor, for his continuous encouragement on this work. I am grateful to Dr. Hajime Yano and Dr. Noboru Ebizuka for observational collaboration and for providing me with the instruments. Dr. Peter Jenniskens who is a principal investigator of the 1999 Leonid Multi-Instrument Aircraft Campaign, gave many constructive comments and suggestions, for which this work has made a great improvement in its final form. I would like to thank Dr. Shigetomo Shiki for helpful suggestions. I gratefully acknowledge helpful discussions with Dr. Yashuhiro Hirahara and Dr. Junko Takahashi on several points in the paper. I also thank Dr. Katsuhito Ohtsuka for orbital calculations of HDTV data. My special thanks are due to Mr. Hideyuki Murayama for providing me with the persistent trains's spectra. The 1999 Leonid Multi-Instrument Aircraft Campaign was made possible by grants from the NASA Exobiology, Planetary Astronomy, and Astrobiology Advanced Missions and Technology Programs, NASA Ames Research Center, and the U.S. Air Force. The authors thank NHK(Nippon Hoso Kyokai) for kindly providing the HDTV-II system to make this observation possible. I appreciate cooperation with Keisoku Giken Co., Ltd.(Mr. Kouich Akiyama, Mr. Hiroshi Tabata, Mr. Michio Uchida) and Space Communications Division of the Communications Research Laboratory(Dr. Yoshiaki Suzuki, Dr. Naoto Kadowaki) for digitization of the HDTV images. I was supported by the travel grant of the National Astronomical Observatory of Japan. The making spectrographs was made possible largely through grants from the National Astronomical Observatory, I would like to acknowledge here.

Table of Contents

TABLE OF CONTENTS—*Continued*

Abstract

During the 1999 Leonids, an intensified HDTV camera was used for slitless meteor spectroscopy at visible and near-UV wavelengths in three night flights of the Leonid Multi-instrument Aircraft Campaign. The HDTV system provided a high dynamic range (digital 10-bit) and a wide field of view of 37 x 21 degrees. The maximum spectral sensitivity is at 405 nm, while the resolving power of the spectrograph was $\lambda/\Delta\lambda \sim 250$. Here, we report on the results for three particularly nice spectrum from Leonid meteors and one spectrum from a Taurid meteor. It is confirmed that sodium is released from the meteoroid earlier than iron and magnesium, just as in meteors of the 1998 Leonid shower. Numerous atomic emission lines of magnesium and iron were detected, with an excitation temperature of $T = 4,500 \pm 300K$ in local thermodynamic equilibrium(LTE). Rovibrational band of N_2 dominate the spectrum in the visible (550 - 800 nm) which are matched by electronic-vibrational temperature $T_{e,v} = 4,500K$. It seems that meteor spectra can be explained well by LTE model. Stereoscopic observations of one spectroscopic meteor have been accomplished for the first time and the real height of emissions were fixed. We also searched for CN band emission at 388 nm related with cometary organic carbon. CN like structures are seen in the spectrum of Taurid, but it is not clear due to the overlap of numerous iron lines.

Spectroscopic observations of a meteor persistent train of Leonid were carried out using a grating spectrograph covering 370 - 640 nm wavelength range. An excellent spectra of a Leonid persistent train was obtained during the 1998 Leonid maximum in Japan. There are thousands of possible emission lines in the 370 - 640 nm wavelength range. Taking all possible atoms into account, we adapted a simple radiative model based on LTE for the persistent train. To explain the obtained spectrum and to decide precise identifications, a comparison with a physical interpretation may be

helpful. The number of 22 emission lines in the spectrum of the persistent train was identified. The abundances of Mg, Na, Fe, Al, Ca and Mn indicate that Magnesium and Iron are the the most dominant atoms in the persistent train while Sodium is also rich in the train. The enhancement of Mg, Fe and Na suggests that these atoms are the source of the persistent trains and of long-lived emitters. The intense emissions of the persistent train could be explained with the temperature of $\sim 2200K$. It seems that cooling time is more rapid than luminosity decay time. It approves of the chemiluminescence mechanism, that is to say, thermal energy has nothing to do with the source of luminosity in the persistent train.

Spectroscopic Study of Meteors and Persistent Trains

Shinsuke Abe, Ph.D.
The Graduate University for Advanced Studies, 2000

Director: Jun-ich Watanabe

During the 1999 Leonids, an intensified HDTV camera was used for slitless meteor spectroscopy at visible and near-UV wavelengths in three night flights of the Leonid Multi-instrument Aircraft Campaign. The HDTV system provided a high dynamic range (digital 10-bit) and a wide field of view of 37 x 21 degrees. The maximum spectral sensitivity is at 405 nm, while the resolving power of the spectrograph was $\lambda/\Delta\lambda \sim 250$. Here, we report on the results for three particularly nice spectrum from Leonid meteors and one spectrum from a Taurid meteor. It is confirmed that sodium is released from the meteoroid earlier than iron and magnesium, just as in meteors of the 1998 Leonid shower. Numerous atomic emission lines of magnesium and iron were detected, with an excitation temperature of $T = 4,500 \pm 300K$ in local thermodynamic equilibrium(LTE). Rovibrational band of N_2 dominate the spectrum in the visible (550 - 800 nm) which are matched by electronic-vibrational temperature $T_{e,v} = 4,500K$. It seems that meteor spectra can be explained well by LTE model. Stereoscopic observations of one spectroscopic meteor have been accomplished for the first time and the real height of emissions were fixed. We also searched for CN band emission at 388 nm related with cometary organic carbon. CN like structures are seen in the spectrum of Taurid, but it is not clear due to the overlap of numerous iron lines.

Spectroscopic observations of a meteor persistent train of Leonid were carried out using a grating spectrograph covering 370 - 640 nm wavelength range. An excellent spectra of a Leonid persistent train was obtained during the 1998 Leonid maximum in

Japan. There are thousands of possible emission lines in the 370 - 640 nm wavelength range. Taking all possible atoms into account, we adapted a simple radiative model based on LTE for the persistent train. To explain the obtained spectrum and to decide precise identifications, a comparison with a physical interpretation may be helpful. The number of 22 emission lines in the spectrum of the persistent train was identified. The abundances of Mg, Na, Fe, Al, Ca and Mn indicate that Magnesium and Iron are the the most dominant atoms in the persistent train while Sodium is also rich in the train. The enhancement of Mg, Fe and Na suggests that these atoms are the source of the persistent trains and of long-lived emitters. The intense emissions of the persistent train could be explained with the temperature of $\sim 2200K$. It seems that cooling time is more rapid than luminosity decay time. It approves of the chemiluminescence mechanism, that is to say, thermal energy has nothing to do with the source of luminosity in the persistent train.

Part I

Spectroscopic Study of Meteors

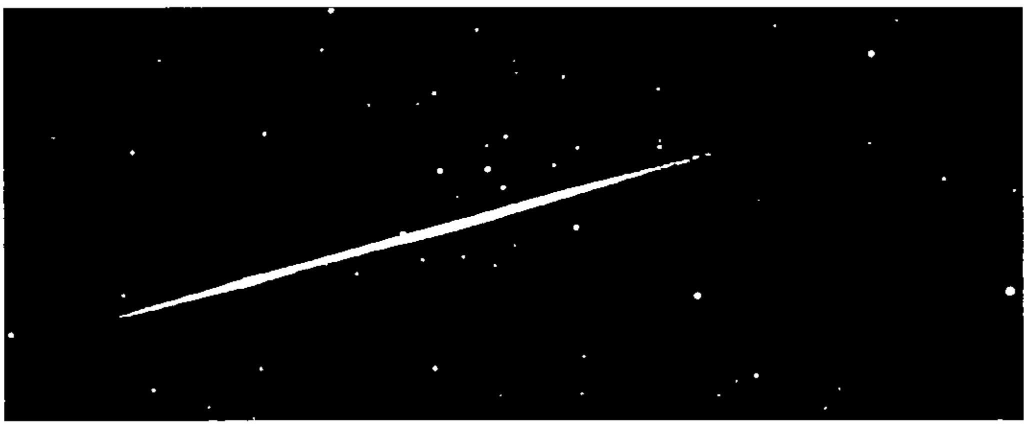

Chapter 1
INTRODUCTION - METEORS -

Meteoric phenomena occur when meteoric bodies, or meteoroids, enter the atmosphere. The terms "meteoric body" and "meteoroid" are equivalent. Owing to the interaction with air molecules, a meteoroid heats up to very high temperatures and begins to melt and vaporize. The luminosity of the meteoroid vapor and air produces the phenomenon known as a "shooting star", called meteor.

Ionization of air takes place along the meteor path, forming an ion train which reflects radio waves in the decameter, 10 - 100 m wavelength range. The ion trains of brilliant meteors are visible even to the naked eye and those of particularly bright meteors may persist for a few dozen seconds or even for some minutes. These phenomena are known as "persistent trains".

Directly behind the meteoroid extends the so-called "wake" of the meteor, whose luminosity is of the same nature as that of the meteor proper motion. The meteoroid loses mass owing to vaporization, fusion, and fragmentation. The process of mass loss by a meteoroid is known as "ablation". Owing to the resistance of the atmosphere, the meteoroid is decelerated. Ablation and deceleration affect one another, since ablation depends on the body's velocity (geocentric velocity) and deceleration on its mass. Hence the mass-loss and deceleration equations for a meteoroid must be solved simultaneously.

Depending on the conditions under which they can be detected, meteoric bodies may be broken down into three groups:

- **Micrometeoroids**. The smallest meteorites are collectively called "micrometeorites" or, more commonly, "interplanetary dust particles (IDPs)" IDPs are so small that they are retarded in the upper levels of the atmosphere before becoming heated to evaporation temperature and before they can become luminous. The concept of micrometeoroids was introduced by Whipple in 1950 (Whipple, 1950). Micrometeoroids cannot be observed by optical or radar methods since they do not produce a significant luminosity and ionization. They are collected from stratosphere, polar ice cores, and deep sea and in-land sediments also suffer from similar selection effects in terms of size, shape, magnetism, time resolution, etc., but to a lesser extent. As yet none of these methods enables the determination of micrometeoroid orbits; their mass distribution can be determined fairly reliably. It may be assumed that the upper end of their mass and size range are 10^{-6} g and $100\mu m$ respectively.

- **Meteoroids**, which produce meteors, i.e., produce sufficient luminosity and ionization upon entering the atmosphere to permit observing by visual, photographic, or radar methods, Using photographic or high-sensitive video observational methods can determine the precise orbit of any meteor, and hence the elements of meteoric orbits can be analyzed statistically. The mass and size range are from 10^{-6} to 10^{-7} g and $100\mu m$ to several 10 cm respectively.

- **Meteorites**, which are best studied with regard to their physics, chemistry, and mineralogy, but accurate orbits are known for a very small number of meteorites. The mass range range of meteorites that have actually been found, from 10^{-2} to 10^{8} g, is based on their final masses, after they have passed through the atmosphere.

Meteors are the luminous ablation of dust particles from parent comets that enter the Earth's atmosphere at a few tens of kilometers per second. They are heated, vaporised, and even partially ionized in the upper atmosphere. Meteor emission originates from a mixture of atoms and molecules ablated from the meteoroid itself as well as from the surrounding air. The Leonid meteor shower is one of the most interesting meteor showers and have occurred roughly every 33 years at least in the

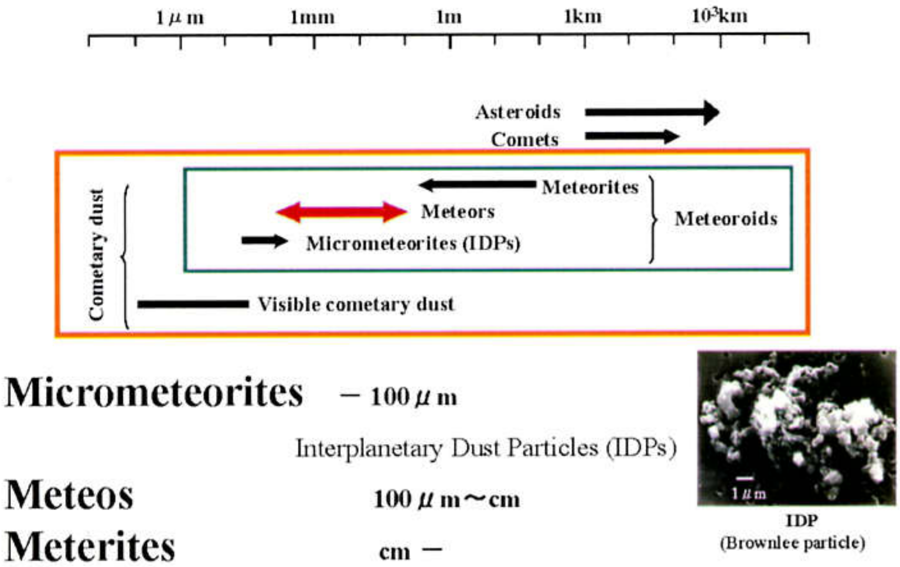

FIGURE 1.1. Dust size distribution in the solar system.

last 100 years recorded in the history. This corresponds to the orbital period of the comet, 55P/Tempel–Tuttle. Comets are the surviving bodies since the genesis of our solar system. They are thought to be remnants of planetesimals at the edge of the protoplanetary disk that could not grow into planets. Through detailed meteor observations and analysis of their interaction with the Earth's atmosphere, physical and chemical properties of cometary meteoroids can be studied. Spectroscopic observations of the flash heating and evaporation reveal not only chemical composition of the interplanetary dust but also emission processes of hypervelocity impacts in the atmosphere, which are difficult to reproduce in laboratory experiments at present.

Millman et al. (1971) first observed meteor spectra by television techniques. TV observations can record fainter meteors with higher temporal resolution than photographic spectroscopic techniques. Most early papers were concerned with line identification. In recent years, J. Borovicka et al. (Borovicka, 1995; Borovicka and Bocek, 1993; Borovicka et al., 1999) have applied this technique to quantitative analysis of spectroscopy of meteors and their persistent trains. Typically, the intensified video data are recorded in an 8-bit($2^8 = 256$) analogue video system in PAL or NTSC format.

Here, we report on the first such spectroscopic observations using Intensified High-Definition TV. Earlier, HDTV imaging was used to monitor the prominent activity of the 1998 Giacobinid meteor shower, associated with comet 21P/Giacobini-Zinner (Watanabe et al., 1999). This technique increases the number of TV lines from about 576(NTSC) to 1150, and has higher 10-bit($2^{10} = 1024$) dynamic range, 4 times higher than previous video systems. For a given field of view, the system is more sensitive than conventional intensified CCD cameras. Meteors as faint as 8th magnitude and stars of 10th magnitude can routinely be observed even with a wide $37^\circ \times 21^\circ$ field lens.

Purposes of Meteor Study;

- To observe the meteor spectra with high quality using HDTV system.
- To reveal compositions of cometary meteoroids.
- To show physical parameters which provide emission processes.
- To observe emission processes of the hypervelocity collisions to the atmosphere.
- To investigate the real height of emission phenomena.
- To search for organic compounds related with parent comet.

Chapter 2

OBSERVATIONS

Our spectroscopic observations were performed by the "blue-sensitive" intensified HDTV camera equipped with a transmission grating with 600 grooves per mm, blazed at 550 nm, made by Jobin Yvon. We operated two HDTV cameras provided by the Japanese Broadcasting Company (NHK) that were mounted on both the "FISTA" and "ARIA" aircraft in NASA's 1999 Leonid Multi-instrument Aircraft Campaign (Leonid MAC) (Jenniskens et al., 2000a). Each HDTV camera was composed of a large diameter image intensifier along with a blue sensitive 1-inch 2M-pixel FIT CCD, which has a resolution of 1150 TV lines (Sunasaki et al., 1997; Yamazaki et al., 1998). Figure 2.3 is a picture of the HDTV-II camera set on observational window of FISTA. Figure 2.6 shows a composite of images from the ARIA camera around the time of the peak.

During flight, the grating was rotated to set the dispersion direction perpendicular to the projected direction of Leonid meteor trajectories on the sky. The camera was mounted in one of the high $\sim 61°$ ports of the FISTA aircraft. This system not only recorded intrinsically faint meteors, but also had a wide field of view of 37 x 21 degrees by using a $f50mm$ F1.0 photographic lens. The resulting dispersion was 0.59 nm/pixel in the first order. That is a resolving power of 250 at 590 nm. The images were recorded in 10-bit monochrome frames at a rate of 33 ms, i.e. 30 frames per second. The limiting magnitude for meteor spectra corresponded to the first order meteor of about +5th apparent visual magnitude.

The spectroscopic observations were carried out intermittently for a total of 297 minutes in the nights of Nov. 16-19, 1999, consisting of 87, 46 and 164 minutes respectively for the 1st, 2nd and 3rd nights. In total 105 meteor spectra were recorded,

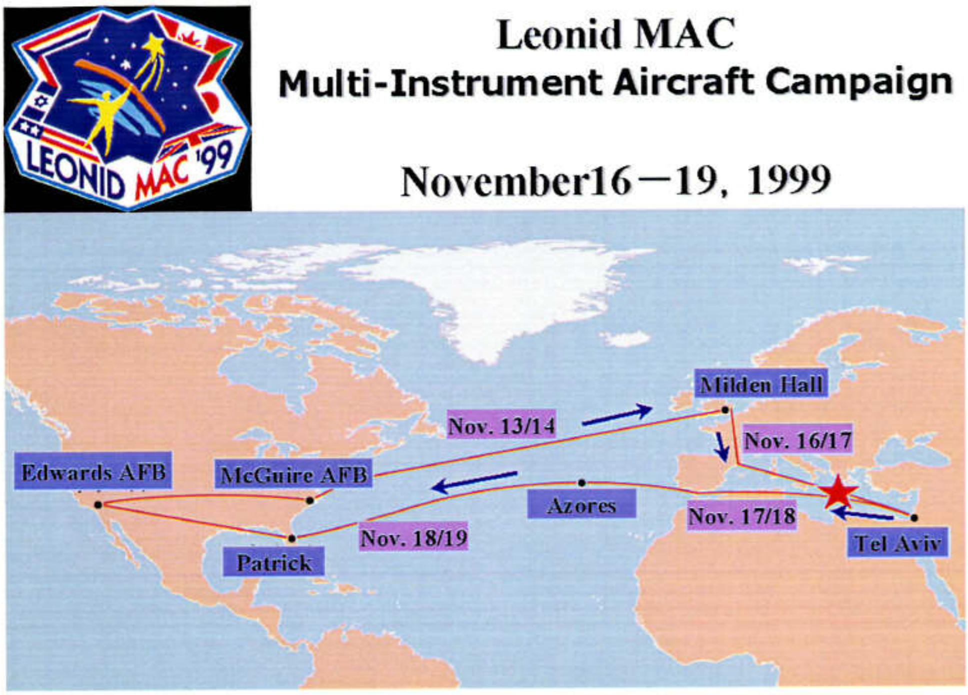

FIGURE 2.1. Observational root map. The Leonid Multi-Instrument Aircraft Campaign (Leonid MAC) is a NASA and USAF sponsored interagency and international effort to study a rare natural phenomenon, a meteor storm, for clues to the composition of meteoroids, cometary debris, and the emission processes. **Two Japanese scientists, Dr. Hajime Yano(ISAS) and Shinsuke Abe(NAOJ), participated in the 1999 mission.**

FISTA aircraft

Modified NKC135-E aircraft

ARIA aircraft

Boeing 707 aircraft equipped With a radar in the nose

FIGURE 2.2. 1999 LEONID MULTI-INSTRUMENT AIRCRAFT CAMPAIGN, FISTA and ARIA observational aircrafts. On the night of November 18, 1999, two aircrafts took off on a mission to rendezvous with the biggest meteor storm since the 19th century. Over the Mediterranean Sea, these aircrafts encounter with the Leonid Meteor Storm, thousands of meteors per hour. From 12 km up, flying about 150 km apart, with over twenty instruments pointing out the Leonids, capturing images and making stereoscopic observations.

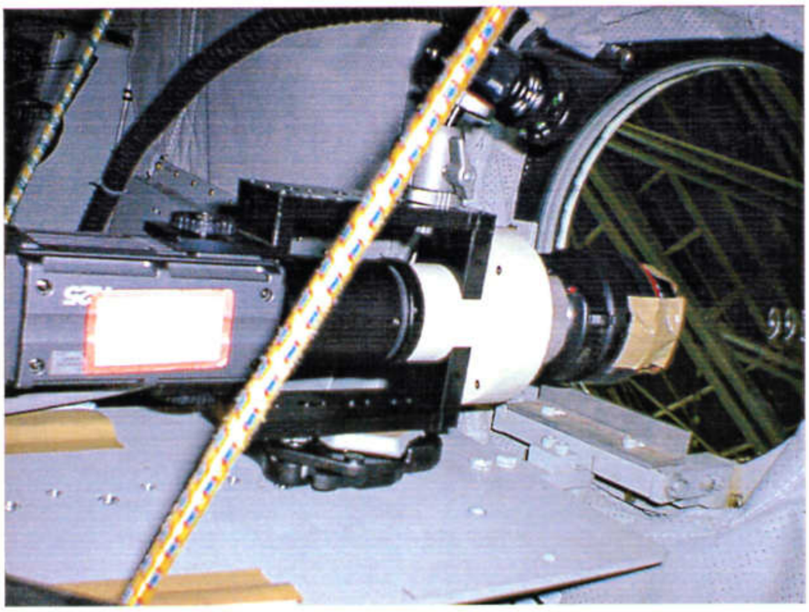

FIGURE 2.3. Intensified High-Definition TV Camera installed on FISTA.

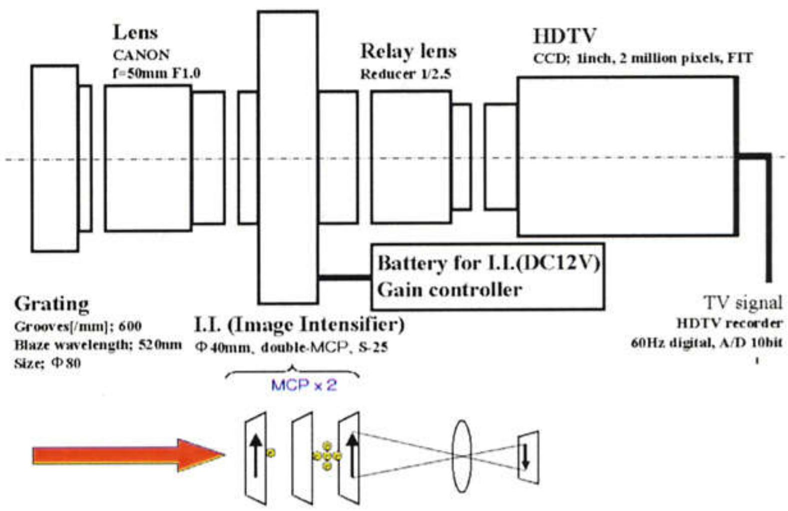

FIGURE 2.4. Schematic of Intensified High-Definition TV Camera.

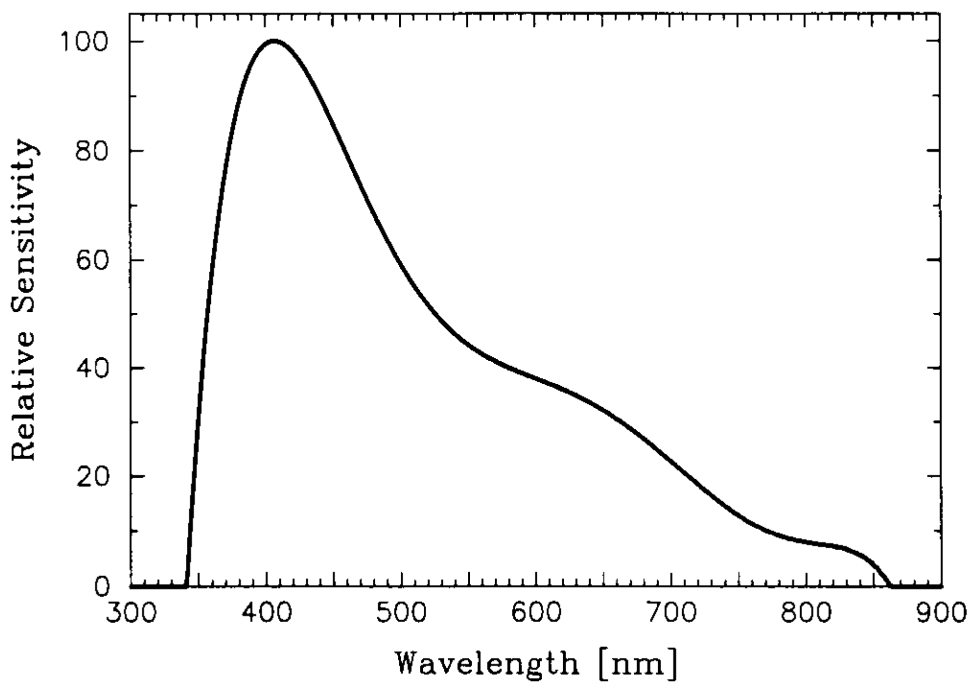

FIGURE 2.5. Spectral sensitivity curve of the intensified HDTV camera operated on FISTA. This system is sensitive in 360 - 850 nm range, with the maximum sensitivity at 405 nm.

FIGURE 2.6. Leonid Meteor Storm. Composite of meteor images recorded from ARIA at the peak of the 1999 Leonid storm. FOV is $60° \times 34°$. Zenith Hourly Rate ZHR $\sim$ 4,000 hr^{-1} at 02:02 UT on November 18, 1999.

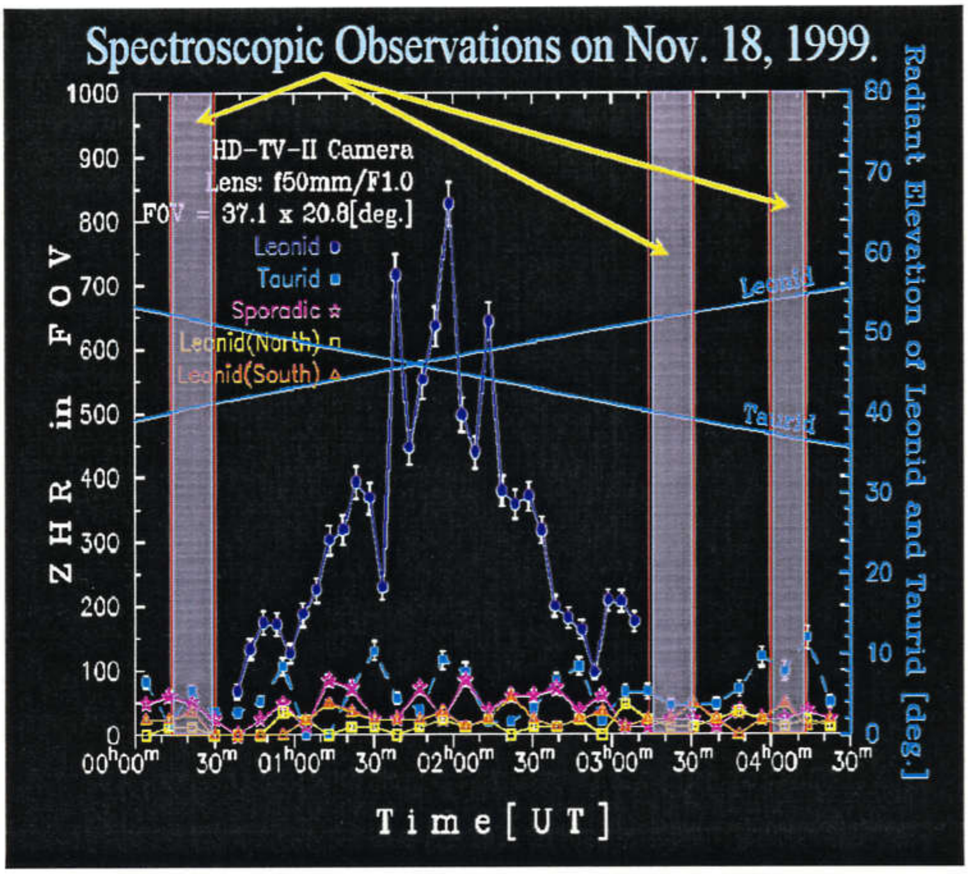

FIGURE 2.7. The peak of the 1999 Leonid storm recorded from FISTA at the peak of the 1999 Leonid storm. Spectroscopic observations were carried out intermittently before and after the peak. The peak activity was around 1h59m UT, November 18 with an peak Zenithal Hourly Rate(Z.H.R.) in FOV($60° \times 34°$) of 826 ± 35 based on 5.0-minute intervals.

which were 76 Leonids, 11 Taurids and 18 sporadics. Most of the Leonid spectra recorded in the night of Nov. 17/18 are meteors belonging to the 1999 Leonid meteor storm. The meteor studied here appeared at 03:24:40 UT, in the Lorentzian tail of the meteor storm (Jenniskens et al., 2000b) or small-scale features of the storm(Arlt et al., 1999; Watanabe et al., 2000).

Chapter 3
DATA ARCHIVES AND ANALYSIS

Selected segments of the HD-CAM tapes were digitized at the studio facilities of Keisoku Giken Co., Ltd., in Yokohama, Japan. The converted frames are 1920 x 1035 pixels 10-bit monochrome files. After the conversion, the image reductions were conducted by using the astronomical image processing software named IRAF(released by National Optical Astronomy Observatories). Both a sky frame subtraction and flat-fielding are applied to the raw data. Flat frames were taken from inside of the aircraft by filming a diffuse white board outside the aircraft before each flight. Also, the same frames obtained before and after meteor spectrum were used for sky frames.

The effective spectral sensitivity curve of the instrument was constructed by measuring a number of spectra of bright main-sequence stars in the observing field. The sensitivity curve is shown in Fig. 2.5 The effective spectral sensitivity covers the range of 360 - 850 nm, with the maximum sensitivity at 405 nm.

The two dimensional images (Fig. 5.1) were reduced to one dimensional spectra by a shift-and-add task, which was repeated to integrate the emission signals along the meteor trajectory and to achieve the highest signal-to-noise ratio (S/N). Typically, the spectrum in each frame consisted of about 10 TV lines. Once the lines were aligned, the combined spectrum was extracted along a trace.

A deconvolution procedure was applied for improving the spectral resolution. The convolution function was based on the point spread function of standard stars in the same frame. The resulting spectral resolution was obtained 2.2 nm in FWHM(Full Width at Half Maximum), which improves over typical video observations by a factor of 4 (Borovicka et al., 1999).

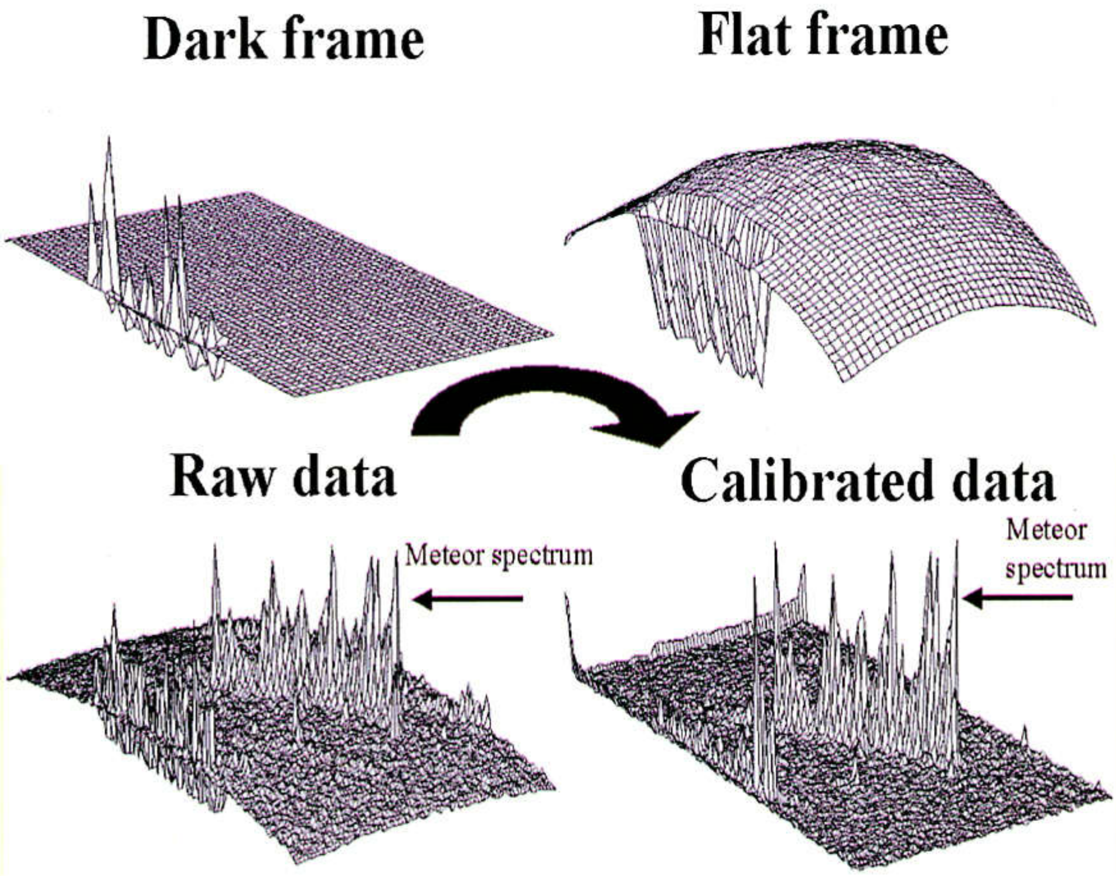

FIGURE 3.1. Raw images are calibrated by dark and flat frames.

3.1 Simplex Method for Spectral Fitting

The simplex method was first introduced by Nelder & Mead (1965) for finding the minimum value of functions. O'Neill (1971) produced a FORTRAN implementation of the simplex method, and Caceci & Cacheris (1984) applied the simplex method to curve fitting and produced a PASCAL program. When the algorithm of the simplex method was re-examined, a redundant mechanism in the process was found. My simplex method is used for Gaussian, Lorentzian or Voigt function fitting to observational spectra. The variance (σ^2) of function $y = f(x_i)$, i=1 – n over k data sets

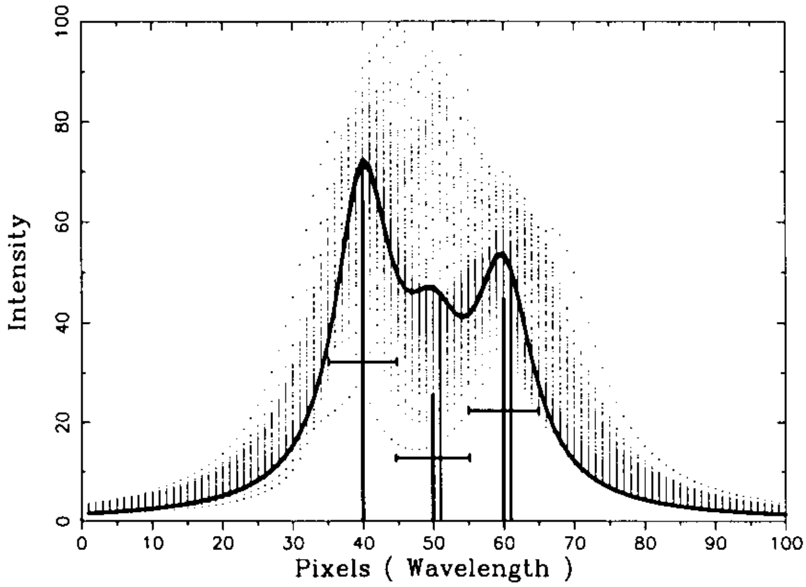

FIGURE 3.2. Simplex method for example. A model spectra is convolved by three Gaussian spectra. Simplex code can separate these combined spectra as they are. Gaussian central wavelengths (pixels) and FWHM are fixed by this method.

is,

$$\sigma^2 = \Sigma_{j=1}^{k} y_i - f(x_{1j}, x_{2j}, x3j, \ldots, x_{nj})^2. \tag{3.1}$$

The coefficients that minimize the variance give the best-fitted function. If we take a simple 2-dimensional function y = ax + b, then the variance will be,

$$\sigma^2 = \Sigma(y_j - \alpha x_j - b)^2) = minimum. \tag{3.2}$$

A graph of the variance versus the coefficients a and b is called a response surface. Each ellipse is a contour of equal variance. The lowest point on the figure will give the appropriate value of the coefficients.

Zernike polynomials are well-known and broadly used functions for describing the wavefront of optical systems in terms of aberrations. Data fitting to Zernike

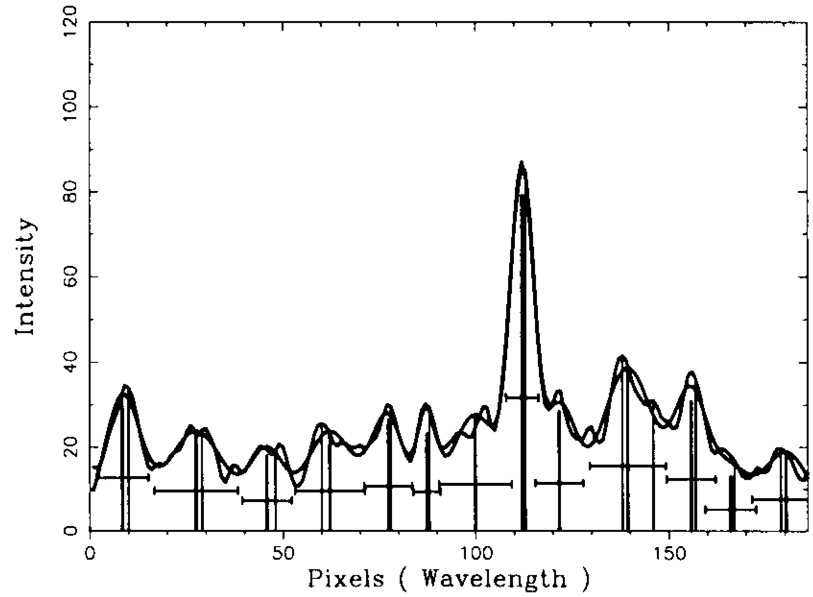

FIGURE 3.3. Simplex method adapted for meteor spectrum. This method has the advantage of meteor spectra.

polynomials has mainly been done by the least-squares method (Malacara et al. 1990; Rayces 1992). However, in order to use the least-squares method, the function to be fitted should have a derivative function, and the function terms should be orthogonal or transformed to be orthogonal (Rayces 1992), to make the calculation easy. The simplex method needs neither the derivative function nor the orthogonality condition. The simplex method is used for curve fitting to Zernike polynomials in Cartesian coordinates.

The spectra consist of numerous overlapping emission lines(5.2). We adopted the simplex method for separation of blended emission lines. The simplex method makes it possible to determine the wavelength and FWHM of each emission line based on an assumed spectral profile. We adopted a Gaussian curve rather than Lorentzian for the fitting function, with free parameters as intensity, position and width of each line.

Chapter 4

Synthetic Atomic and Molecular Spectra

4.1 Boltzmann Distribution

The two-level atom represents a special case of the application of the Boltzmann distribution of population. The general case, specifying the fraction of the total number of atoms or molecules in any given state, requires consideration of all possible energy levels. It is necessary to evaluate a quantity called the *partition function* or *state sum* which can be thought of as a normalization factor. Under conditions of local thermodynamic equilibrium (LTE) at a temperature, T, the number density, n_j, of atoms or molecules in the excited state, j, is (Boltzmann, 1872; Brush 1966)

$$n_j = n_0 \frac{g_j}{g_0} exp\left(-\frac{E_j}{kT}\right), \tag{4.1}$$

where E_j is the excitation energy (energy above ground level) of the j state, n_0 is the number of molecules in the ground state, and g_i is the statistical weight of the s state. An energy level with total angular quantum numbers, J, has $g_i = 2J + 1$, and for a multiplet term with quantum number L and S, the $g_i = (2S+1)(2L+1)$. Eq. (4.1) governs the distribution of particles over different energy states, and is known as the Boltzmann formula. The sum of all n_j must equal the total number density n of the species, so

$$n = \sum_{j=0}^{\infty} n_j = \frac{n_0}{g_0} \sum_{j=0}^{\infty} g_j \, exp\left(-\frac{E_j}{kT}\right) \equiv \frac{n_0}{g_0} Q(T), \tag{4.2}$$

where the partition function $Q(T)$ is defines by

$$Q(T) = \sum_{j=0}^{\infty} g_j \, exp\left(-\frac{E_j}{kT}\right) \tag{4.3}$$

$$= g_0 + g_1 \, exp\left(-\frac{E_1}{kT}\right) + g_2 \, exp\left(-\frac{E_2}{kT}\right) + \cdots. \tag{4.4}$$

Therefore $n_0/g_0 = n/Q(T)$, and the population of the j the level is given by

$$\frac{n_j}{n} = \frac{g_j}{Q(T)} exp\left(-\frac{E_j}{kT}\right). \tag{4.5}$$

The partition function for one molecule, Z, is given by

$$Z = Z_{trans} \cdot Z_{rot} \cdot Z_{vib} \cdot Z_{el}, \tag{4.6}$$

where the subscripts translate, rot, vib, and el denote, respectively, the translational, rotational, vibrational, and electronic partition functions. These partition functions are given by

$$Z_{trans} = \left(\frac{2\pi MkT}{h^2}\right)^{3/2} V, \tag{4.7}$$

$$Z_{rot} = \frac{8\pi^2 IkT}{h^2\sigma} = \frac{kT}{h\nu_{rot}\sigma}, \tag{4.8}$$

$$Z_{rot} = \frac{8\pi^2}{\sigma}\left(\frac{2\pi IkT}{h^2}\right)^{3/2}, \tag{4.9}$$

$$Z_{vib} = \left[1 - exp\left(\frac{-h\nu_{vib}}{kT}\right)\right]^{-1}, \tag{4.10}$$

$$Z_{el} = Q(T), \tag{4.11}$$

Taking the logarithm, Eq. (4.1) becomes:

$$ln\left(\frac{n_j}{g_j}\right) = ln\left(\frac{n_0}{g_0}\right) - \frac{E_j}{kT}. \tag{4.12}$$

Graphically, the LTE temperature T is thus obtained from the slope of the line joining the ground state to the electronic state under consideration. For a gas in

LTE, this temperature is level-independent because all levels lie on a straight line. Therefore, if the gas is in LTE, the LTE temperature characterizes the electronic distribution with respect to the ground state, every probed level yields a different LTE temperature. In that case, different LTE temperature have no physical meaning and are only indicative of a non-Boltzmann distribution.

The number density of an excited state can be accessed by emission spectroscopy by probing the radiative transitions issued from that state. Transitions from atomic electronic levels produce spectral lines that span a narrow spectral range, typically a few angstroms. Atomic transitions are therefore more easily accessed than molecular transitions that span very large spectral ranges, typically several thousand angstroms. For this reason, electronic temperatures are determined in the present work from atomic transitions only.

4.2 Radiative Transfer

The amount of energy emitted in volume dV, solid angle $d\Omega$, frequency range $d\nu$, and time dt is, by definition,

$$j_\nu dV d\Omega d\nu dt. \tag{4.13}$$

Since each atom contributes an energy $h\nu$ distributed over 4π solid angle for each transition, this may also be expressed as

$$\frac{h\nu}{4\pi}\phi(\nu)n_i A_{ji} dV d\Omega d\nu dt, \tag{4.14}$$

so that the emission coefficient is

$$j_\nu = \frac{h\nu}{4\pi}\phi(\nu)n_i A_{ji}\phi(\nu), \tag{4.15}$$

$$I_{ij} = \frac{h\nu}{4\pi}N_i A_{ij} = \frac{N_i}{g_i}\frac{g_i h\nu A_{ij}}{4\pi}, \tag{4.16}$$

then

$$\frac{N_i}{g_i} = \frac{4\pi I_{ij}}{g_i h\nu A_{ij}}, \qquad (4.17)$$

4.3 Abundances

From (4.5), (4.17), we can find the ratio of the numbers of radiating atoms N_a and N_b, for two elements a and b, from the intensities of lines i and j :

$$\frac{N_a}{N_b} = \frac{I_{ija}}{I_{ijb}} \frac{Q(T)_a}{Q(T)_b} \frac{g_{ib}}{g_{ia}} \frac{A_{ijb}}{A_{ija}} exp\left(\frac{-(E_{jb} - E_{ja})}{kT}\right). \qquad (4.18)$$

The line-of-sight spectrum $I(\lambda)$ was then determined by either assuming that the medium is optically thin to all radiation, or by solving the radiative transport equation. In the optically thin case, the spectral emission coefficient in each slab is multiplied by the thickness x of the slab. In the case of self-absorption computations, the radiative transport equation is solved.

$$\frac{dI(\lambda)}{dx} = \epsilon(\lambda) - \kappa(\lambda)I(\lambda) \qquad (4.19)$$

Note that this method is only justified when the gas in in LTE, that is when collisional processes are sufficiently effective so as to prevent the absorption of radiation from modifying the population of the electronic states. Under non-LTE conditions, rays coming from all directions would affect the population, and hence the absorption and emission coefficients.

4.4 Radiative Model

Bound-bound transitions occur between two bound electronic states of atoms or molecules. The spectral position of the line center, the integrated line intensity, and the line shape function are determined in the radiative model.

4.5 Line Center

The location of the line center is determined from the difference of energy between the two bound states u and l as:

$$\lambda_0 = \frac{hc}{E_u - E_l}. \tag{4.20}$$

For molecules, they are decomposed into the sum of electronic, vibrational, and rotational term energies:

$$E_{e,v,J} = T_e + G(v) + F_v(J), \tag{4.21}$$

where $G(v)$ and $F_v(J)$ were calculated using polynomial expansions of the form:

$$G(v) = \omega_e(v + \frac{1}{2}) - \omega_e\chi_e(v + \frac{1}{2})^2 + \omega_e y_e(v + \frac{1}{2})^3 + \omega_e z_e(v + \frac{1}{2})^4 + \cdots, \tag{4.22}$$

$$F_v(J) = B_v J(J + 1) - D_v J^2(J + 1)^2 + \cdots, \tag{4.23}$$

with

$$B_v = B_e - \alpha_e(v + \frac{1}{2}) + \gamma_e(v + \frac{1}{2})^2 + \delta_e(v + \frac{1}{2})^3 + \cdots, \tag{4.24}$$

$$D_v = D_e + \beta_e(v + \frac{1}{2}) + \cdots. \tag{4.25}$$

Klein-Dunham coefficients : $(\omega_e, \omega_e\chi_e, \cdots, B_e, \alpha_e, D_e, \beta_e, \cdots)$

These expressions are in fact the so-called Klein-Dunham polynomial expansions, but arbitrarily truncated to the second or third term.

4.6 Integrated Line Intensity

The integrated intensity of the line is:

$$I[W/cm^3 sr] = \frac{N_u A_{ul} \Delta Eul}{4\pi}. \quad (4.26)$$

The radiative transition probability of a single rotational line of a diatomic molecule can be decomposed in a first approximation as the product of three terms: the square of the electronic transition moment, R_e^2, the Franck-Condon factor, $q_{v'v''}$, and the Honl-London factor, $S_{J''\Lambda''}^{J'\Lambda''}$. These tree terms correspond to the probability of a transition between the two electronic levels, the two vibrational levels, and the two rotational levels, respectively. For most systems, however, the electronic transition moment depends on the vibrational pair involved. This dependence can be accounted for by assuming that R_e^2 is a function of the vibrational pair through the so-called r-centroid $\bar{r}_{v'v''}$.

$$A_{ul} = \frac{64\pi^4 \nu^3}{3hc^3} (R_e(\bar{r}_{v'v''}))^2 q_{v'v''} \frac{S_{J''\Lambda''}^{J'\Lambda'}}{2J'+1}. \quad (4.27)$$

Usually, $(R_e)^2$ is expressed in multiples of $(ea_0)^2$ where e is the charge of the electron in electrostatic units ($e = 4.8 \times 10^{-10}\, e.s.u.$) and a_0 is the first Bohr radius ($a_0 = 0.53^{-8}\, cm$).

Definitions:

v'	; Upper state of the transition
v''	; Lower state of the transition
$T_{v'v''}$	; Term energy, in cm^{-1}
$q_{v'v''}$	; Franck-Condon factor
λ	; Wavelength, in *angstroms*
$\bar{r}_{v'v''}$	; r-centroid, in *bohrs*
$A_{v'v''}$	; Band Einstein A coefficient, in $second^{-1}$
$f_{v'v''}$	; Band absorption oscillator strength
$\sum(R_e^{v'v''})^2$	; Sum of the squared electronic-vibrational transition moments, in $(ea_0)^2$

The fraction of population in a given electronic level e' is then:

$$\frac{N_{e'}}{N_{total}} = \frac{Q_{el}^{e'} \sum_{v',J'} Q_{vib}^{e',v'} Q_{rot}^{e',v',J'}}{\sum_{e',v',J'} Q_{el}^{e'} Q_{vib}^{e',v'} Q_{rot}^{e',v',J'}}. \tag{4.28}$$

where

$$Q_{el}^{e'} = g_{e'} exp\left(-\frac{\epsilon_{e'} - \epsilon_{e'=0}}{kT}\right), \tag{4.29}$$

$$Q_{vib}^{e',v'} = exp\left(-\frac{\epsilon_{v'} - \epsilon_{v'=0}}{kT}\right), \tag{4.30}$$

$$Q_{rot}^{e',v',J'} = (2J'+1)\, exp\left(-\frac{\epsilon_{J'} - \epsilon_{J'=0}}{kT}\right), \tag{4.31}$$

are respectively the electronic, vibrational, and rotational partition functions.

Detailed calculations of partition functions are given by Irwin (atoms and molecules). However, for the approximate purposes of this paper, the partition function may simply be regarded as the effective statistical weight of the atoms or iron under existing conditions of excitation. Except in extreme conditions it is approximately equal to ten weight of the lowest ground term. (The part of the partition function associated with these high-n term is dependent on both temperature and electron pressure.) The ground term weight g_0 is therefore given and this can normally be extrapolated along the isoelectronic sequences to give the approximate partition function for any ion. Table 4.1 shows statistical weights and partition functions of typical elements in neutral(I) and ionization(II) states.

4.7 Lineshape

Spectral lines are broadened by three major processes, namely, natural broadening, Doppler broadening, and pressure broadening. Natural broadening originates from the uncertainty principle of the quantum mechanics, and FWHM of this profile is small enough to be neglected for meteor spectra observations. The FWHM of Doppler

TABLE 4.1. Partition function (T=5040K)

	I		II	
Element	g_0	$logU$	g_0	$logU$
H	2	0.30	1	0.00
N	4	0.61	9	0.95
O	9	0.94	4	0.60
Na	2	0.31	1	0.00
Mg	1	0.01	2	0.31
Al	6	0.77	1	0.00
Si	9	0.98	6	0.76
K	2	0.34	1	0.00
Ca	1	0.07	2	0.34
Mn	6	0.81	7	0.89
Fe	25	1.43	30	1.63
Co	28	1.52	21	1.46
Ni	21	1.47	10	1.02

broadening and pressure broadening is the same order of magnitude, which is generally more than ten times larger than of natural broadening in the meteor emission environment.

However, as Park has pointed out, it is deemed impractical to describe a line shape even with high accuracy accounting for all these broadening mechanisms(Park, 1990). Following this standpoint, this paper introduce the Voigh profile in an approximated form(Olivero 1977), in which both the dispersion profile and Gaussian shape are synthesized. The line shape function is given by

$$\begin{aligned}\Phi(\lambda) &= A\left[(1-t)exp(-2.772L^2) + \frac{t}{1+4L^2}\right. \\ &\left. +0.016(1-t)\left\{exp(-0.4L^{2.25}) - \frac{10}{10+L^{2.25}}\right\}\right] \qquad (4.32)\end{aligned}$$

where

$$A = \frac{1}{w_v(1.065 + 0.477t + 0.058t^2)} \tag{4.33}$$

$$L = \frac{\lambda - \lambda_c}{w_v} \tag{4.34}$$

$$t = \frac{w_L}{w_v} \tag{4.35}$$

$$w_v = \frac{w_L}{2} + \sqrt{(w_{L/2})^2 + w_G^2} \tag{4.36}$$

w_G, w_L; full width at half maximum of Gaussian and Lorentzian line spectra, respectively, m

λ; wavelength, m

λ_c; line center wavelength, m

4.8 Line Selection for Calculation

TABLE 4.2. Calculated molecules.

Molecular species and Electronic system name	Spectroscopic notation (upper state $\longrightarrow$ lower state)
CN violet	$B^2\Sigma^+ \longrightarrow X^2\Sigma^+$
N_2 first positive	$B^3\Pi_g \longrightarrow A^3\Sigma_u^+$

Chapter 5

RESULTS

5.1 Time Series of Meteor Spectra

Figure 5.1 shows a set of time series spectra between 3:24:40.20 and 3:24:40.57 UT on November 18, 1999. The time resolution is 0.033 seconds(1/30 seconds). The zeroth order meteor image disappears from the field of view. The dispersing direction is from right(short-wavelength) to left(long-wavelength). The forbidden OI line at 557.7 nm is delayed behind the meteor image (Halliday, 1958, Millman, 1962). The spectrum covers the first order image below 720 nm and an overlap of 1st and 2nd order images above that.

The spectra consist of numerous overlapping emission lines. Figure 5.2 shows the spectrum taken at 3:24:40.30 UT, at time t = 0.167s along the meteor trajectory (Fig. 5.1). The thin line is the spectrum as it was observed. The thick line shows the spectrum after correction for the spectral sensitivity of the system (Fig. 2.5). About 60 emission lines are seen in the 360 - 850 nm wavelength range.

Once the wavelength and FWHM of each line are determined using simplex method, the temperature and abundances of each atoms can be calculated by as-

TABLE 5.1. Observational frame data.

No.	Date	Start Time(frame) hh:mm:ss.ss	End Time(frame) hh:mm:ss.ss	frames	order
Leo-32	18-Nov.	03:24:40.20(06)	03:24:40.57(17)	12	1st
Leo-18	19-Nov.	08:55:22.90(27)	08:55:23.23(08)	12	0th,1st
Leo-10	18-Nov.	04:07:50.77(23)	04:07:51.13(04)	12	0th,1st
Tau-02	17-Nov.	03:51:01.43(13)	03:51:02.17(05)	23	0th,1st

suming local thermodynamic equilibrium(LTE). It is an assumption that all energy levels are populated by collisional and radiative processes which were characterized by a Maxwellian velocity distribution for all radiating particles. Relative intensities obtained by calibrated spectrum allow us to estimate the excitation temperature. The identified lines imply an excitation temperature of about $T = 4,500 \pm 300$. This excited temperature is calculated mainly from intensities ratio of the Fe lines and applies to the mean intensities along the meteor trajectory shown in Fig. 5.1.

The time evolution of spectrum Leo-32, Leo-18, Leo-10 and Tau-02 are shown in Fig. 5.3, Fig. 5.4, Fig. 5.5 and Fig. 5.6 respectively. Observational frame data of each spectrum are shown in Fig. 5.1. Fig. 5.7, Fig. 5.8, Fig. 5.9 and Fig. ?? indicate the light curves of different spectral lines during a meteor event. Geocentric velocity of Leonids are $\sim 71km/s$ while Taurids are $\sim 27 - 29km/s$. This is why the meteoric duration time of Taurids are about 2 times longer than Leonids.

5.2 Orbital Calculations of Meteors

We(Hajime and I) operated "Air-to-Air stereoscopic observations" from two aircrafts. If we could observe a same meteor from different places, we can calculated the orbital elements of meteoroid as a triangulation method. FISTA aircraft kept the distance about 150 - 200 km from ARIA aircraft and we could know the GPS positioning data of the mission aircrafts through head-set radio communications. We tried to aim each HDTV camera to the sky area where same meteors could be observed. The stereoscopic observations operated for 20 minutes every hour and have been accomplished. This is the first attempt to calculate the orbit of meteor using spectroscopic and imaging data sets. The zeroth order of spectroscopic meteor was used for measuring the position on the field. The 5th order polynomial fitting function was adopted for calculating the plate constant. However, the position error was over 30 seconds in the FOV of $37.1 \times 20.8deg.$ because the objective grating spectrograph caused large aberration. Table 5.2 and 5.3 indicate the meteor trajectory of Leo-18. Each observational frame was composed of interlaced image of 1/30 seconds. There are 3 points to be measured, head, center and behind, because meteors moved in the frame during the 1/30 seconds. Moreover, meteors decelerate in the upper atmosphere caused by collisions. Orbital calculation results, height(km) and distance(km), shown in Table 5.3. The accuracy of height is $\sim \pm 3.0km$.

- ◊ FISTA aircraft ◊
- Observation: Spectroscopic mode
- FOV = $37.1 \times 20.8deg.$ (HDTV with f=50mm(F1.0) camera lens)
- 08:55:22 UT, 19-NOV-1999(Leo-18)
- FISTA position(UTC=08:55:20)
  Longitude = $33°.28419N$, Latitude = $-62°.03203E$,
  Height = 9146.4384 m, Velocity = 468.3 km/h, Heading = 248°.2
- ◊ ARIA aircraft ◊
- Observation: Imaging mode
- FOV = $32.7 \times 18.3deg.$ (HDTV with f=58mm(F1.2) camera lens)
- 08:55:22 UT, 19-NOV-1999(Leo-18)
- ARIA position(UTC=08:55:20)
  Longitude = $32°.07383N$, Latitude = $-61°.43850E$,
  Height = 9120.5304 m, Velocity = 452.7 km/h, Heading = 247°.5

TABLE 5.2. Leonid meteor trajectory from FISTA

No.	GPS Time (U T) hh mm ss.sss	α meteor(behind) hh:mm:ss.ss	δ meteor(behind) o:mm:ss.ss	α meteor(center) hh:mm:ss.ss	δ meteor(center) o:mm:ss.ss	α meteor(head) hh:mm:ss.ss	δ meteor(head) o:mm:ss.ss
01.	08:55:22.900	10:19:44.71	+61:50:54.33,	10:19:39.02	+61:54:47.00,	10:19:34.76	+61:59:53.85
02.	08:55:22.933	10:19:01.47	+62:15:34.30,	10:18:57.06	+62:20:41.06,	10:18:40.93	+62:24:43.50
03.	08:55:22.967	10:18:12.74	+62:36:30.74,	10:17:59.22	+62:43:01.33,	10:17:45.59	+62:49:31.84
04.	08:55:23.000	10:17:16.63	+63:01:18.34,	10:17:02.71	+63:07:48.55,	10:16:47.28	+63:13:04.42
05.	08:55:23.033	10:16:18.92	+63:26:04.30,	10:16:04:58	+63:32:34.07,	10:15:40.80	+63:40:27.14
06.	08:55:23.067	10:15:18.17	+63:49:34.17,	10:14:56.65	+63:59:55.12,	10:14:33.52	+64:09:01.54
07.	08:55:23.100	10:14:18.41	+64:15:30.38,	10:13:56.20	+64:25:50.46,	10:13:22.61	+64:36:18.83
08.	08:55:23.133	10:13:08.29	+64:44:01.16,	10:12:45.25	+64:54:20.14,	10:12:10.63	+65:04:47.07
09.	08:55:23.167	10:11:57.01	+65:13:42.73,	10:11:31.81	+65:22:46.33,	10:10:54.84	+65:31:57.55
10.	08:55:23.200	10:10:13.26	+65:48:40.50,	10:09:54.91	+65:53:52.42,	10:09:36.44	+65:59:04.14
11.	08:55:23.233	10:09:06.34	+66:16:51.19,	10:08:36.75	+66:23:23.71,	10:08:08.07	+66:31:09.78
12.	08:55:23.267	10:07:26.53	+66:51:29.15,	10:06:55.82	+66:57:59.89,	10:06:35.96	+67:03:09.38

TABLE 5.3. Leonid meteor trajectory from ARIA

No.	GPS Time (U T) hh mm ss.sss	α meteor(behind) hh:mm:ss.ss	δ meteor(behind) o:mm:ss.ss	α meteor(center) hh:mm:ss.ss	δ meteor(center) o:mm:ss.ss	α meteor(head) hh:mm:ss.ss	δ meteor(head) o:mm:ss.ss km	Height km	Distance
01.	08:55:22.900	00:42:11.22	+81:10:22.07,	00:41:30.20	+81:07:53.56,	00:40:38.56	+81:03:17.75	*119.60*	*233.41*
02.	08:55:22.933	00:36:31.85	+80:45:41.51,	00:35:41.97	+80:41:53.86,	00:35:05.49	+80:38:01.76	*117.60*	*232.35*
03.	08:55:22.967	00:31:08.33	+80:17:05.17,	00:30:17.99	+80:13:33.31,	00:29:50.63	+80:09:22.59	*115.01*	*230.99*
04.	08:55:23.000	00:26:37.63	+79:51:26.08,	00:25:29.90	+79:44:44.98,	00:24:41.70	+79:38:15.33	*113.24*	*230.08*
05.	08:55:23.033	00:22:18.72	+79:21:26.71,	00:21:17:03	+79:14:44.17,	00:20:26.42	+79:07:27.70	*111.09*	*228.98*
06.	08:55:23.067	00:18:16.43	+78:52:59.94,	00:17:14.12	+78:46:01.26,	00:16:20.74	+78:37:26.35	*109.00*	*227.94*
07.	08:55:23.100	00:14:41.18	+78:25:31.35,	00:13:42.02	+78:17:13.80,	00:12:53.56	+78:08:39.04	*106.88*	*226.90*
08.	08:55:23.133	00:11:27.72	+77:57:14.69,	00:10:27.94	+77:48:56.73,	00:09:32.93	+77:39:20.36	*104.91*	*225.96*
09.	08:55:23.167	00:08:18.77	+77:28:11.14,	00:07:28.47	+77:20:08.69,	00:06:47.69	+77:11:04.18	*102.97*	*225.04*
10.	08:55:23.200	00:05:13.90	+76:57:04.24,	00:04:33.68	+76:51:21.89,	00:04:05.79	+76:42:49.99	*100.97*	*224.11*
11.	08:55:23.233	00:02:28.60	+76:26:46.60,	00:01:51.58	+76:22:06.14,	00:01:26.50	+76:13:36:00	*098.99*	*223.21*
12.	08:55:23.267	23:59:43.57	+75:58:18.37,	23:59:34.03	+75:53:41.28,	23:59:11.71	+75:47:15.51	*098.48*	*222.98*

- **Radiant Point:** $\alpha = 158°.261, \delta = +53°.672$

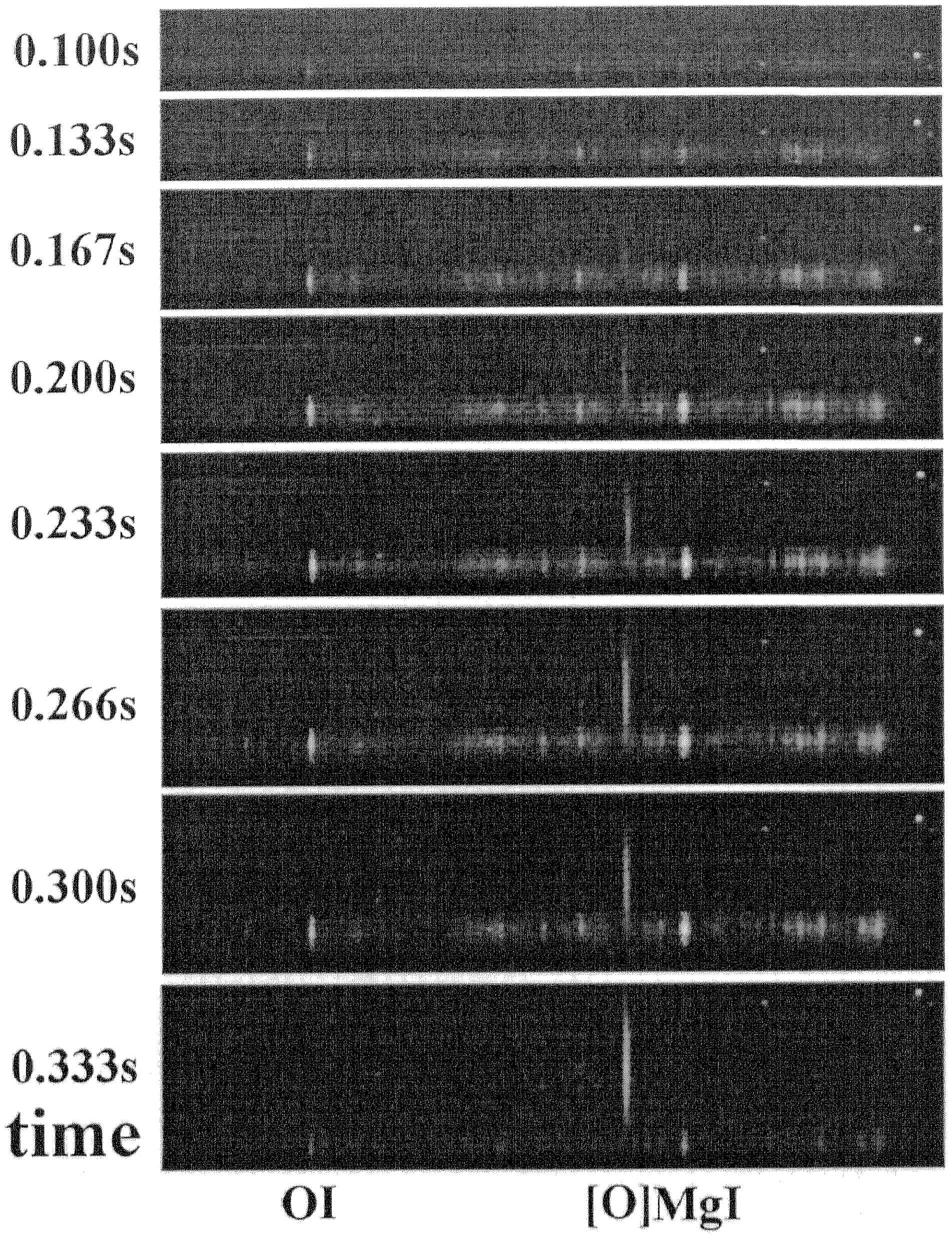

FIGURE 5.1. Time sequence (top to bottom) of spectra recorded from Leonid meteor 03:24:40 UT at a rate of 30 frames/s.

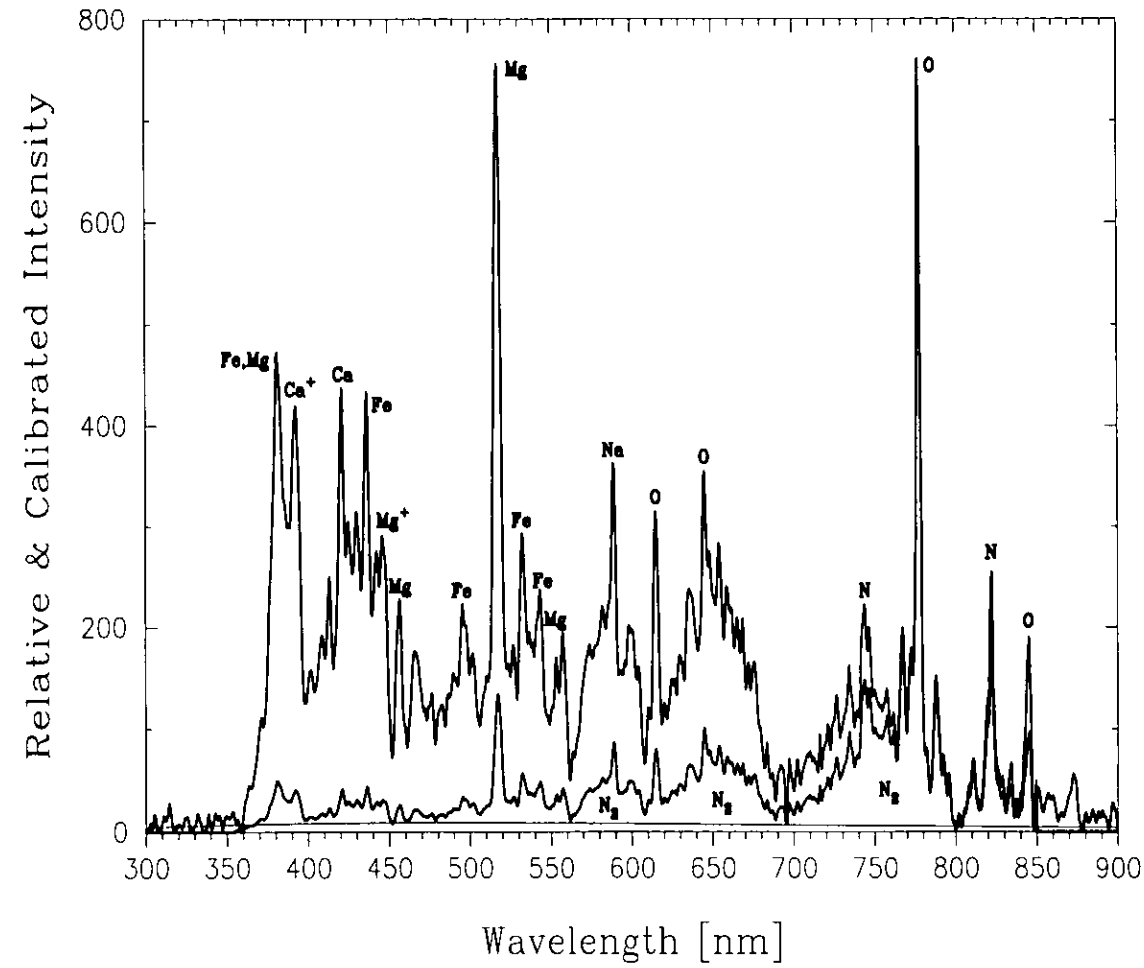

FIGURE 5.2. The identification of spectral lines in the 03:24:40 UT Leonid at t=0.266s. Thin line shows the observational spectrum after a deconvolution procedure. The thick line shows the spectrum after calibrated by the spectral sensitivity of the observed system.

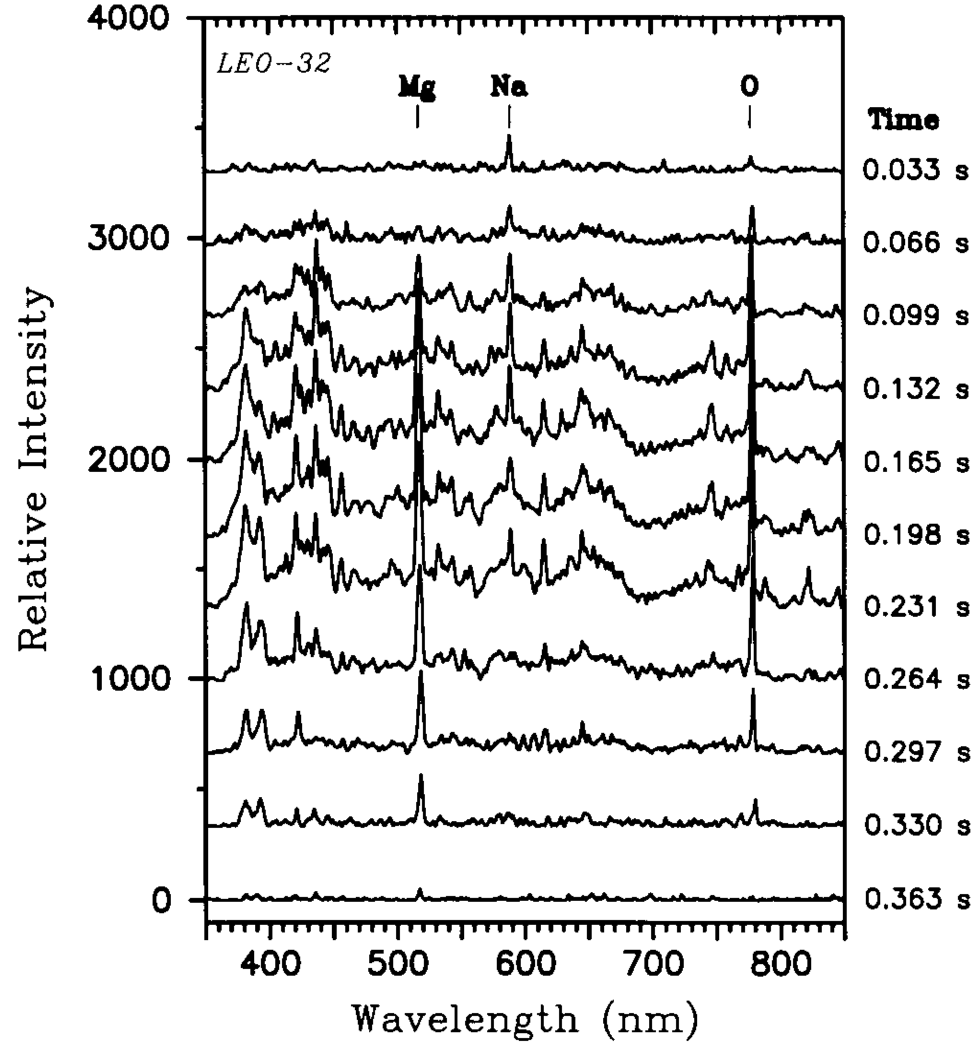

FIGURE 5.3. Time evolution of Leonid spectrum (Leo-32) as it was observed(before calibration for spectral sensitivity). The spectra extracted individual HDTV frames are shown as individual profiles from the top to the bottom. Three brighten lines of MgI(517 nm), NaI(589 nm) and OI(777 nm) are indicated.

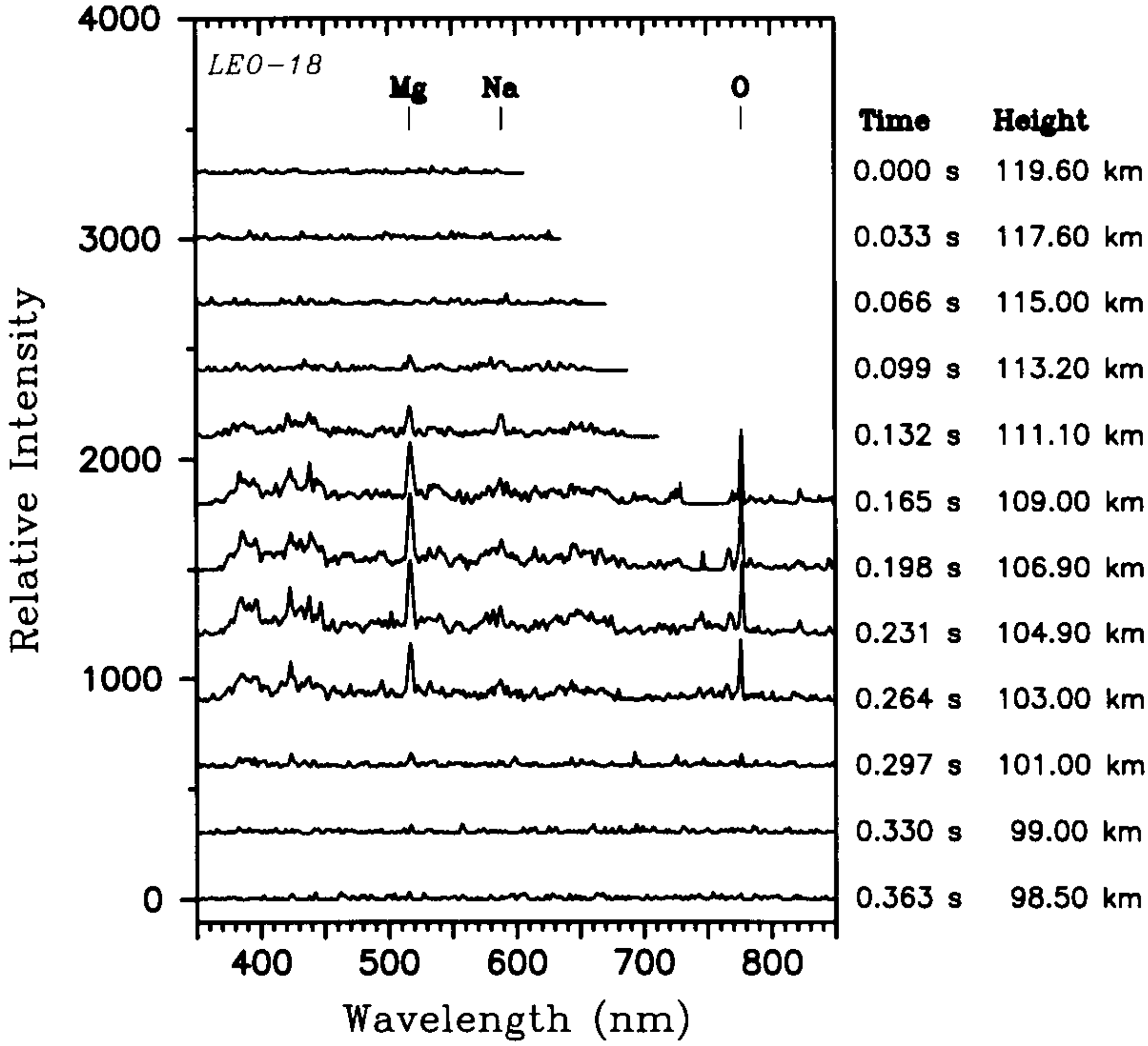

FIGURE 5.4. Time evolution of Leonid spectrum (Leo-18) as it was observed(before calibration for spectral sensitivity). The spectra extracted individual HDTV frames are shown as individual profiles from the top to the bottom. Three brighten lines of MgI(517 nm), NaI(589 nm) and OI(777 nm) are indicated.

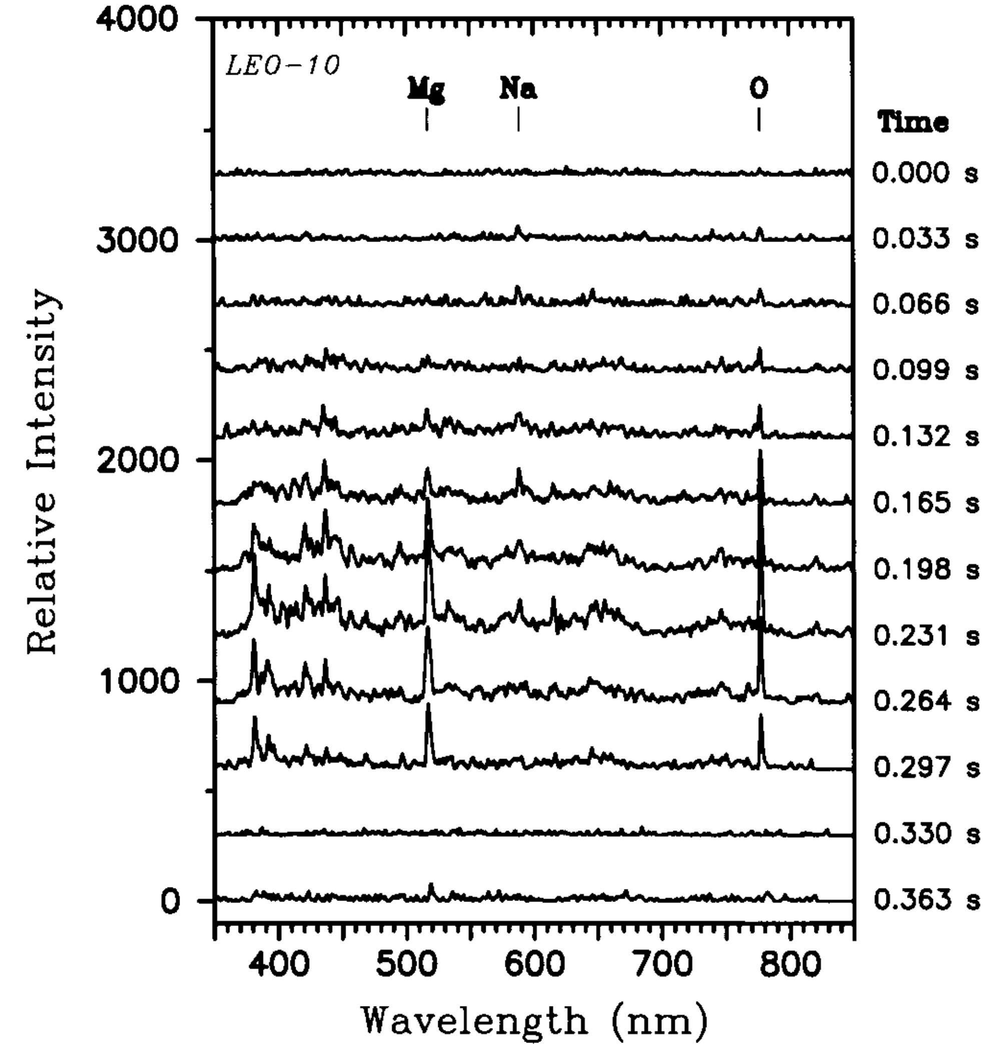

FIGURE 5.5. Time evolution of Leonid spectrum (Leo-10) as it was observed(before calibration for spectral sensitivity). The spectra extracted individual HDTV frames are shown as individual profiles from the top to the bottom. Three brighten lines of MgI(517 nm), NaI(589 nm) and OI(777 nm) are indicated.

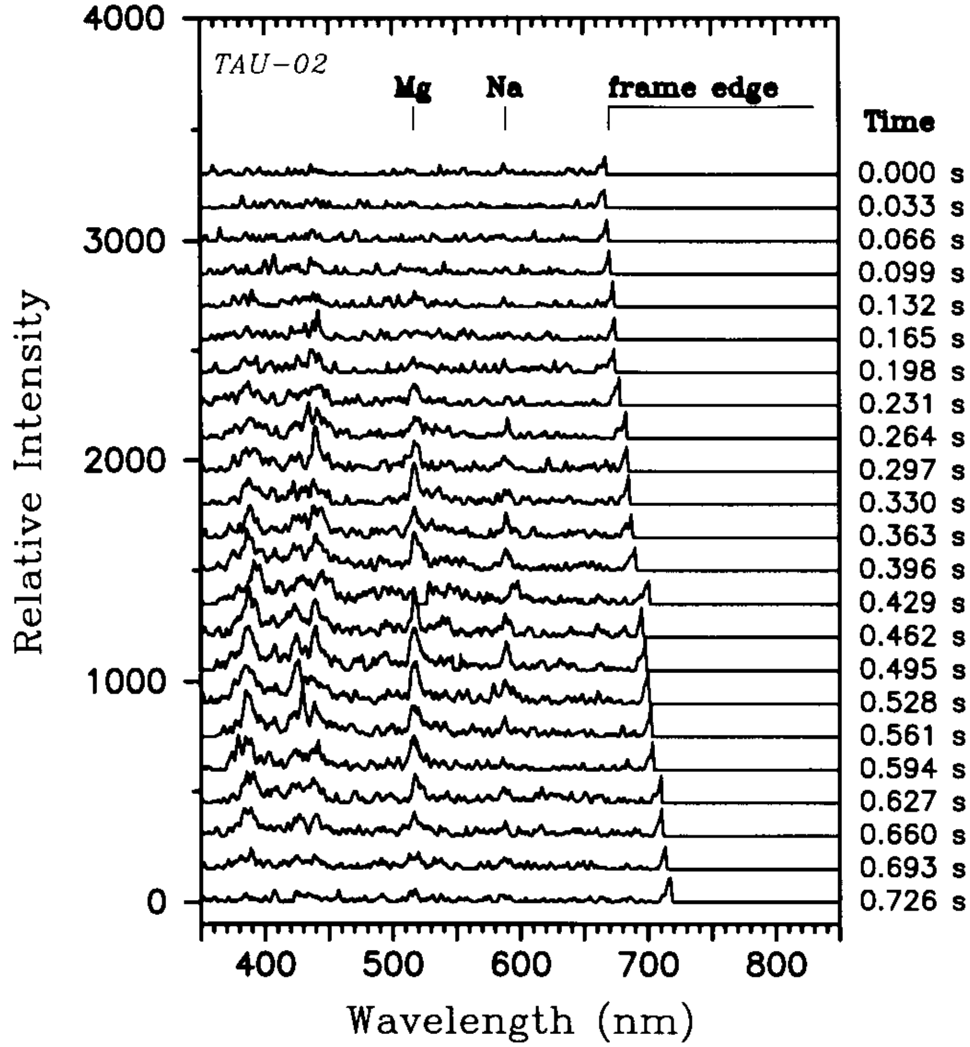

FIGURE 5.6. Time evolution of Taurid spectrum (Tau-02) as it was observed(before calibration for spectral sensitivity). The spectra extracted individual HDTV frames are shown as individual profiles from the top to the bottom. Three brighten lines of MgI(517 nm), NaI(589 nm) and OI(777 nm) are indicated. Right gap is not a emission line which is caused by the observational frame edge.

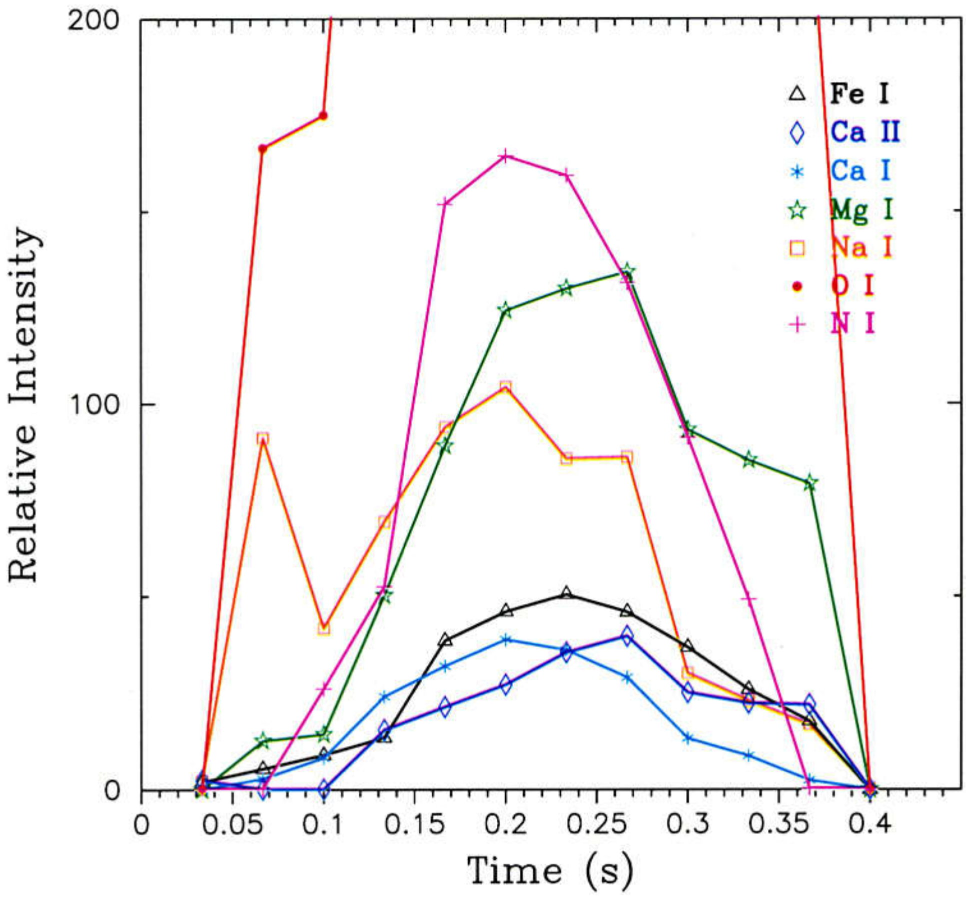

FIGURE 5.7. Relative intensity curves of the spectral emissions from six atomic species in the 03:24:40 UT Leonid(Leo-32).

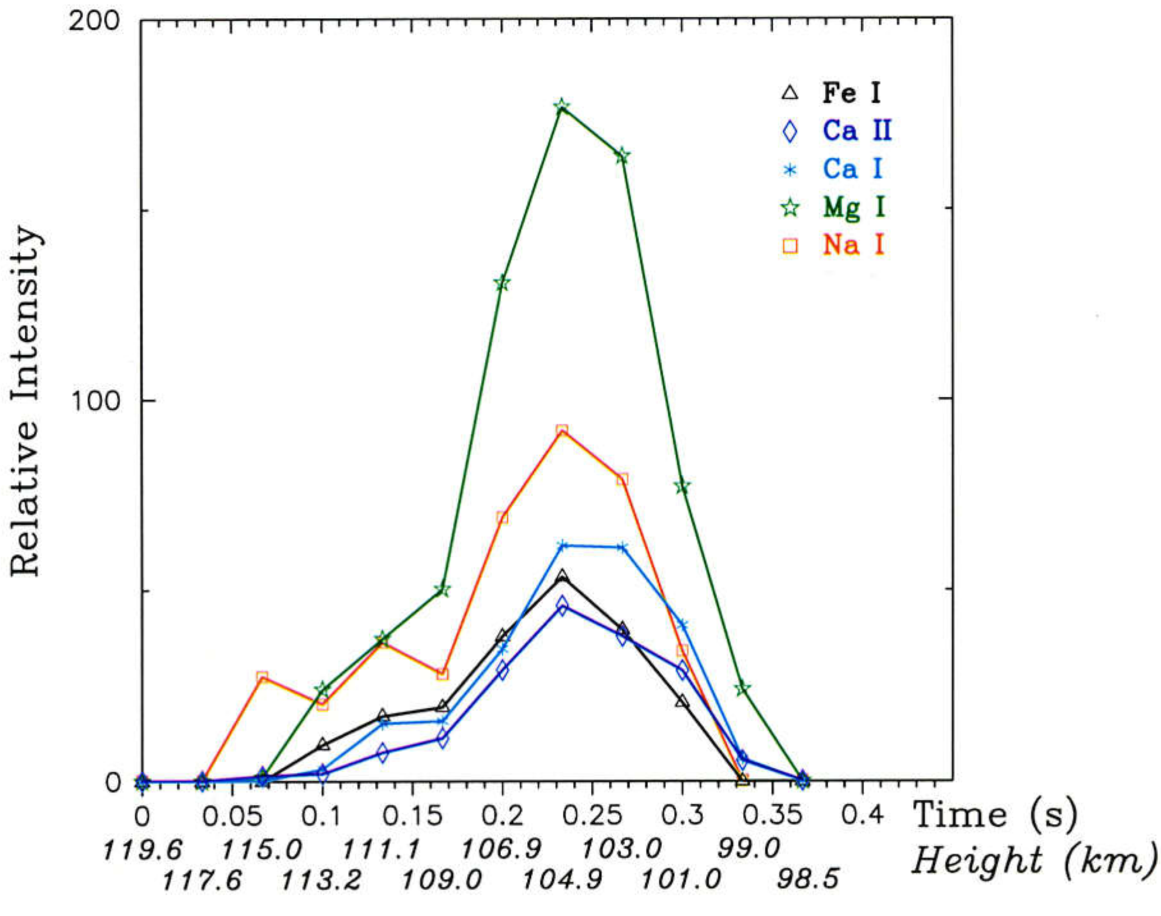

FIGURE 5.8. Relative intensity curves of the spectral emissions from six atomic species in the 8:55:22 UT Leonid(Leo-18).

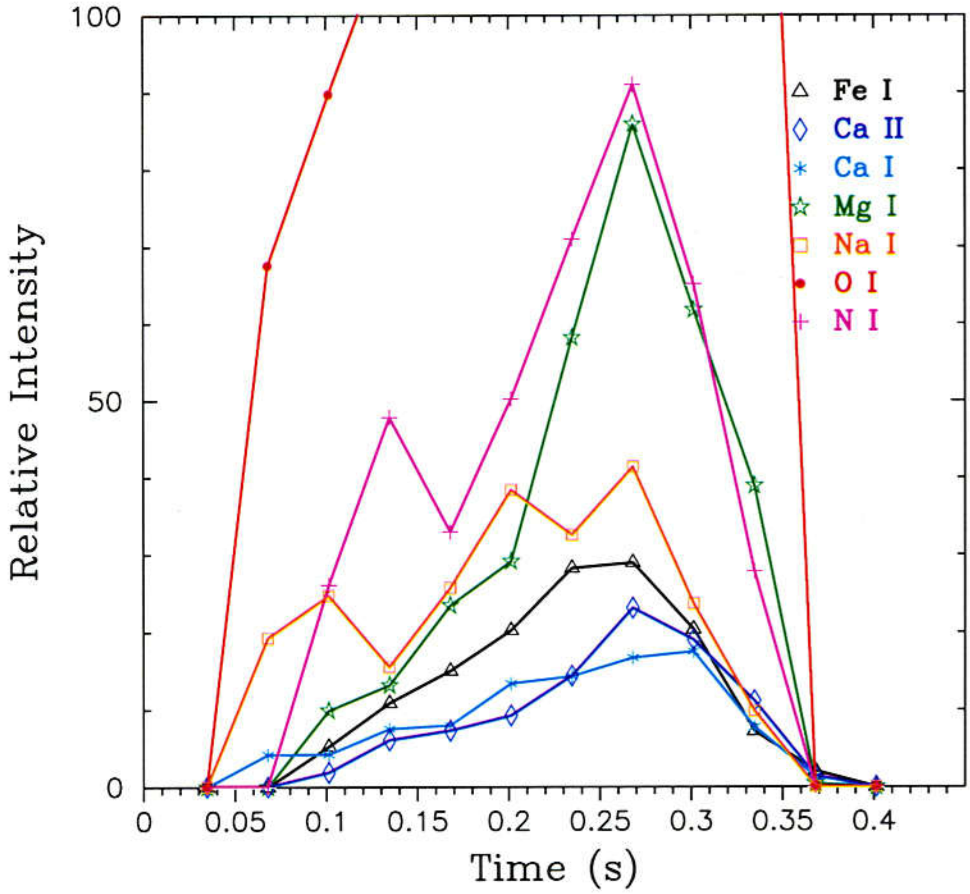

FIGURE 5.9. Relative intensity curves of the spectral emissions from six atomic species in the 4:07:50 UT Leonid(Leo-10).

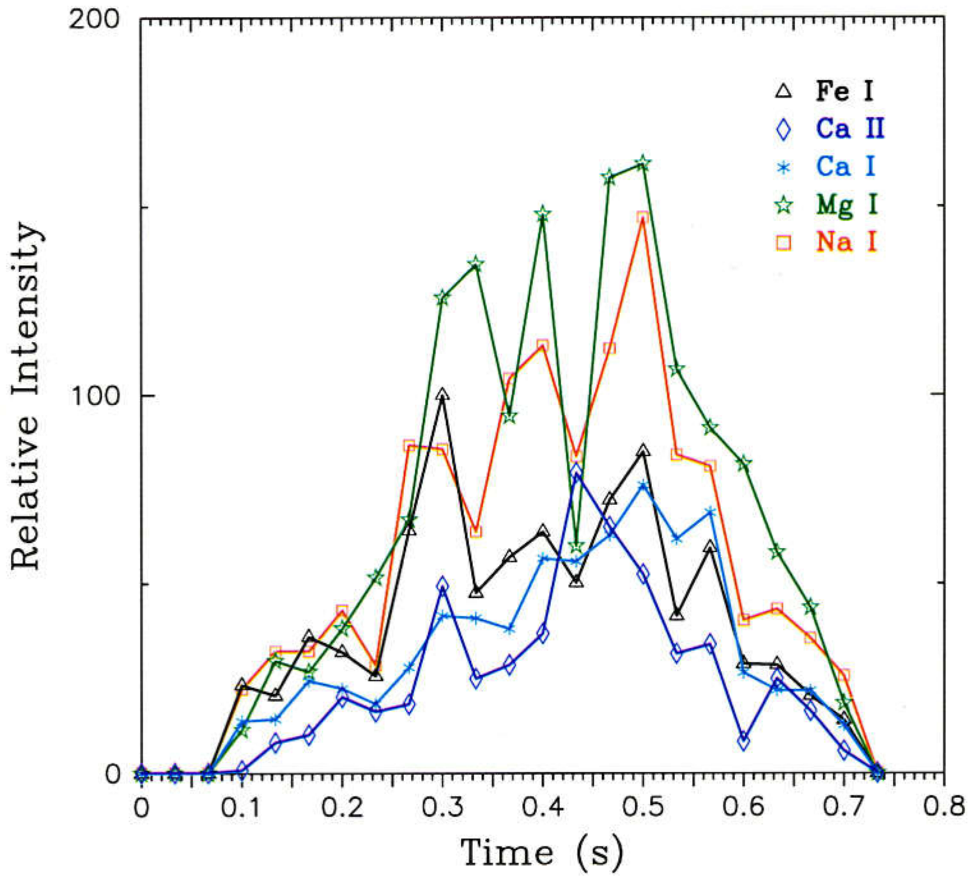

FIGURE 5.10. Relative intensity curves of the spectral emissions from six atomic species in the 3:51:01 UT Taurid(Tau-02).

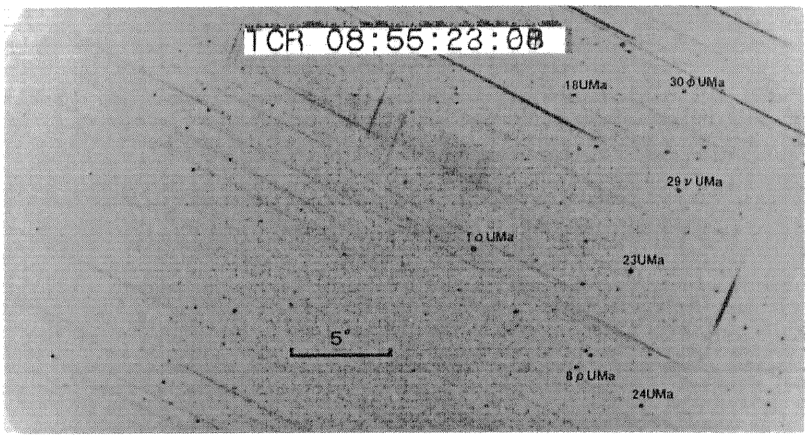

FIGURE 5.11. Air-to-Air stereoscopic observations; stereoscopic observations of Leonid(Leo-18) from FISTA.

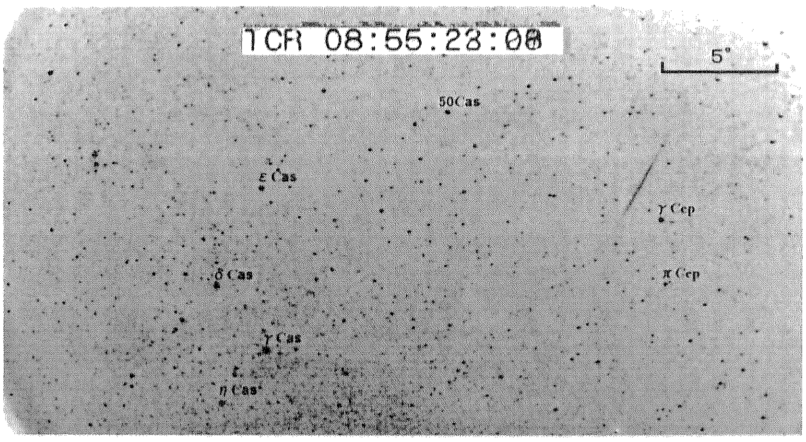

FIGURE 5.12. Air-to-Air stereoscopic observations; imaging observations of Leonid(Leo-18) from ARIA.

Chapter 6
DISCUSSION

6.1 Chemical compositions

In Table 6.1, the elements unambiguously detected in Leonid spectra are listed. For each elements, numbers of detected multiplets(Moore, 1945) are given. Individual lines within multiplets are not listed because they are usually unresolved. The lines of ionized Ca and Mg (at 395 nm and 448 nm respectively) belong to the high-temperature component, other meteoric emission belong to the low-temperature component. Some additional elements(e.g., Cr, Mn) probably contribute to some features in the spectra but remain unsolved.

TABLE 6.1. Elements and multiplets identified in Leonid spectra.

Elements	Major multiplets	Faint multiplets
O	1,4,9,10,11,12;1F	13,14,15,16,17,18,21
N	1,2,3	8,21,24
N_2	first positive	
Mg	2	1,9,11
Mg^+	4	
Na	1	
Fe	41	1,2,15,42,43,318
Ca	2	
Ca^+	1	

Figure 5.7, 5.8 and 5.9 show the relative intensities of the most dominant emissions. Iron and magnesium follow a similar ablation profile than atmospheric oxygen emission. However, the atomic sodium emission is depleted significantly earlier than the other metal atom emissions. This effect was earlier observed for the 1998 Leonid

meteors, and is now confirmed for the 1999 Leonids. This confirmation is significant in light of results by Murray et al.(2000), that the light curves for 1998 and 1999 Leonids differed significantly, with the 1999 Leonids being less finely fragmented. Further study should reveal whether the sodium release from the 1999 Leonids is significantly different from those of 1998.

The average mutual ratios of Na, Fe, Mg, and Ca line intensities have been converted to relative abundances of these elements. Thermal equilibrium at a temperature of 4,500 K and a column density of Mg I and Fe I atoms of the order of $10^{14} cm^{-2}$ were assumed for the main spectral component. From the mean multiplet intensity ratios, we derived the atomic ratios in the radiating gas of Leonid and Taurid meteors(Table 6.2). Owing to all uncertainties of the procedure used, these values may be in error by a factor of 3. Because Na and Ca are highly ionized at 4,500 K, the Saha equation had to be used to convert neutral atom ratios to elemental ratios. The ionization degree depends also on density. Fortunately, changes of density affect all elements in nearly the same way for a given temperature, and the density estimate is therefore not so critical.

A comparison of Leonid with Taurid meteors showed that for NaI/MgI abundances at high altitude(first stage), Leonid meteors are more abundant than Taurid meteor(Fig. 6.1, 6.2, 6.3). This can be explained by their lower velocity - $71 km/s$ for Leonid, and $28 km/s$ for Taurid meteors.

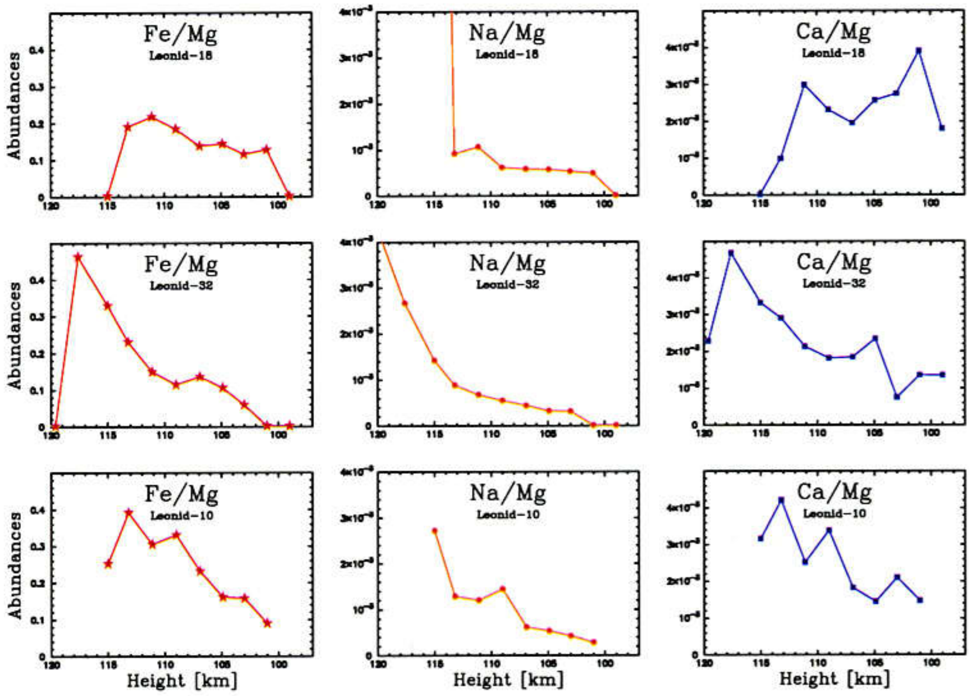

FIGURE 6.1. Abundances of Leonids at each height(km).

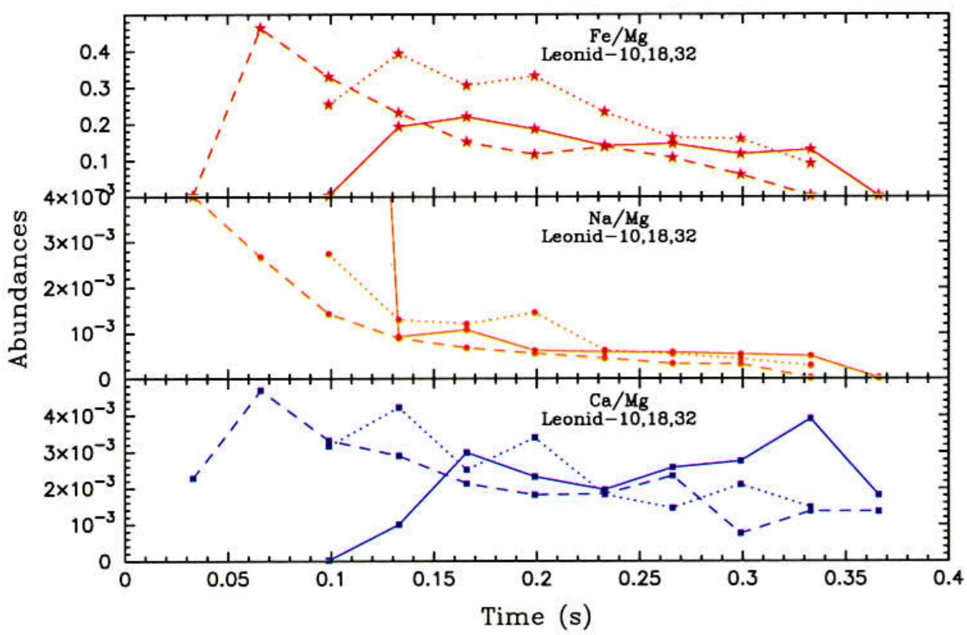

FIGURE 6.2. Abundances of Leonids at each time.

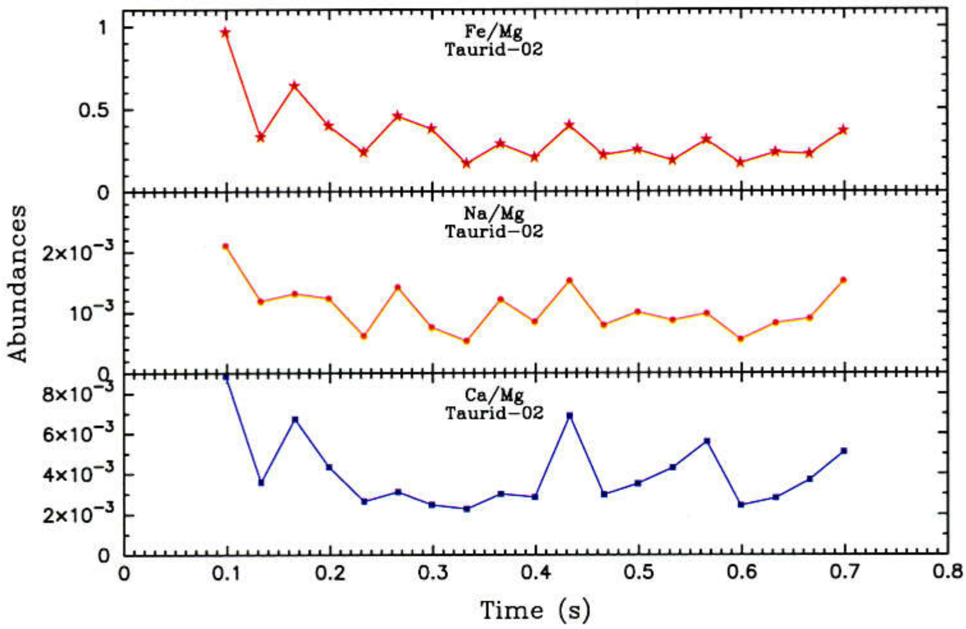

FIGURE 6.3. Abundances of Taurids at each time.

6.2 Excitation Temperature

Figure 6.4 shows the Boltzmann distribution. The so-called Boltzmann temperature T_B is defined by the distribution of excited electronic levels.

$$n_{u1} = n_{u2} \frac{g_{u1}}{g_{u2}} exp\left(-\frac{E_{u1} - E_{u2}}{kT_B}\right), \tag{6.1}$$

Although LTE and Boltzmann temperatures are not independent(6.1 is the ratio of 4.1 written for two electronic levels), the Boltzmann temperature offers several advantages. First, it has a physical meaning, because even when the gas is not in LTE, T_B represents the kinetic temperature of the free electrons if the probed levels are close to the ionization limit. This stems from the fact that high-lying electronic levels tend to be in equilibrium with the free electrons. Second, in contrast to the LTE temperature, no assumption needs to be made about the ground state number density since it is not involved. Finally, the Boltzmann temperature is more sensitive to a possible non-equilibrium distribution of the electronic levels. However, the latter point

TABLE 6.2. Relative abundances of meteors at each time and height. (normalized by Mg)

	Leonid-32	Leonid-18	Leonid-10	Taurid-02
Na (ratio in number)	7.04×10^{-4}	6.12×10^{-4}	7.84×10^{-4}	9.14×10^{-4}
Na (ratio in mass)	6.66×10^{-4}	5.79×10^{-4}	7.41×10^{-4}	8.64×10^{-4}
Mg (ratio in number)	1.00	1.00	1.00	1.00
Mg (ratio in mass)	1.00	1.00	1.00	1.00
Ca (ratio in number)	2.09×10^{-3}	2.55×10^{-3}	$\times 10^{-3}$	3.45×10^{-3}
Ca (ratio in mass)	3.44×10^{-3}	4.21×10^{-3}	$\times 10^{-3}$	5.69×10^{-3}
Fe (ratio in number)	1.33×10^{-1}	1.37×10^{-1}	2.04×10^{-1}	2.73×10^{-1}
Fe (ratio in mass)	3.06×10^{-1}	3.14×10^{-1}	4.69×10^{-1}	6.28×10^{-1}

also implies that the Boltzmann temperature cannot be determined as accurately as the LTE temperature because it includes the Einstein coefficients of two transitions, and these are not yet known very precisely.

Calculated excitation electronic temperature is $4,500 \pm 300K$, which is the average temperature through the meteor phenomena ($< 1 second$). Though the excitation temperature changes time by time between 4,000 - 5,000 K, we may say that LTE assumption is not bad. We found an evidence to support LTE assumption. The maximum sensitivity of HDTV camera is near-UV region, but still sensitive in near-IR region. There are many iron lines below 550 nm range, but less contamination in 600 - 850 nm range. There are many broadband emissions from molecular emissions. The near-IR and visible region is dominated by molecular emission from first positive bands of N_2. Other broad features are simply blends of atomic lines, OI at 615.7 nm, 626.2 nm, 645.4 nm, 648.9 nm 665.4nm and NI at 747 nm.

Many Einstein coefficients, Frank-Condon factors, and r-centroids for nitrogen band systems have been published previously. Synthetic spectra of nitrogen were carried out using a structured SPRADIAN package(Fujita and Abe, 1997) with nitrogen data base(Gilmore et al., 1992). Figure 6.5 shows observed spectrum of Leonid(thick line) and theoretical spectrum of N_2 first positive(thin line).

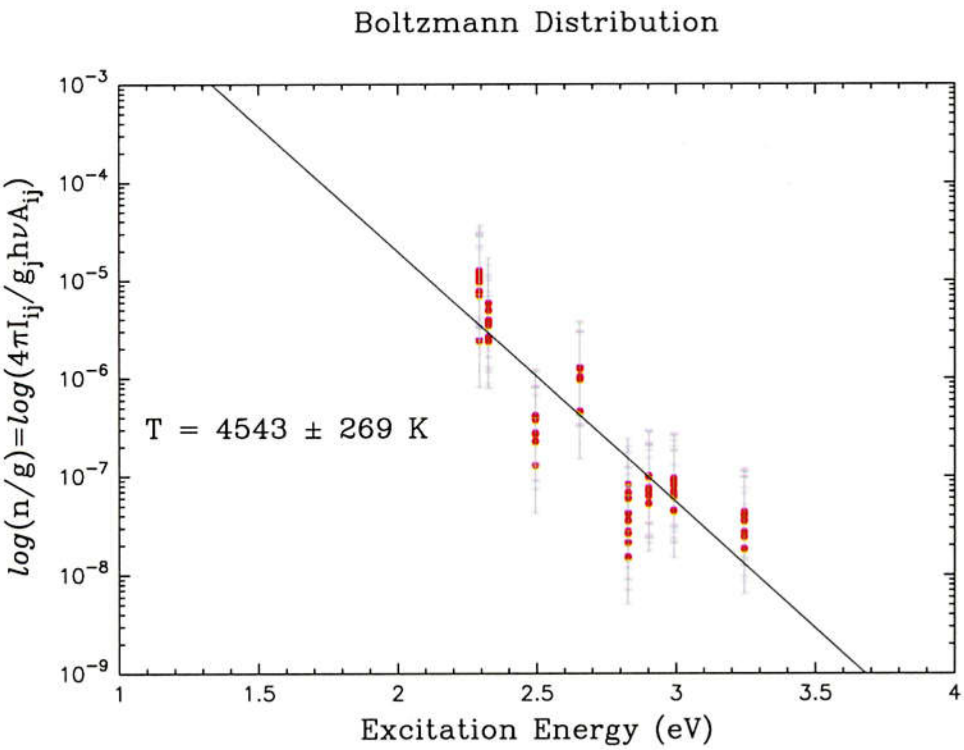

FIGURE 6.4. Boltzman distribution of Fe spectra.

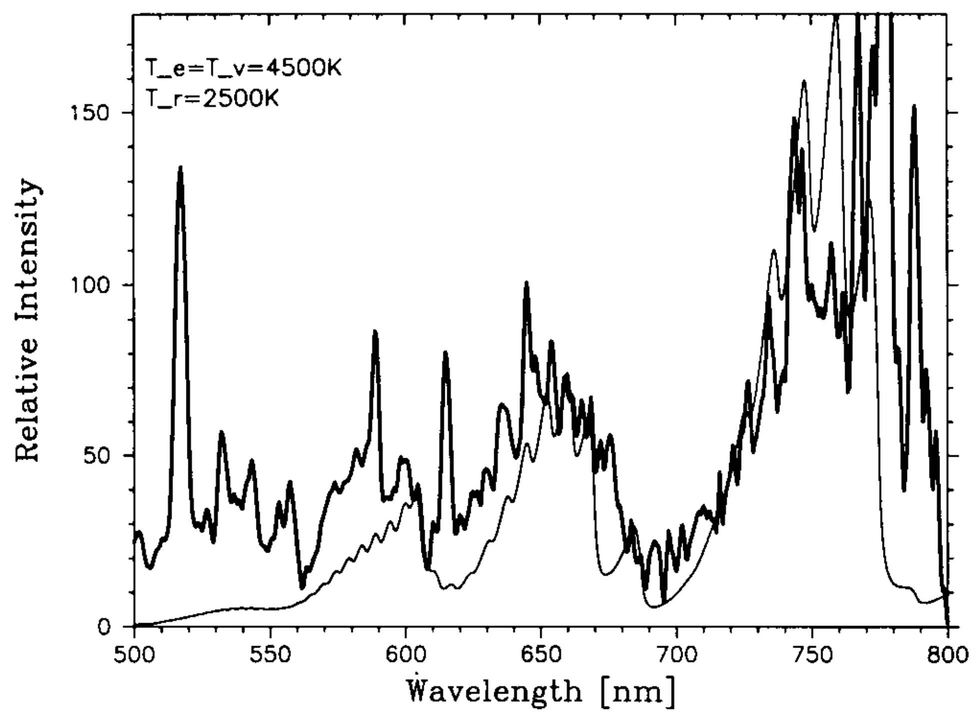

FIGURE 6.5. Leonid spectrum at 500 - 800 nm range(thick line). The spectrum is calibrated by spectral sensitivity of HDTV system. The thin line shows the first positive bands of N_2 convolved by observational FWHM of Gaussian profile.

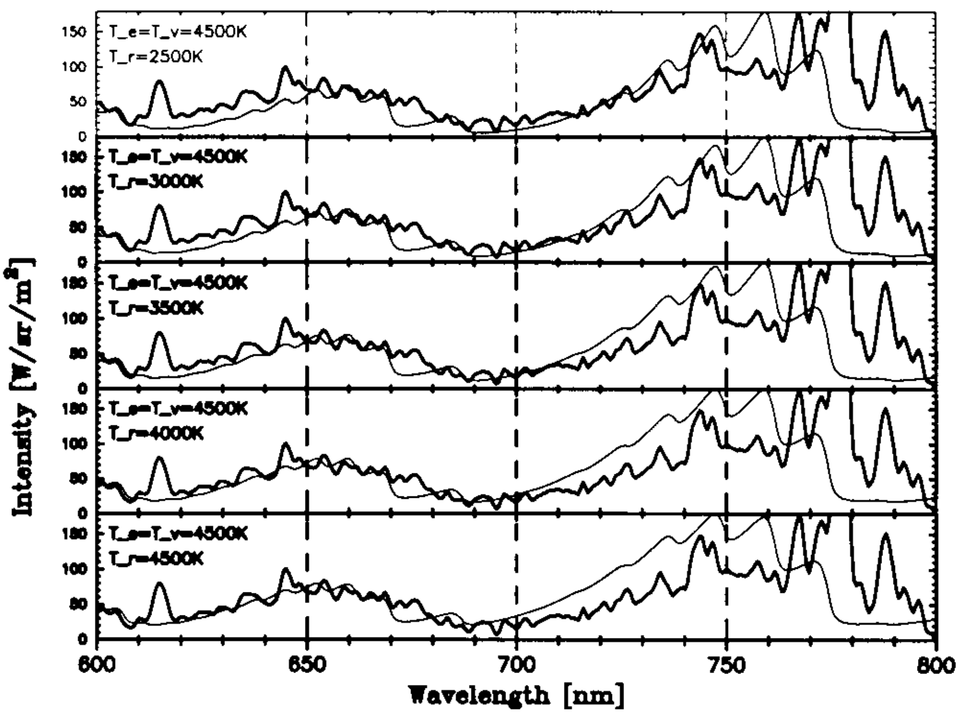

FIGURE 6.6. Observational spectrum in 600 - 800 nm range compared with synthetic spectrum of N_2 first positive band ($B^3\Pi_g \longrightarrow A^3\Sigma_u^+$).

Figure 6.6 shows same synthetic spectra of N_2 first positive(thin line) and observed Leonid spectrum(thick line), but the combination of the electronic-vibrational temperature T_e and the rotational temperature T_r make change. The radiation strength of meteor, LTE has been measured for temperature of $4,500 \pm 300K$ using many atomic irons in short wavelength range, 400 - 550 nm. Prior studies discussed only at shorter wavelength where the emission lines of ablated meteoric metal atoms dominate because of instrument or calculation problems. Our new measurements have been compared to the temperature of N_2 first positive band in long wavelength 550 - 800 nm(top of Fig. 6.6). Entry speed of Leonid meteor is enough to excite N_2 molecules, so the Leonid is the best meteor shower for N_2 or N_2^+ researches. Ionization potentials of typical atoms and molecules are shown in Table 6.3.

TABLE 6.3. Ionization potentials of atoms and molecules.

Atoms	Ionization Potential (eV)
N	14.53414
O	13.61806
Na	5.13908
Mg	7.64624
Al	5.98577
Si	8.15169
Ca	6.11316
Mn	7.43402
Fe	7.9024
Molecules	**Ionization Potential (eV)**
CN	14.17
N_2	15.58
N_2^+	27.1
O_2	12.07
C_2	12.15

Herzberg, G. 1950, *Spectra of Diatomic Molecules*(Krieger, Florida.)

It seems that meteor spectra can be explained well by LTE model. However, there are differences between the vibrational temperature of $T_{e,v} = 4,500K \pm 300K$ and estimated the rotational temperature of $T_r = 2,500K \pm 500K$. It means that meteor

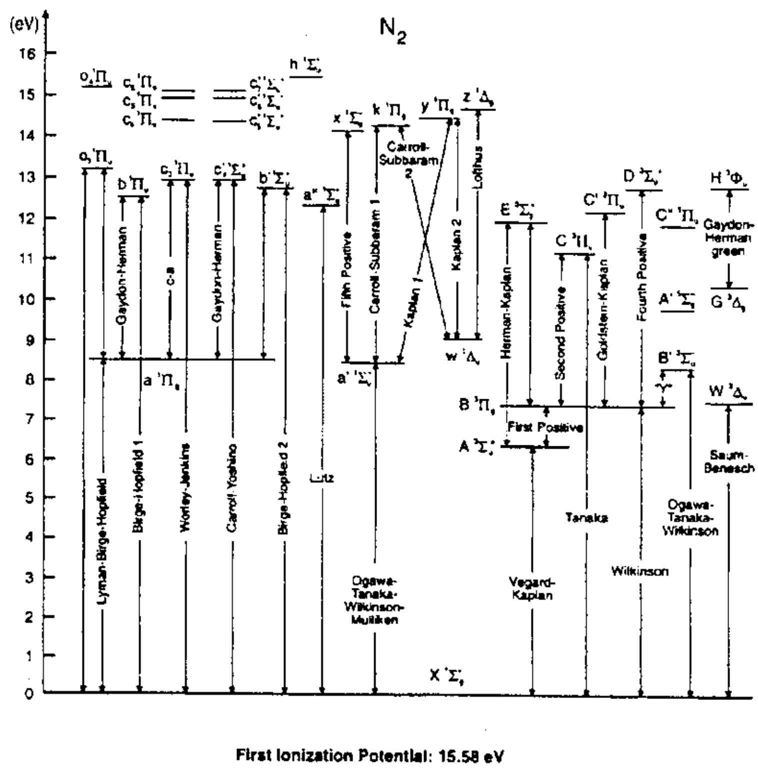

FIGURE 6.7. Grotrian Diagrams of N_2

spectra are not completely explained by thermal equilibrium in detail. I leave the problem untouched because it needs more spectral resolution power in observations to explain the spectra precisely.

The radiation of N_2^+ is not usually observed. The first indication of possible presence of N_2^+ bands was obtained by Millman, Cook and Hemenay in 1969, during a television recording of Perseid spectra. However, since the resolution was low ($\sim 4nm$ in the first order), the presence of bands of the first negative system of nitrogen could only be presumed. The first negative system of bands of N_2^+ cannot be obtained in our spectra.

6.3 Relationship between Meteoroids and Comets

Direct information on the composition of solid cometary particles was very scare prior to the spacecraft and ground-based observations of comet 1P/Haley. Since then, observations of a number of other comets have also contributed significantly to our understanding of comet dust. The physical and chemical characteristics of cometary dust have been reviewed by Grün and Jessberger(1990), Mumma et al.(1993), and Weissmann and Campins(1993). The GIOTTO and VEGA spacecraft probes measured the elemental composition of dust grains in the coma of comet 1P/Halley and found many to be rich in the elements C, H, O and N(Kissel and Krueger, 1987; Jessberger et al., 1998). Refractory organic carbon is thought to be an abundant compound of cometary meteoroids, making up some 23 % of the comet mass fraction and some 66 % of meteoroid mass once the volatile compounds have evaporated(Greenberg, 2000). This organic carbon was mixed intimately with the silicate component and has high molecular mass. Most of it is expected to survive exposure to the vacuum of space and the gentle warming when grains come as close to the Sun as Earth's orbit($T \sim 300K$). When these meteoroids encounter the Earth's atmosphere, the organic carbon is ablated either 1) early on at a relatively cool temperature (400 - 750 K) in the classical case where the grains are heated throughout and the evaporation is the key ablation process, or possibly 2) together with the silicate grains when the ablation process is like sputtering and thermal conductivity is low(Jenniskens et al., 2000c).

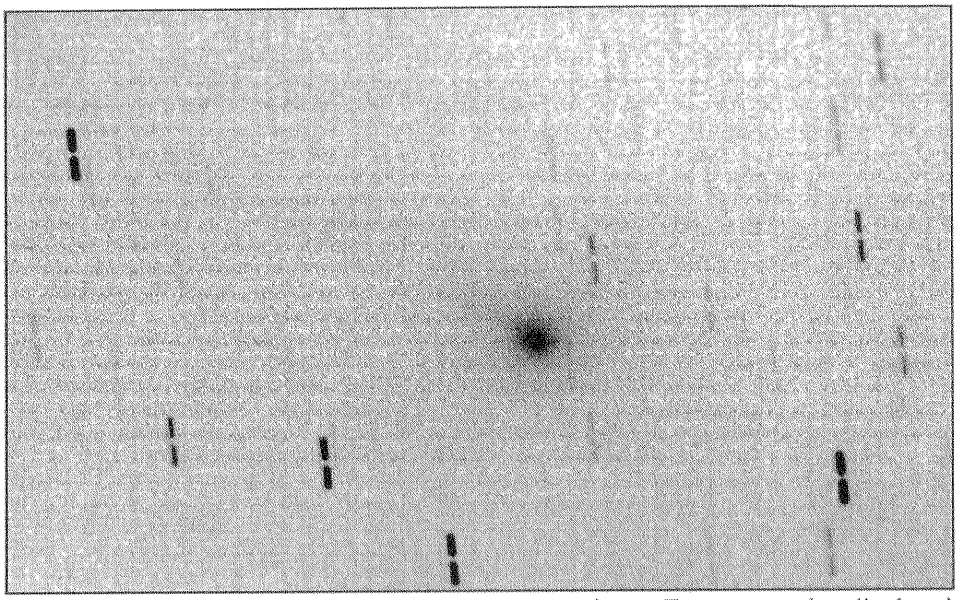

1998年　２月17日，18時26分（JST）
1998, Feb. 17, 09h 26m (UT)

口径50cmカセグレン式反射望遠鏡（F 12→F 7.31，レデューサ使用）
冷却ＣＣＤカメラ（MUTOH CV-16）
露出時間：３分×８，フィルタ：R-60，疑似カラー処理，画像範囲：12.91×8.02′
観測場所：国立天文台（三鷹）

H. Fukushima, T. Nakamura and T. Sekiguchi 国立天文台 広報普及室

FIGURE 6.8. 55P/Tempel–Tuttle observed by 50 cm diameter telescope of Public Information Center of National Astronomical Observatory, Japan. The 1998 was a recurrent year of comet Tempel-Tuttle which orbital period is 33 years. On the night of 17th - 19th November, 1998-2001 when the earth moved through the path of comet Tempel-Tuttle, Leonids meteor shower caused by sand to pea sized debris left in the trail of this comet.

6.3.1 Leonid and Comet 55P/Tempel–Tuttle

CN radical is the most easily detected because of a strong $B \longrightarrow X$ transition of low energy potential. This electronic transition has a band head at 388.3 nm in the near-UV. Figure 6.9 shows the spectrum of comet C/1996B2 (Hyakuteke) obtained at the European Southern Observatory's 1.5-m telescope(Zwitter et al, 1996). Strong CN violet is shown in this spectrum. We searched for CN violet($B^2\Sigma^+ \longrightarrow X^2\Sigma^+$) at 388.3 nm related with comets. The transition probabilities of the CN violet system are computed using the electronic transition moment of Bauschlicher and Langhoff(1998). Synthetic spectra were calculated and convolved with a Voigh profile in which both the dispersion profile and Gaussian shape are synthesized. Spectral resolution of HDTV system is $\lambda/\Delta\lambda \sim 250$, which means the resolution is about 1.6 nm at 400 nm. Three temperature, electronic, vibrational and rotational temperature, assumed to be 4,500 K obtained by meteor spectra.

Figure 6.11 shows the magnified spectrum (uncorrected data) of the Leonid meteor(Leo-32) in the 360-410 nm wavelength region. This part of the spectrum is dominated by lines of iron, causing the broad features at 382 and CaII, causing the band at 392-395 nm. Our HDTV camera has a high sensitivity in the near-UV region and thus can be used to search for the band head of CN at 388 nm, of particular interest to astrobiology (Jenniskens and Butow, 1999). CN emission was not detected significantly above the blends of metal atom lines, not even at the higher altitudes where metal atom lines are less dominant. A comparison with theoretical line spectra is needed to bring out any emission hidden in the blended atomic lines.

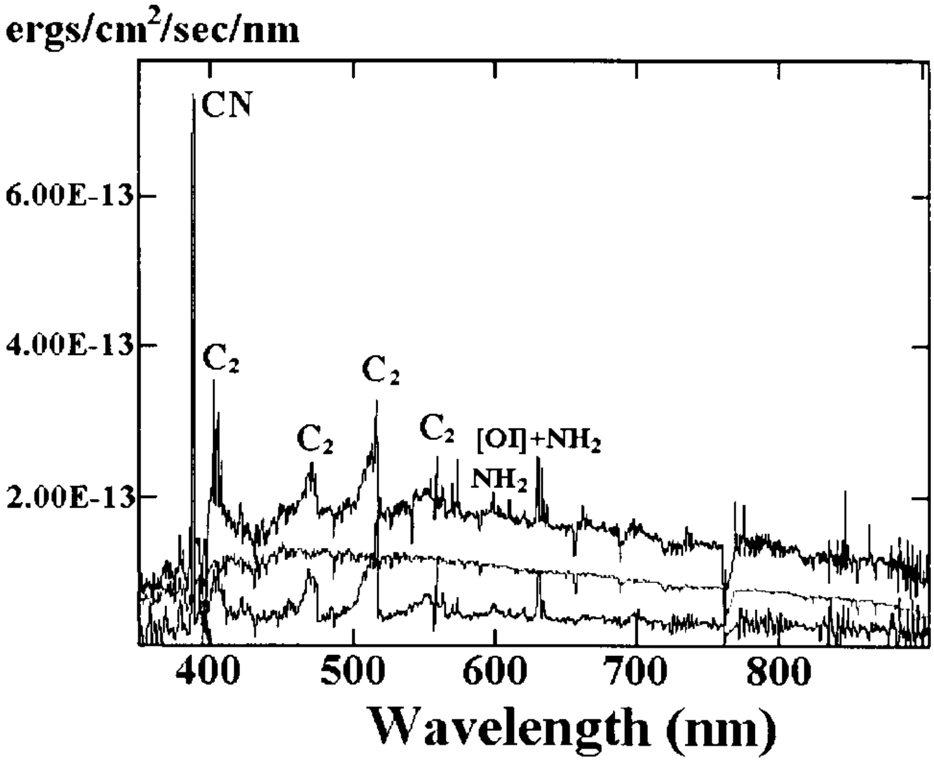

FIGURE 6.9. Spectrum of Comet C/1996 B2 (HYAKUTAKE). A spectrogram (range 340-910 nm) of C/1996 B2 was obtained at the European Southern Observatory's 1.5-m telescope (+ Boller & Chivens spectrograph + CCD) on Feb. 8.2 UT, 1996. The slit (width 2", length 14") was positioned on the comet nucleus. The reflected solar spectrum accounts for the vast majority of the recorded flux, with all major absorption lines markedly visible. The strongest cometary emission is from CN(0,0) at 388 nm, followed by the C3 complex at 405 nm. The strongest C2 Swan band is that of (0,0) at 516 nm, followed by that of (1,0) at 474 nm, with that of (2,0) at 438 nm being barely detectable. The CN(0,1) 422-nm band is in moderate emission, while no cometary NaI D emission is observed.

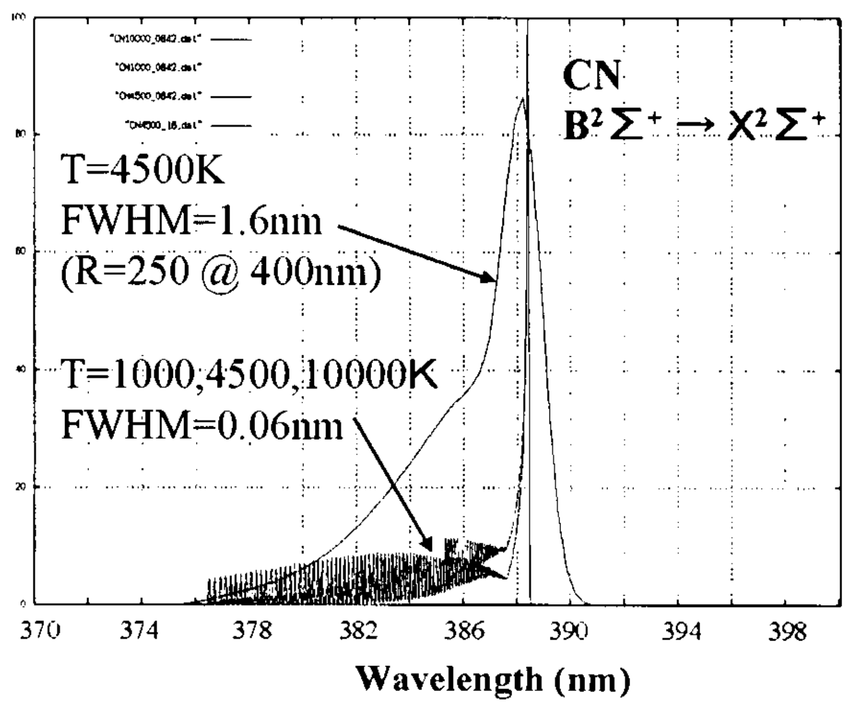

FIGURE 6.10. Synthetic spectra of CN violet($B^2\Sigma^+ \longrightarrow X^2\Sigma^+$). FWHM =1.6 nm and FWHM = 0.06 nm spectra were shown in this figure.

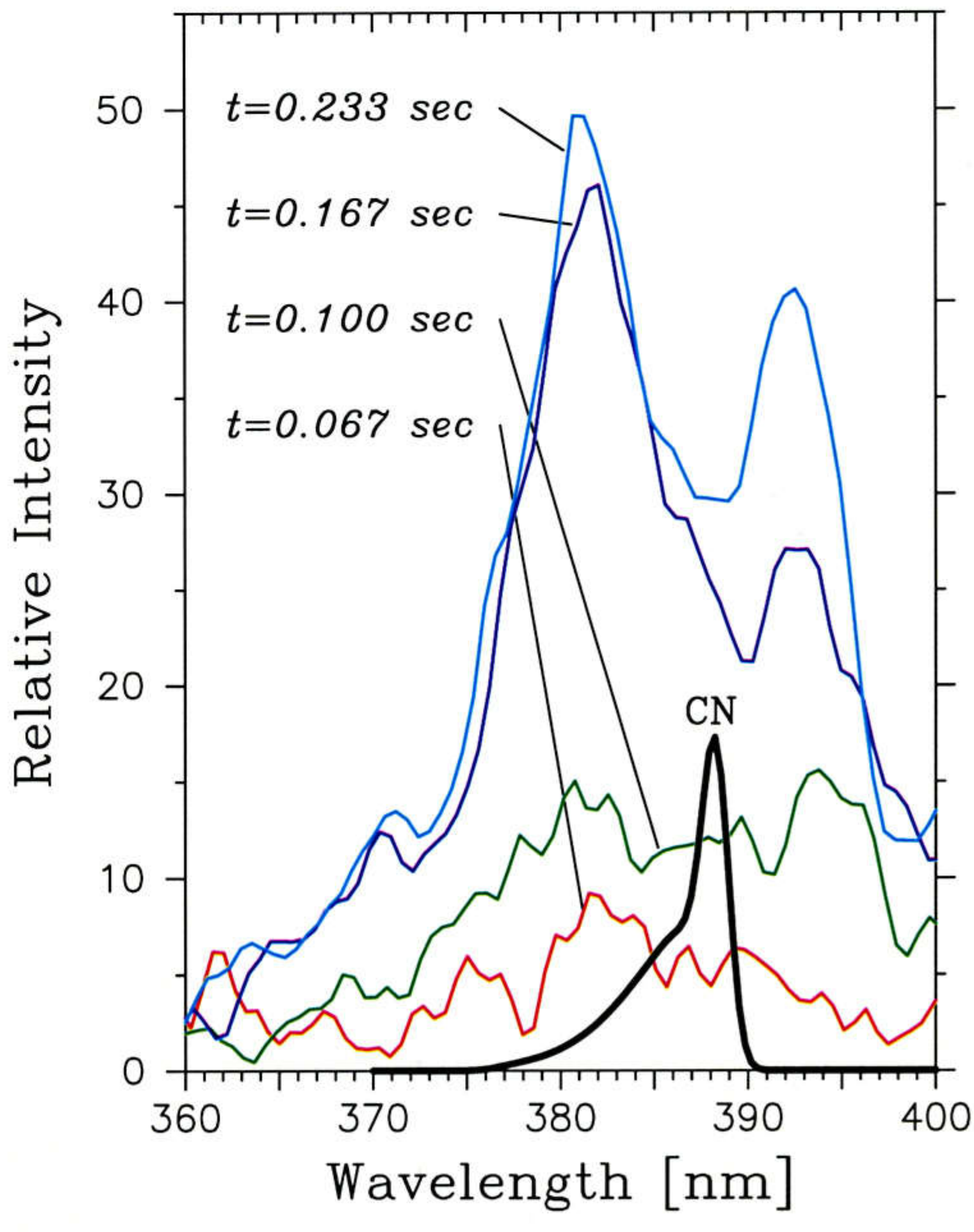

FIGURE 6.11. The 03:24:40 UT Leonid spectrum(Leo-32) in near-ultraviolet region with synthetic CN spectrum. These four spectra show a time profile of one Leonid meteor. The two strong features are caused by neutral FeI, MgI at 382, 383 nm and ionized CaII at 392, 395 nm. The lower spectra were observed at the beginning of meteor ablation, with relatively weak CaII lines. The upper spectra show meteor spectra at the lower altitude. The CN spectrum was calibrated by spectrum sensitivity of observational system, but the intensities is relatively.

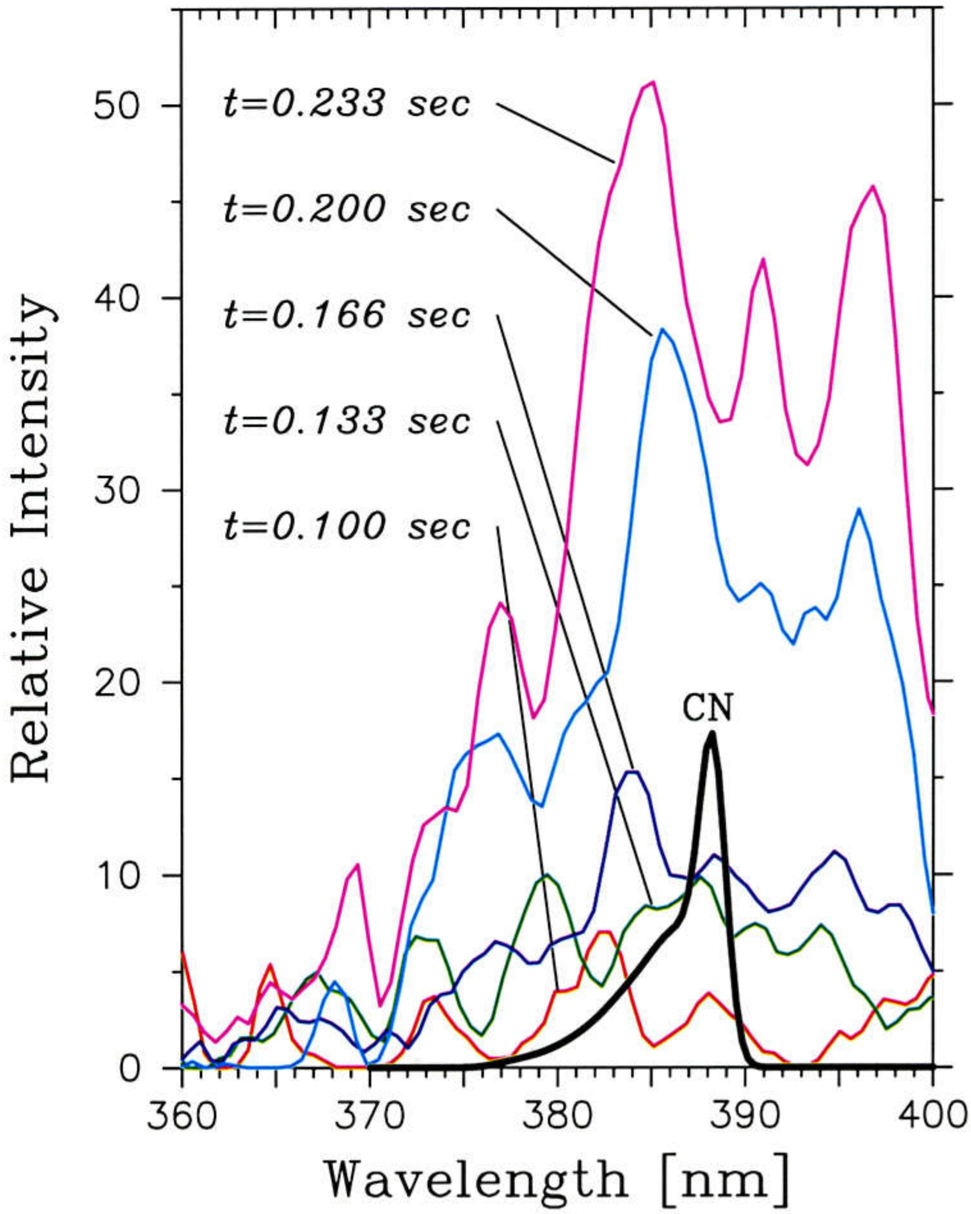

FIGURE 6.12. The 8:55:22 UT Leonid spectrum(Leo-18) in NUV with synthetic CN spectrum(T_e, v, r = 4,000K). The CN spectrum was calibrated by spectrum sensitivity of observational system, but the intensities is relatively.

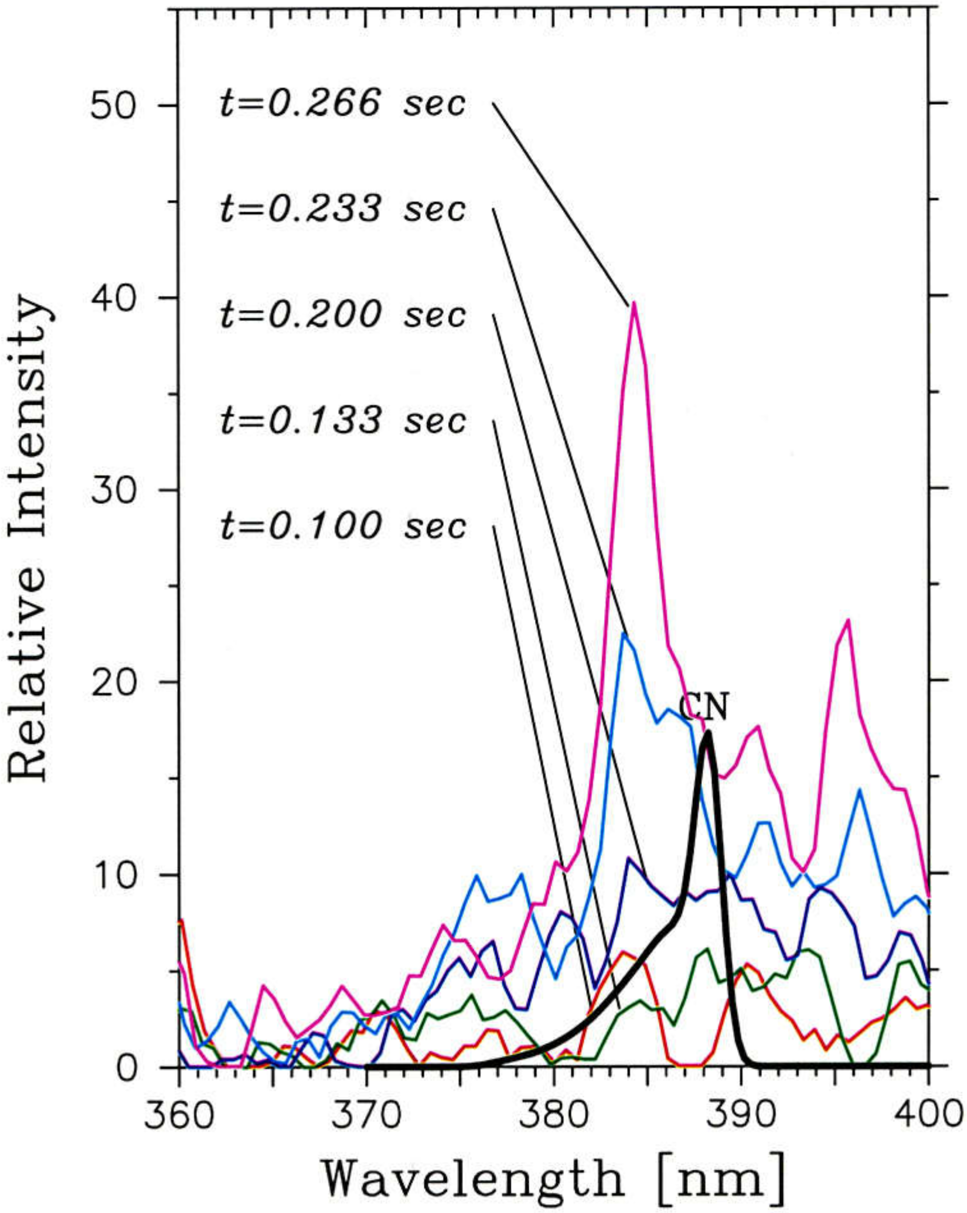

FIGURE 6.13. The 4:07:50 UT Leonid spectrum(Leo-10) in NUV with synthetic CN spectrum(T_e, v, r = 4,000K). The CN spectrum was calibrated by spectrum sensitivity of observational system, but the intensities is relatively.

6.3.2 Taurid and Comet 2P/Encke

Comets produce a lot of dust, and that dust is responsible for bright infrared emission. Cometary dust trail were first observed by the Infrared Astronomical Satellite (IRAS) (Skyes and Walker, 1991). 6.14 is a picture of comet 2P/Encke observed by the Infrared Space Observatory (ISO) using the mid-infrared camera (ISOCAM($3.6\mu m - 100\mu m$)) on July 14th, 1998(Fernndez et al., 2000). When the Earth passes through one of these "trails" we see a lot of large meteors entering the atmosphere. That is the "Taurid" meteor shower. Considering that the solid particles are even harder to get off of the comet than gas molecules, the comet must actually be composed of a solid rocky material, not just ice with a few dust particles. Fe/Mg abundance of Taurids is about 2 times higher than that of Leonids. It is possible to build up a hypotheses. Comet 2P/Encke is more rocky comet than comet 55P/Tempel–Tuttle. Observations of the nuclei of comet 2P/Encke showed that the active fraction of their nuclear surface was 0.44%, 13% for comet 1P/Halley(A'Hearn et al., 1995). Because comet 2P/Encke is gradually faint, comet 2P/Encke thought to be a extinct or dormant comet(known as Comet-Asteroid Transition(CAT) Objects) among the NEOs(Near Earth Objects; one of the asteroids), it seems rather improbable that any set of observations would capture an infrequent outburst. More interesting things is CN like structures which are seen in the spectrum of Taurid(Fig. 6.15). It needs further consideration of atomic emission lines(Fe, Mg and Ca^+) that contaminate the true CN band.

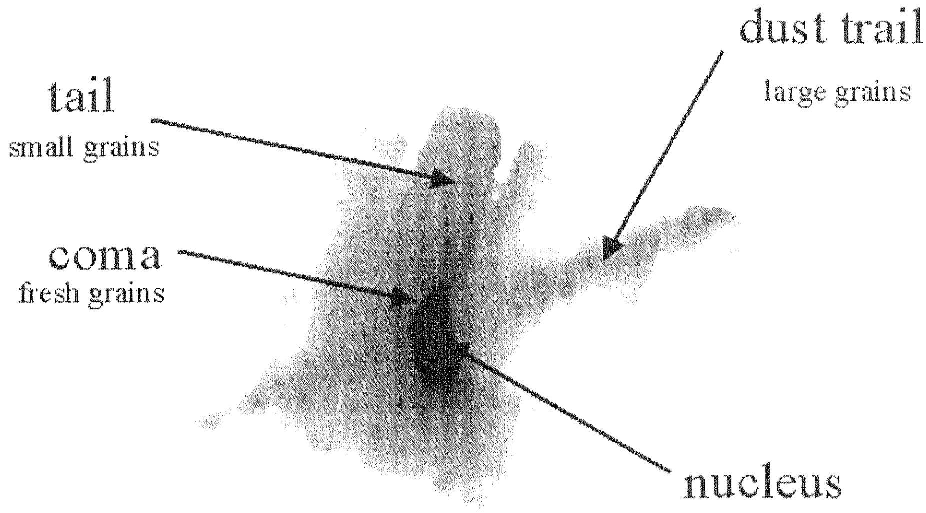

FIGURE 6.14. Cometary dust tail is well-known from the appearance of the comet in visible, which is due to very small dust particles $\sim mum$ and also emission from ices and vapors emitted by the comet. The large dust particles, called cometary dust trail, are source of meteor. Dust trails are different from cometary dust tail. Large particles are blown off of the comet relatively gently and then they slowly drift away. While, the small particles move more quickly away from the comet because of the radiation pressure from sunlight and the fast-moving cometary gas.

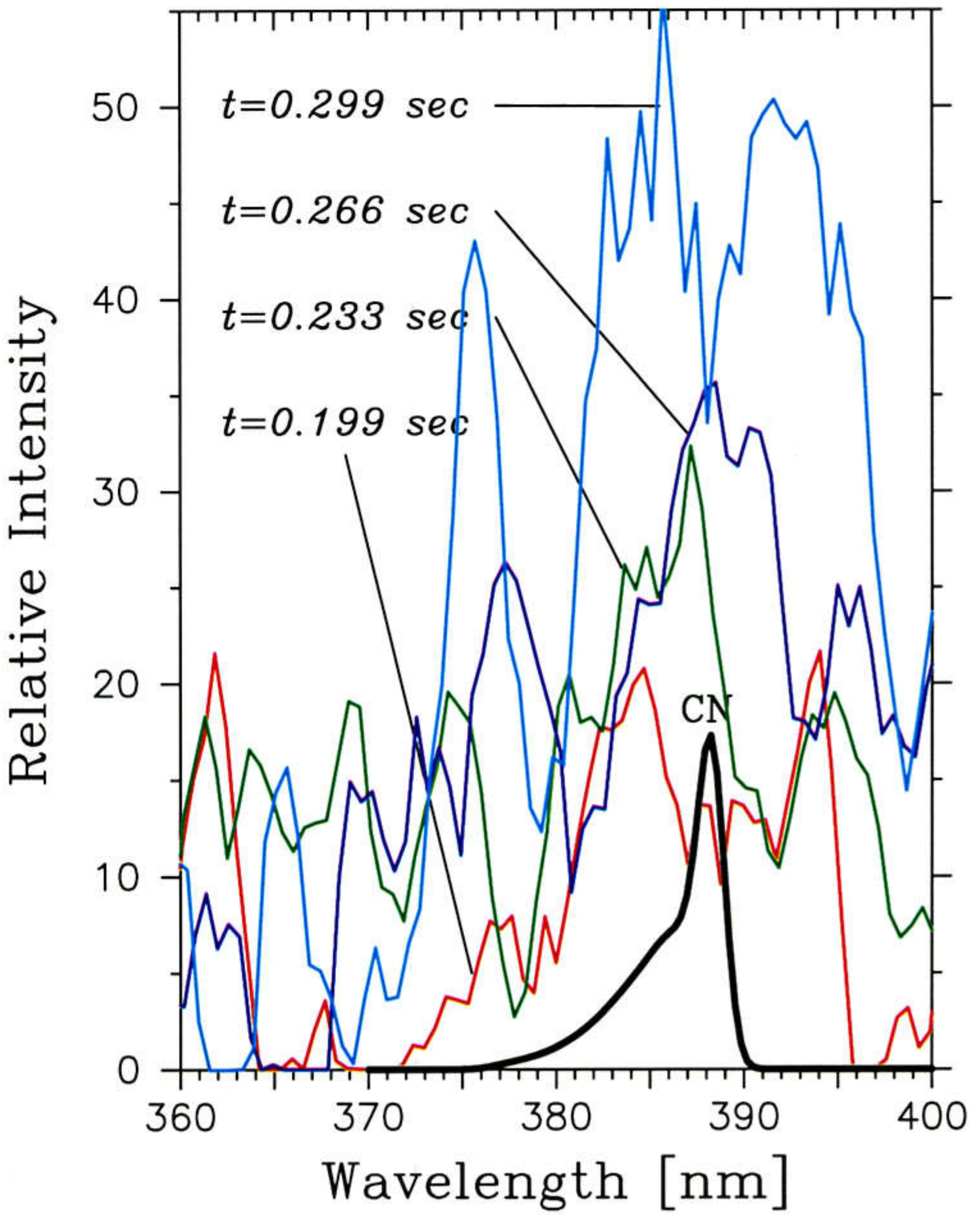

FIGURE 6.15. The 3:51:01 UT Taurid spectrum(Tau-02) in NUV with synthetic CN spectrum($T_e, v, r = 4,000K$). The CN spectrum was calibrated by spectrum sensitivity of observational system, but the intensities is relatively.

Part II

Spectroscopic Study of Persistent Trains

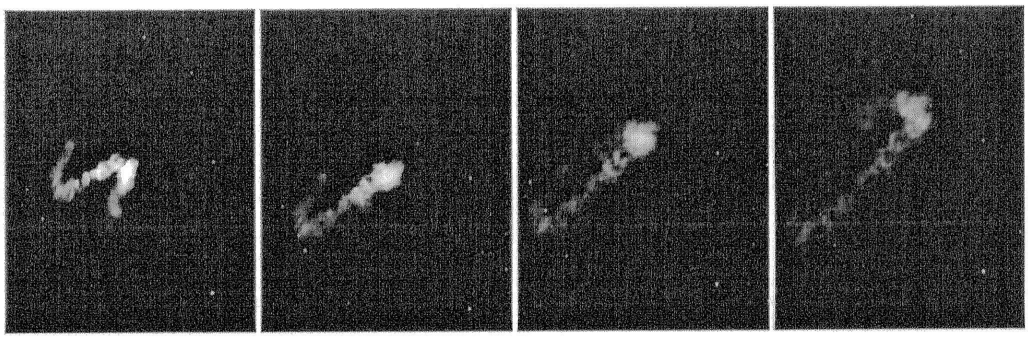

Chapter 7

INTRODUCTION - PERSISTENT TRAINS -

Meteor persistent trains are luminous clouds formed by meteors which persist long after the disappearance of mother meteor. It is considered that the clouds consist of a mixture of atoms and molecules ablated from the meteoroid itself as well as from the surrounding air. From color observations of meteor trains in early years, several emission lines are emitted from trains. While green lines are strong for Leonid meteors, Perseid meteors are more likely to be yellowish (Trowbridge, 1907). The best method to investigate these emitted line is spectroscopic observation. Meteor spectrography has been in existence since the end of 19th century. More than 1000 meteor spectra were observed and it has been known that the most common emission lines for Leonid meteors originate from Mg, Fe and Co, while less frequently seen are the emission lines of Na, Ca, and Mn (Nagawasa, 1978). It is evident that short time duration trains, called the wake, which last several seconds at the most, emit a forbidden line of $[OI]$ at 557.7 nm known as the aurora green line (Halliday, 1958; Millman, 1962). After a rapid decay in intensity, bright meteors often leave persistent trains that last several or several ten minutes. However, the physical processes of long-lived meteor trains are still not well known. The main reason is that spectroscopic observations of the persistent trains are not easy because of its rareness phenomena.

Recently, photographic spectra program of persistent trains at Banska Bystrica Observatory in Slovakia observed six spectra(Rajchl and Peresty, 1992) and four spectra of persistent trains have been observed in Japan during the 1993 Perseid maximum(Rajchl et al, 1995). All these spectra has shown two main emissions; multiplets of MgI at 518 nm and NaI at 589 nm. On the other hand prominent forbidden lines of ionized atoms, $[OII]$ at 372.6 nm, $[SII]$ at 406.9 nm and $[OIII]$ at 500.7 nm,

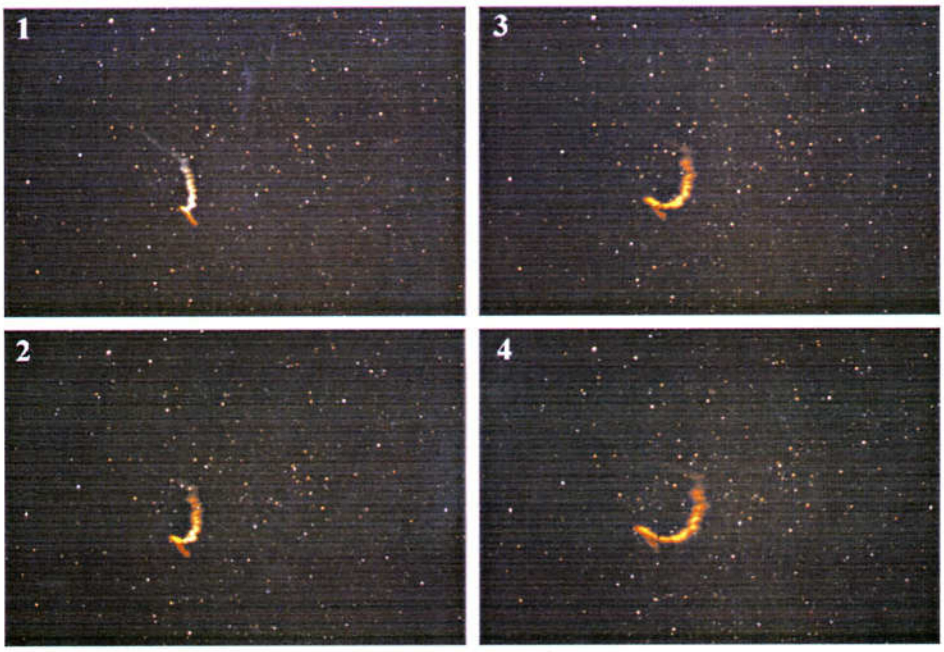

FIGURE 7.1. Persistent train's pictures on November 18, 1998. The photographs has been obtained by Mr. Kenich Watanabe at Usuda, Nagano prefecture near the spectroscopic observational station. Each exposure time is 10 seconds from (1)4:14:10, (2)4:14:25, (3)4:14:40 and (4)4:14:55.

which are known as gaseous nebular lines were identified in a train Borovička(1996). However, all these spectra have no conclusive evidence of emitters due to lack of the 0th order image and sufficient resolution. Although several spectroscopic observations have been made on persistent trains, little is known about the emission mechanism.

The Leonid meteors tend to leave long-lasting persistent trains because of the high entry velocity of the meteoroids, $\sim 71km/s$. Comet 55P/Tempel-Tuttle of which orbital period is 33 years passed perihelion on February 28, 1998. On the night of 17th - 18th November, 1998 when the earth crosses the outer regimes of the dust trail of comet Tempel-Tuttle, Leonid was expected to show a strong display(Yeomans, 1981; Jenniskens, 1996). Because the epoch of the nodal crossing correspond to about 20h UT on November 17 in 1998, many expeditions, including NASA's Leonid Multi-Instrument Aircraft Campaign(Leonid MAC), were performed in east Asia (Jenniskens and Butow, 1999). Leonid returns of 1998 and 1999 is a favorite opportunity to obtain spectra of persistent trains.

Chapter 8

OBSERVATIONS

The observations were carried out using a 35mm size photographic camera with a grating at 20km east from Nobeyama radio observatory(138°.47E, 36°.03N, H=1150m), Japan on November 17, 1998. The grism is a dispersing optical element, consisting of a transmission grating and a prism, is used for astronomical spectrograph(Ebizuka et al., 1998a, 1998b). The camera was used with a f=85mm F/1.2 lens and a panchromatic film Kodak TMAX400. The transmission grating made by BAUSCH & LOMB with 300 grooves/mm, blazed wavelength of 490 nm and blazed angle 14°.6 was equipped for a dispersing element. The resulting dispersion was 38.8 nm/mm in the 1st order. The effective spectral region 370 - 640 nm was covered. The 2nd order image is overlapped onto the position of the wavelength above 700 nm image of 1st order. In order to prevent from blending of the 1st and the 2nd order on the image, we used a filter L-37 of Kenko which cut off sharply below 350nm and transmissibility of 50% at 370 nm.

One Leonid of magnitude -8 appeared at 19h13m55s UT on November 17 and this meteor left the persistent train which was visible by naked eye for more than 15 minutes. Spectra of the persistent train were obtained by means of our spectroscopic system. The exposures started from 12 seconds after the mother meteor's disappearance. Every exposure time was 10 seconds at 2 seconds intervals. A series of spectra was obtained by automatically.

Many photographs and video images were possible to determine the mother meteor trajectories and a real height of the persistent train. The height of the appearance, maximum brightness and extinct points of the meteor are 177 km, 86 km and 78 km respectively. The distance between the observational point to the persistent train is

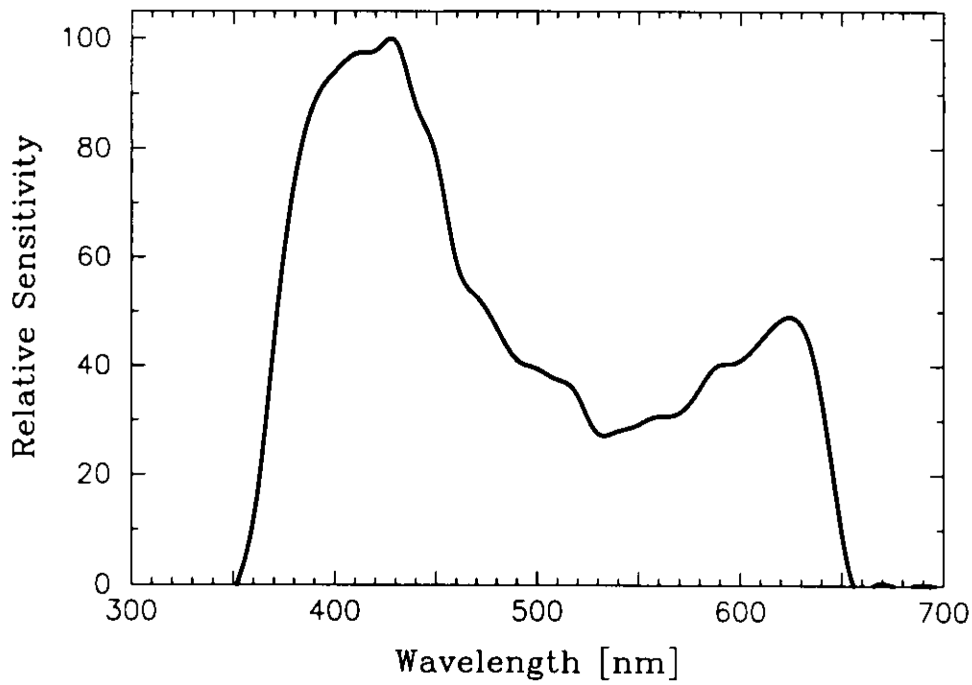

FIGURE 8.1. Relative spectral sensitivity of the observational system. The system is sensitive in the 370 - 640 nm range. The sensitivity curve is normalized to 100.0 at the peak wavelength, ~ 428 *nm*.

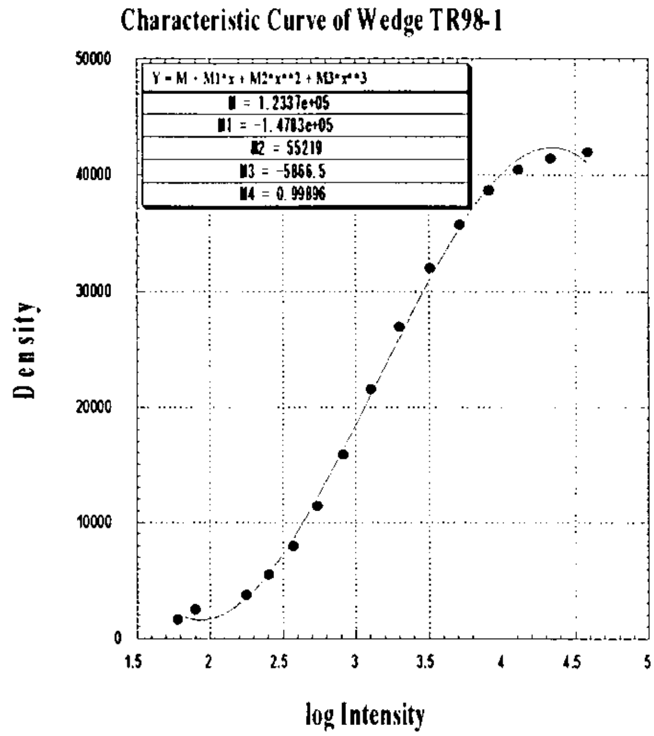

FIGURE 8.2. Characteristic curve of photographic plate obtained by photographic wedge. This curve used for reducing the reading of film density to the linear scale in magnitude for the persistent train spectrum No.1. - No.4.

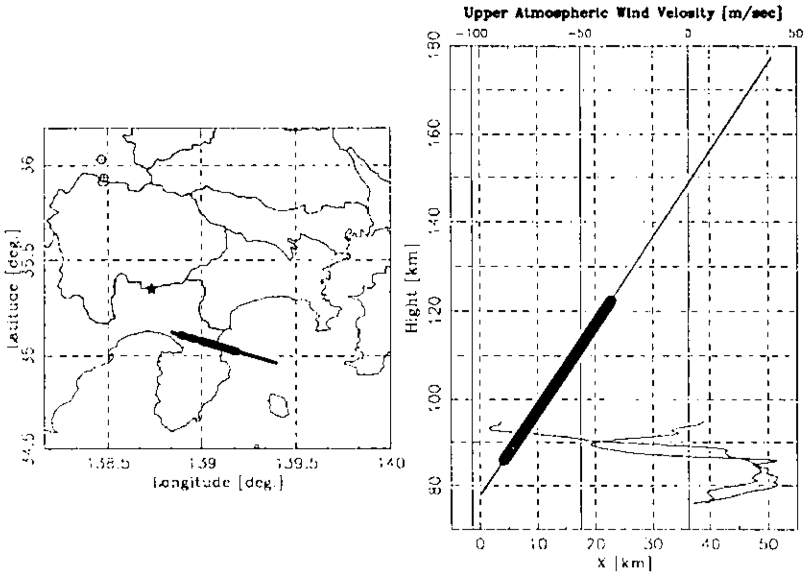

FIGURE 8.3. Meteor orbit on longitude-latitude plane(left) and EW-height plane(right).

about 140 km and the obtained spectra correspond to a part of the train at 86 km - 95 km height. At the moment, the upper atmospheric wind profile showed a large east-west wind maximum approaching $90m/s$ in magnitude at 87 km altitude, observed by MU radar observatory(136°.11E, 34°.85N), Radio Atmospheric Science Center, Kyoto University. Hence, the morphology of the persistent train changed rapidly with time. The train was also observed by a high-sensitivity color High-Definition TV(HD-TV) camera which was developed by NHK(Nippon Housou Kyoukai, Japan Broadcasting Corporation) (Sunasaki et al., 1997; Yamasaki et al., 1998). This color video images showed color variations and transformations of the train in the real time.

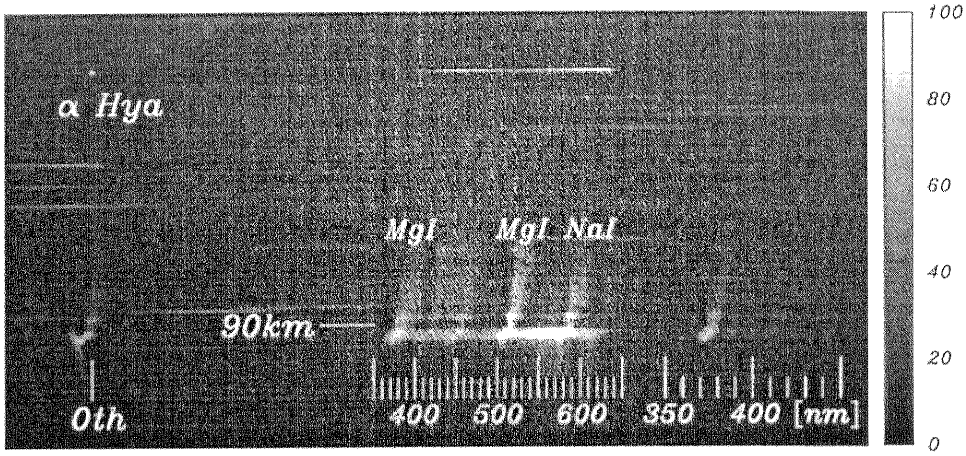

FIGURE 8.4. Spectrum of Persistent train No. 1. between 12-22 seconds after mother meteor's disappearance. The 0th order image is on the left part. The dispersion direction is from left to right. The 1st order spectra stand around the center and a part of the 2nd order spectra is on the right part. α *Hya* is above the spectra on the same frame.

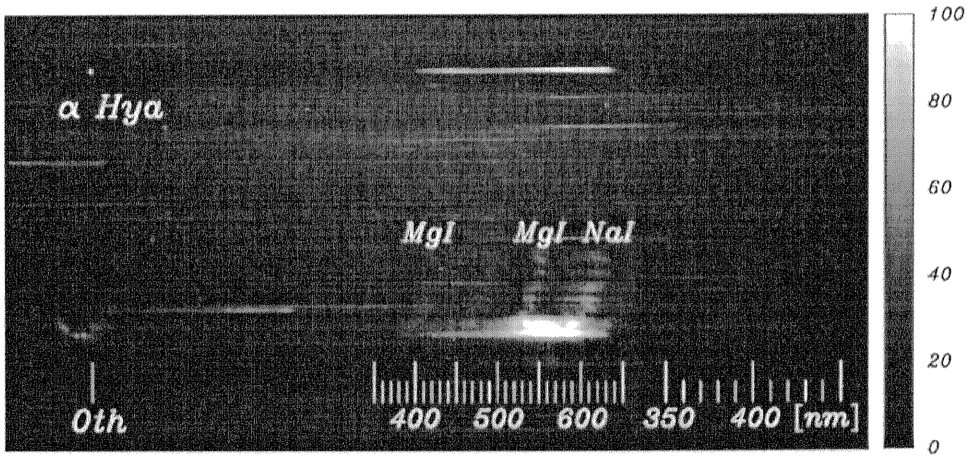

FIGURE 8.5. Spectrum of Persistent train No. 2. between 24-34 seconds after mother meteor's disappearance.

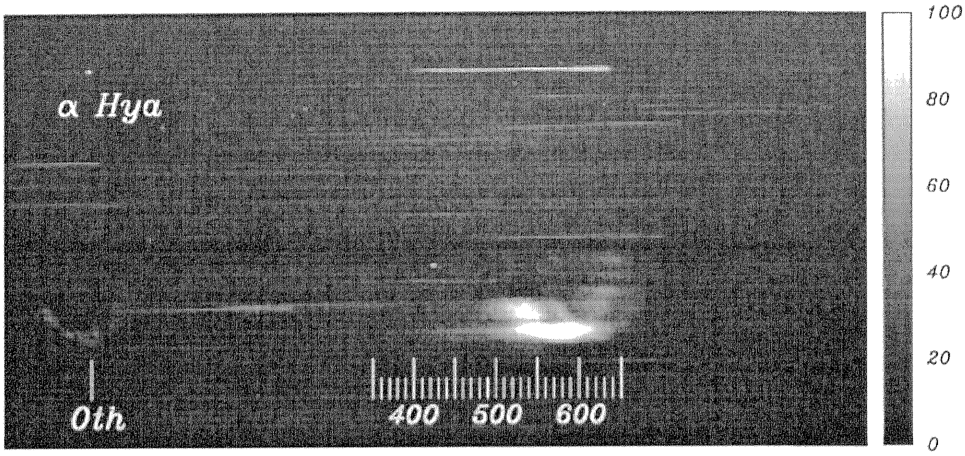

FIGURE 8.6. Spectrum of Persistent train No. 3. between 36-46 seconds after mother meteor's disappearance.

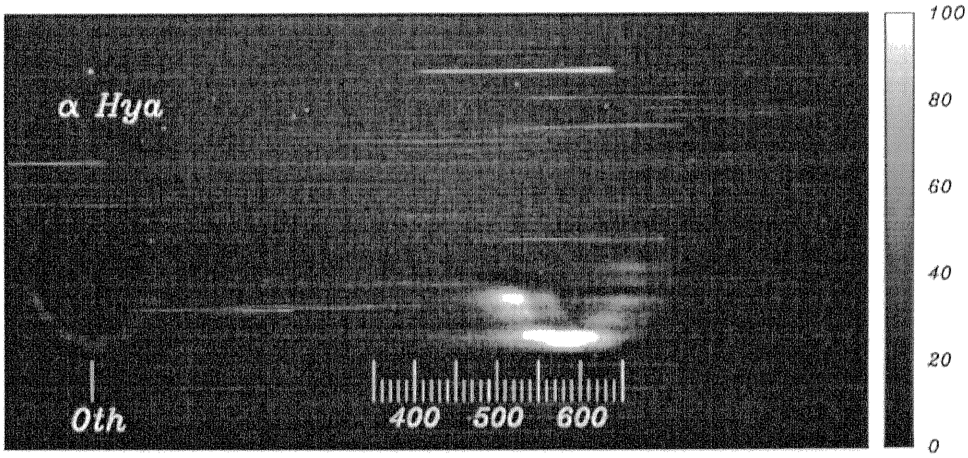

FIGURE 8.7. Spectrum of Persistent train No. 4. between 48-58 seconds after mother meteor's disappearance.

Chapter 9

Data Analysis and Results

9.1 Deconvolution and Sensitive Calibration

The photographs are digitized with 1024 intensity levels. To account for the background radiation and the systematic aberration, a polynomial function was fitted to a train-less field on the same frame. Dark frame subtracting and flat-fielding are applied to the digital images using the polynomial function. The digitized data of the persistent train is shown in Fig. 1. A bright star α-Hya(α=9h27.6m, $\delta = -8°40'$), m_v = 2.0 mag., K3II-III spectral type, was fortunately located within the same frames of the persistent train's spectra images. We used this star as a standard for calibration. The spectral sensitivity curve calibrated by the spectrum of α-Hya is shown in Fig. 2. The observational system is sensitive in the 370 - 640 nm range. The 0th order, the 1st order and a part of the 2nd order images were recorded. The wavelength of the spectra were measured with 0th order image. The image is not a point source but rather a diffused distribution caused by the motion of the train. The observed data was convoluted by atmospheric and instrumental effect, which deteriorate the true spectrum. The deconvolution method is applied to estimate a undisturbed spectrum under the ideal condition. After the deconvolution, the spectrum became sharp than the raw spectrum. This processing not only enhances the S/N of the data, but also measure the precise wavelength for each lines. The deconvolved spectrum was used for identifications.

9.2 Line Identifications

The results reported here are based on the detailed analysis of a high-quality spectrum at a height of 87 km. The spectrum data is consisted mainly with about 20 lines. It is difficult to identify many weak lines because thousands atomic lines exist in 370 - 640 nm wavelength region with hard blending. Most papers are concerned simply with the description of the spectra and the identification of lines without physical interpretation, Borovička(1993) studied meteor spectra taking into account physical conditions in detail.

9.2.1 Synthetic Spectral for Persistent Train

We made a synthetic persistent train's spectrum model compared with the observed spectrum, assuming that the persistent train is approximately in local thermodynamic equilibrium(LTE) for a short time scale. Namely, all radiating particles are assumed to have a Maxwellian velocity distribution characterized by a common temperature T. Because a train could be dealt in optically thin, the effect of self-absorption in the train can be neglected. In order to determine the radiative contribution of each atoms and the chemical composition of the persistent train, LTE is the most simple assumption. The free parameters of the model are the temperature T, the relative abundances of each atoms and the number density of total atoms N. Assuming the number density of total atoms N equal to the electron number density N_e, we obtain $N \sim 1.6 \times 10^{17} cm^{-1}$, using the relationship between the meteor magnitude M and N_e in the meteor trail, $M = 35.0 - 2.5 log N_e$(McKinley, 1961). The atoms of O, Na, Mg, Al, Si, Ca, Ti, Cr, Mn, Fe, Co and Ni are taken into account and more than 3000 lines are calculated. The initial abundances of neutral atoms start with the solar abundances(Anders, 1989) and the computations are performed by multidimensional minimization algorithms. The wavelength, radiative transitions and energy levels in atoms are taken from the NIST(National Institute of Standards and Technology) atomic spectra database(Martin et al., 1999). The most favorable conditions for meteor trains are around an altitude of 87 km. The results of line identifications of the persistent train at the 87 km show in Fig. 3. The identifications of all atomic

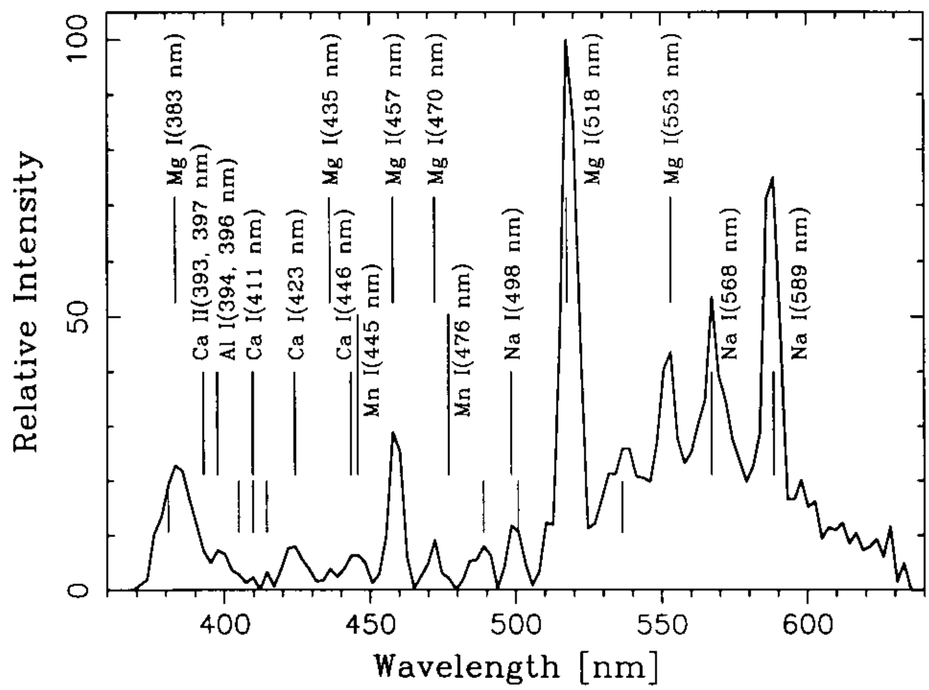

FIGURE 9.1. Identifications of spectra lines for the persistent train at the height of 87 km. The number of 22 emission lines were identified from the results. The each lines shows the identified point on the observed spectrum. Iron lines is indicated on the extreme down without the atomic name. The relative intensity is normalized to 100.0 at *MgI* 518 nm.

features are summarized in Table 10.1.

As the spectrum, which can be seen from Fig. 9.1 and Table 10.1, indicates the number of 22 emission lines were identified. The most significant lines are a series of *MgI* at 518 nm, 553 nm, 457 nm, 383nm, 470 nm and 435 nm, *NaI* at 589 nm, 568 nm and 498 nm in intense order and many other *FeI* lines. The abundances of Na, Al, Ca, Mn and Fe normalized by Mg were calculated, and the results is shown in table 2. On the other hand, O, Si, Ti, Cr, Co and Ni atoms were not identified in the persistent train.

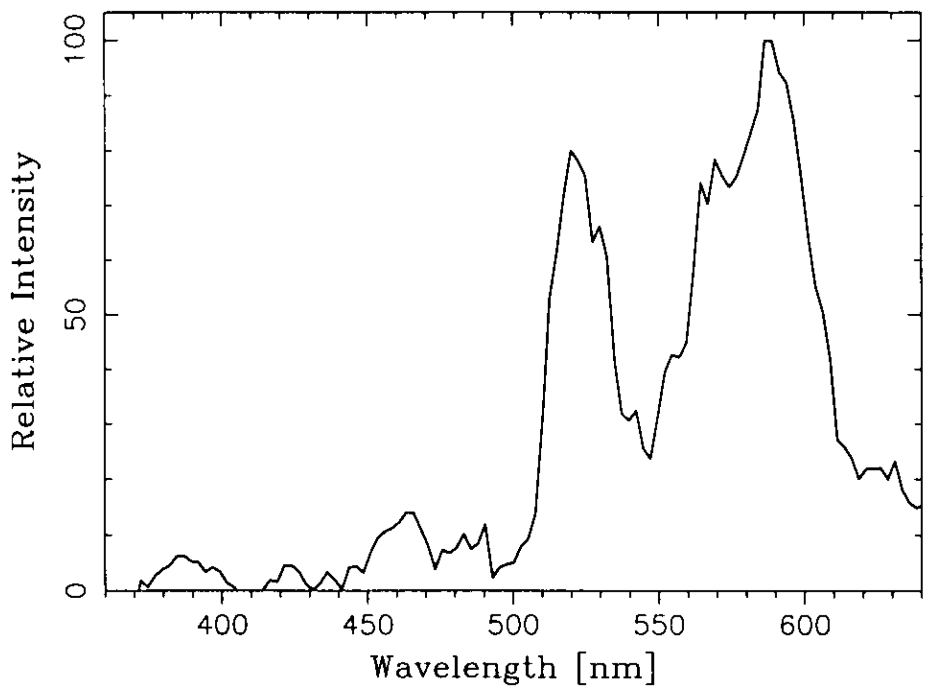

FIGURE 9.2. Identifications of spectra lines for the persistent train No. 2.

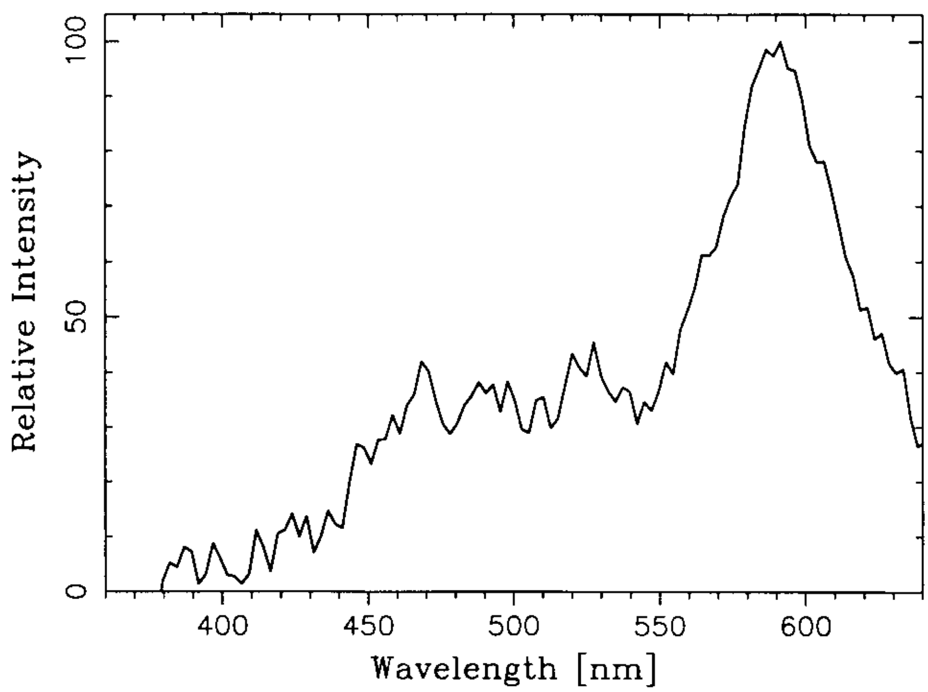

FIGURE 9.3. Identifications of spectra lines for the persistent train No. 3.

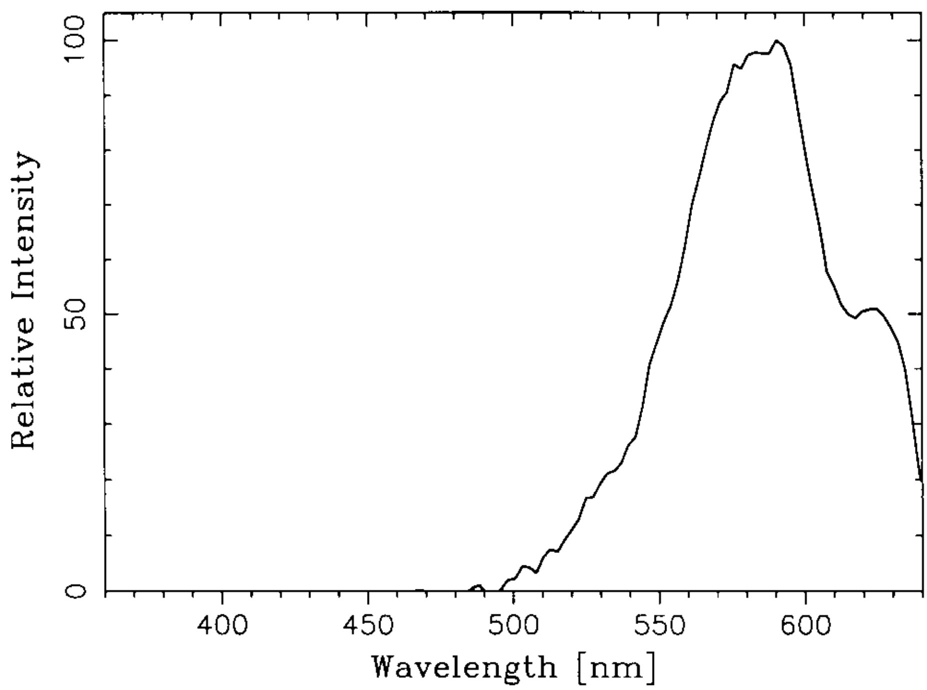

FIGURE 9.4. Identifications of spectra lines for the persistent train No. 4.

Chapter 10
Discussion

10.1 Excitation Temperature of Persistent Trains

The comparison between observational results and model spectrum are given in Fig. 10.1. The global emission feature of the persistent train is well reproduced with the appropriate atom of temperature $\sim 2200K$. It seems reasonable to suppose that the LTE model can apply to the observed spectrum of the persistent train because most of intense emission lines could be proved. Our model is very effective in identifying strong lines and in estimating physical parameters, such as temperatures and abundances in the persistent train. Let us now look at the differences between the observed and modeled spectrum in detail. The model spectrum does not fit the observational spectrum completely. It means that the model with LTE assumption is not a perfection in everything. The main reason is that the spectrum data was composed of 10 seconds integration, and the physical environment including temperature and density, should have changed with time. In addition to this, the train was blown away by the upper atmosphere wind at the rate of about 90 m/s at that time and the morphology of the train changed every second. In these case, the LTE is not appropriate, even though it seems reasonable to suppose that the LTE apply to the meteor spectrum(Borovîcka, 1993; Nagasawa, 1978). Non-equilibrium model is needed for persistent trains in the future.

10.2 Elemental Abundances of Persistent Trains

The abundances in the persistent train tell us that Magnesium and Iron are the the most dominant and Sodium is the next rich atoms(Table 10.1). Moreover, the ob-

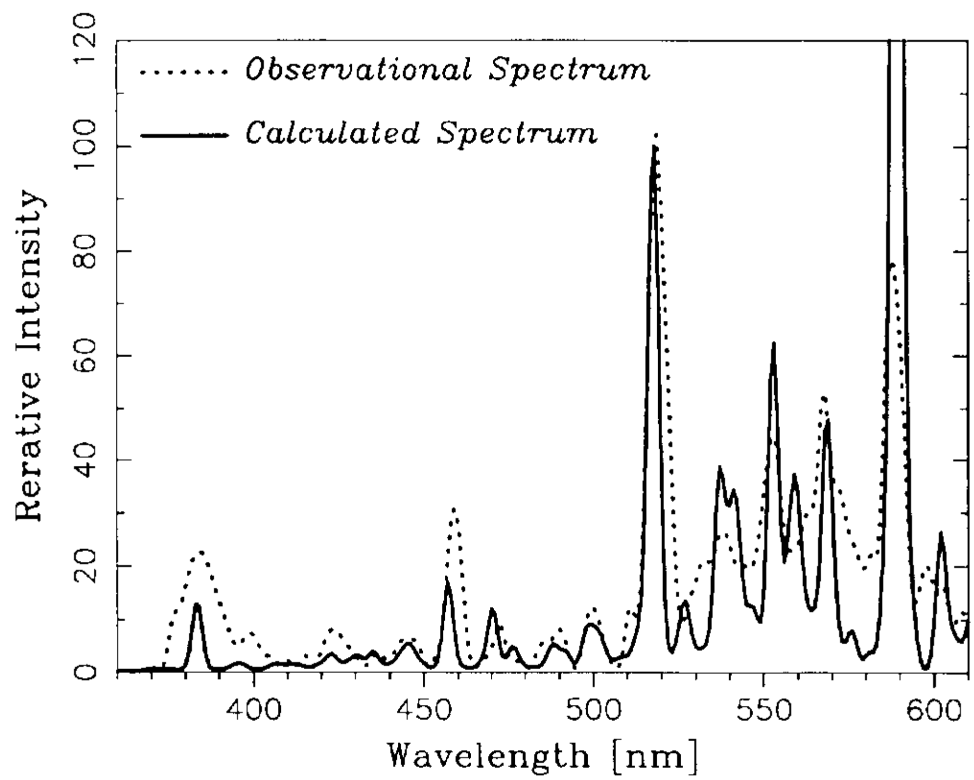

FIGURE 10.1. Comparison between the calculated model spectrum and observed spectrum. The dotted line represents the observational spectrum, while the thick line shows the spectrum of model calculation. Both spectra have been normalized to 100.0 at *MgI* 518 nm.

served spectrum's enhancement of the background in 500 - 600 nm wavelength seems to be a large number of FeI lines. The enhancement of Mg, Fe and Na atoms considerable evidence to show that these atoms are the source of the persistent trains and have a strong relationship with long-lived emitters. The 1998 Leonid persistent train's observations carried out with SOR, the Air Force Research Laboratory Starfire Optical Range, New Mexico in US, also suggested the enhancement of Na atoms (Chu et al., 2000). Enhancements of Mg, Fe and Na atoms may account for chemiluminescence in the train.

10.3 Emission Processes of Persistent Train

Emissions from meteor can be classified under three physical phases;

1. The emission from the mother meteor; $\mu \sim mm\ sec.$

   The central mass along the meteor trail cools very rapidly mainly due to emission of hard UV radiation, leading to extensive dissociation and ionization of the surrounding air. The fireball temperatures were found to be about 4000 K in the main spectrum and 10,000 K in the second spectrum respectively(Borovička, 1994). This main radiative phase lasts for $\mu \sim mm$ seconds order.

2. The emission from the short-time duration train, called wake; $1 \sim 10sec.$

   The emissions form short-time duration trains have been identified with the radiation of the forbidden line of neutral oxygen at 557.7nm, which was excited by the shock region along the meteor trail. This secondary radiative phase lasts up to about 10 seconds. The video images of the train in series, obtained by NHK color HD-TV, indicated the existence of the strong bluish green emission at the highest point of the train during the first several seconds.

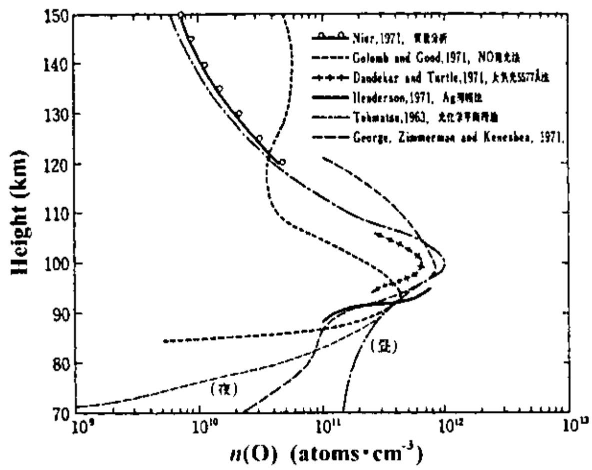

FIGURE 10.2. Earthly O density profile.

3. The emission from the long-lived train, called persistent train; $10sec. <$

The persistent train radiates for a long time, $10sec. \sim 1hour$. After the disappearance of the bluish green emission, the upper region decayed rapidly and the lower region of the train lived for a long time with a orange color, which was observed by NHK color HD-TV. The temperature is expected to have gone down steeply. However, the high temperature was kept in our results against the expectation.

Chapman(1939,1959) and Baggaley(1975,1976) suggested that an oxidation-reduction cycle may excite meteoric neutral atoms and provide a long-lasting meteor train.

$$O_3 + M \longrightarrow MO^* + O_2,$$
$$MO^* \longrightarrow MO + h\nu \ (band\ emission),$$
$$MO + O \longrightarrow M + O_2.$$

The atmospheric sodium nightglow and luminescence of meteor trails, both of which occur at mesospheric altitudes of 85 - 95 km, are emitted by sodium atoms.

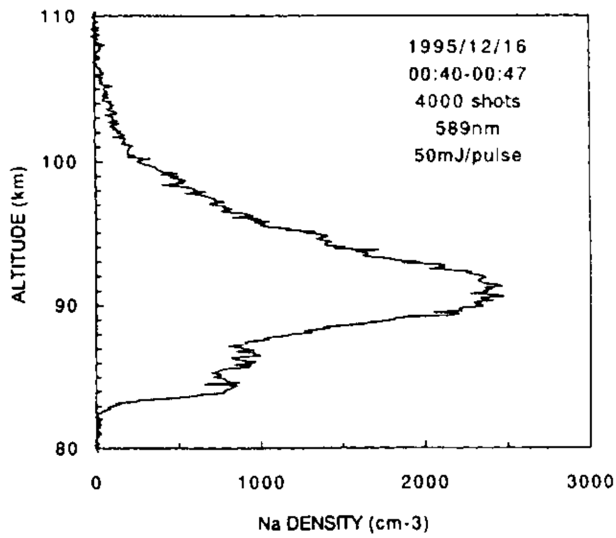

FIGURE 10.3. Earthly Na density profile at the height of 90km.

The sodium layer is believed to result naturally from meteors ablation(Richter and Sechrist, 1979). Meteoric metal atoms M, such as Mg, Fe and Na, combine with O_3 molecules and change into excited monoxides, MgO^*, FeO^* and NaO^*, which radiate band emissions. The most likely explanation is that the enhanced abundances of neutral atoms of Mg, Fe and Na in the train are the source of the excited monoxides and they radiate for a long time as MgO, FeO and NaO. However, we deal with only atoms in this study. The expected band emission from the excited monoxides should be taken into account in the future study. Much still remains to be done.

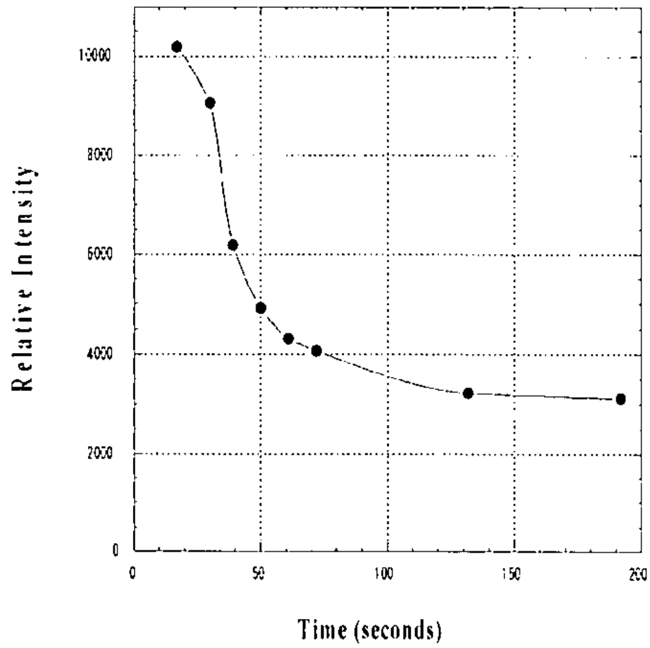

FIGURE 10.4. Luminosity decay curve of persistent train.

TABLE 10.1. Line Identifications of Persistent Train*

Observed Feature		Identified Lines						
λ nm	Intensity 100 × Int./(518nm)	Atom	λ nm	A_{21}[2] $10^8 s^{-1}$	B_{12}[8]	E_1[3] cm^{-1}	E_2[9] cm^{-1}	Terms of lower and upper levels
381	19.2	Fe I	381.58	0.13E+01	0.22E+00	11976.234	38175.350	3F-3D*
		Fe I	(378-387)					
383	22.7	Mg I	382.93	0.94E+00	0.62E+00	21850.405	47957.058	3P*-3D
		Mg I	383.23	0.13E+01	0.47E+00	21870.464	47957.027	3P*-3D
		Mg I	383.82	0.47E-01	0.62E-02	21911.178	47957.058	3P*-3D
		Mg I	(382-383)					
393	7.1	Ca II	393.36	0.15E+01	0.68E+00	0.000	25414.400	2S-2P*
		Al I	394.40	0.49E+00	0.12E+00	0.000	25347.756	2P*-2S
398	7.2	Al I	396.15	0.98E+00	0.12E+00	112.061	25347.756	2P*-2S
		Ca II	396.84	0.14E+01	0.33E+00	0.000	25191.510	2S-2P*
405	2.8	Fe I	406.35	0.68E+00	0.17E+00	12560.930	37162.740	3F-3F*
		Fe I	407.17	0.77E+00	0.19E+00	12968.549	37521.157	3F-3F*
410	2.3	Ca I	410.85	0.90E+00	0.32E+00	21849.634	46182.399	1D-1F*
		Fe I	411.85	0.58E+00	0.17E+00	28819.946	53093.521	1H-1I*
415	3.3	Fe I	418.17	0.36E+00	0.13E+00	22838.318	46744.988	3P-5D*
424	8.0	Ca I	422.67	0.22E+01	0.18E+01	0.000	23652.304	1S-1P*
		(Ca I	430.25	0.14E+01	0.38E+00	15315.943	38551.558	3P*-3P)
		Ca I	(422-431)					
436	3.9	Mg I	435.19	0.21E+00	0.99E-01	35051.264	58023.246	1P*-1D
443	6.2	Ca I	445.47	0.87E+00	0.36E+00	15315.943	37757.449	3P*-3D
		Ca I	(442-445)					
446	6.4	Mn I	445.15	0.80E+00	0.24E+00	23296.670	45754.270	4D-4D*
		Mn I	(440-450)					
458	28.9	Mg I	457.10	0.43E-05	0.40E+00	0.000	21870.464	1S-3P*
472	9.1	Mg I	470.29	0.26E+00	0.14E+00	35051.264	56308.381	1P*-1D
477	2.1	Mn I	476.15	0.54E+00	0.36E+00	23818.870	44814.730	4D-4F*
		Mn I	(470-482)					
489	8.0	Fe I	487.13	0.22E+00	0.56E-01	23110.937	43633.534	7F*-7D
		Fe I	487.21	0.24E+00	0.85E-01	23244.834	43763.980	7F*-7D
		Fe I	489.07	0.21E+00	0.75E-01	23192.497	43633.534	7F*-7D
		Fe I	489.14	0.29E+00	0.81E-01	22996.676	43434.629	7F*-7D
		Fe I	492.05	0.35E+00	0.10E+00	22845.868	43163.327	7F*-7D
		Fe I	(480-493)					
498	11.7	Na I	497.85	0.41E-01	0.30E-01	16956.172	37036.774	2P*-2D
		Na I	498.28	0.82E-02	0.31E-02	16973.368	37036.774	2P*-2D
		Na I	498.28	0.49E-01	0.27E-01	16973.368	37036.754	2P*-2D
501	10.6	Fe I	501.49	0.30E+00	0.81E-01	31805.067	51739.920	3F*-3D
		Fe I	(496-505)					
518	100.0	Mg I	516.73	0.12E+00	0.14E+00	21850.405	41197.403	3P*-3S
		Mg I	517.26	0.35E+00	0.14E+00	21870.464	41197.403	3P*-3S
		Mg I	518.36	0.57E+00	0.14E+00	21911.178	41197.403	3P*-3S
537	25.9	Fe I	536.48	0.55E+00	0.33E+00	35856.400	54491.040	5G*-5H
		Fe I	536.74	0.58E+00	0.32E+00	35611.619	54237.160	5G*-5H
		Fe I	536.99	0.47E+00	0.25E+00	35257.319	53874.260	5G*-5H
553	43.6	Mg I	552.84	0.20E+00	0.15E+00	35051.264	53134.642	1P*-1D
567	53.5	Na I	568.26	0.10E+00	0.10E+00	16956.172	34548.766	2P*-2D
		Na I	568.81	0.21E-01	0.10E-01	16973.368	34548.766	2P*-2D
		Na I	568.82	0.12E+00	0.87E-01	16973.368	34548.731	2P*-2D
589	75.0	Na I	588.99	0.62E+00	0.65E+00	0.000	16973.368	2S-2P*
		Na I	589.59	0.62E+00	0.32E+00	0.000	16956.172	2S-2P*

*Atomic parameters refer the atomic spectra database of NIST(National Institute of Standards and Technology).

[2]Einstein A-coefficient for spontaneous emission.

[8]Einstein B-coefficient for stimulated emission.

[3]Transition energy of upper level.

[9]Transition energy of lower level.

TABLE 10.2. Relative abundances of elements, in persistent train, meteors, and the Sun*

	Na	Fe	Al	Ca	Mn
Persistent train	0.45	0.99	0.24	0.09	0.08
Meteor 1A [1]	$4.0 \cdot 10^{-4}$	0.09	–	$8.5 \cdot 10^{-5}$	–
Meteor 1B [2]	$1.4 \cdot 10^{-9}$	0.28	–	$2.2 \cdot 10^{-4}$	–
Meteor 2A [3]	0.075	1.00	0.0025	0.008	0.012
Meteor 2B [4]	0.025	1.67	$3.3 \cdot 10^{-4}$	$1.6 \cdot 10^{-3}$	0.003
Sun and CI Chondrites [5]	0.068	0.97	0.10	0.070	0.011

$mass/Mg$

[1]Nagasawa(1978), spectrum No. 56.

[2]Nagasawa(1978), spectrum No. 59.

[3]Borovička(1993), spectrum EN151068 at maximum value.

[4]Borovička(1993), spectrum EN151068 at minimum value.

[5]Anders(1989).

Part III

Summary & Future

Chapter 11

Summary of Meteors and Persistent Train and Future Works

11.1 First Results of High-Definition TV Spectroscopic Observations of Meteors

The large pixel format of the HDTV camera makes it a very suitable instrument for time-resolved slit-less spectroscopy of meteors. The large number of resolution elements helps to resolve lines in the meteor spectrum and still be able to compare spectral line intensities at wavelength far apart. In addition, the large dynamic range improves the measurement of the line intensity ratios for lines that are much different in intensity. In the near future, we expect to have our own system for digitization of the HDTV images, which will make a more comprehensive analysis of the present data set possible. Also, we plan to make a new HDTV-II spectroscopic instruments with UV sensitivity for Leonid 2001 and 2002.

11.2 First Results of Physical Treatment of N_2 First Positive Band in the Meteor Spectra

The radiation strength of meteor, LTE has been measured for temperature of $4,500 \pm 300K$ using many atomic irons in short wavelength range, 400 - 550 nm. This measurements have been compared to the N_2 first positive band's temperature(electronic-vibrational temperature) of $4,500 \pm 500K$ in long wavelength 550 - 800 nm. It seems that meteor spectra can be explained well by LTE model. However, there are differences between the vibrational temperature of $T_{e,v} = 4,500K \pm 300K$ and estimated the rotational temperature of $T_r = 2,500K \pm 500K$. It means that meteor spectra are not completely explained by thermal equilibrium in detail. It needs more spectral resolution power in observations to explain the spectra precisely.

11.3 Ablation and Chemical Properties of Meteors

In the Leonid meteors, Fe and Mg follow a similar ablation profile than atmospheric O emission. However, the Na emission is depleted significantly earlier than the other metal atom emissions. This effect was earlier observed for the 1998 Leonid meteors, and is now confirmed for the 1999 Leonids.

A comparison of Leonid with Taurid meteors showed that for NaI/MgI abundances at high altitude(firster stage), Leonid meteors are more abundant than Taurid meteor. This can be explained 1) by their lower velocity - $71km/s$ for Leonid, and $28km/s$ for Taurid meteors, or 2) by volatile Na is lost from a thin surface layer of meteoroids when they are orbiting Sun.

11.4 First Results of Air-to-Air Stereoscopic Observations of Meteors

We operated "Air-to-Air stereoscopic observations" from two aircrafts for the purpose of calculating the real height of various emission phenomena. The operation have been accomplished. The spectroscopic Leonids meteor(Leo-18) emitted from 119.6 km to 98.5 km height with accuracy of $\sim \pm 3.0km$.

11.5 Organic Compounds(CN) from Comet?

Cometary organic carbon was mixed intimately with the silicate component and most of it is expected to survive exposure to the vacuum of space. When these meteoroids encounter the Earth's atmosphere, the organic carbon is ablated. In cometary coma, CN radical is the most easily detected because of a strong $B \longrightarrow X$ transition of low energy potential. We searched for CN violet($B^2\Sigma^+ \longrightarrow X^2\Sigma^+$) at 388.3 nm in the cometary meteoroids, meteors. CN like structures which are seen in the spectrum of

Taurid. It needs further consideration of atomic emission lines(Fe, Mg and Ca^+) that contaminate the true CN band.

11.6 Elements of Persistent Trains

The abundances in the persistent train tell us that Mg and Fe are the the most dominant and Na is the next rich atoms(Table 10.1). Enhancements of Mg, Fe and Na atoms may account for chemiluminescence in the train.

11.7 Excitation Temperature in the Persistent Train

The global emission feature of the persistent train is well reproduced with the appropriate atom of temperature $\sim 2200K$ at the time of $\sim 20sec$ after the meteor's disappearance, $\sim 1000K$ at the time of $\sim 30sec$. It seems that cooling time is more rapid than luminosity decay time. It approves of the chemiluminescence mechanism, that is to say, thermal energy has nothing to do with the source of luminosity.

11.8 Persistent Mechanism

The most likely explanation is that the enhanced abundances of neutral atoms of Mg, Fe and Na in the train are the source of the excited monoxides and they radiate for a long time as MgO, FeO and NaO. However, we deal with only atoms in this study. The expected band emission from the excited monoxides should be taken into account in the future study. The physical and chemical properties of the persistent train which depends on the chemical reactions and elapsed time will be appeared in the future.

BIBLIOGRAPHY

[1] A'Hearn, M. F., Millis, R. L., Schleicher, D. G., Osip, D. J., and Birch, P. V.(1995) The ensemble properties of comets: Results from narrow band photometry of 85 comets. *ICARUS*, **118**, 223-270.

[2] Anders E. and Grevesse, N.(1989) Abundances of the elements - Meteoritic and solar. *Geochim. Cosmochim. Acta*, **53**, 197-214.

[3] Arlt, R., Rubio, L. B., Brown, P., and Gyssens, M.(1999) Bulletin 15 of the International Leonid Watch: First Global Analysis of the 1999 Leonid Storm. *WGN, the Journal of IMO*, **27(6)**, 286-295.

[4] Atkins, P. W.(1990) *Physical Chemistry Forth Edition.* Oxford Univ..

[5] Baggaley W. J.(1975) The role of the oxides of meteoric species as a source of meteor train luminosity. *Mon. Not. R. Astron. Soc.*, **173**, 497-512.

[6] Baggaley W. J.(1976) Meteor trains and chemiluminescent processes. *Mon. Not. R. Astron. Soc.*, **174**, 617-620.

[7] Bauschlicher, C. W., and Langhoff, S. R.(1988) Theoritical study of the dissociation energy and the red and violet band system of CN. *Astrophys. J.*, **332**, 531-538.

[8] Borovička, J. and Bocek J.(1993) A fireball spectrum analysis. *Astron. Astrophys.*, **279**, 627-645.

[9] Borovička J.(1994) Two components in meteor spectra. *Planet. Space Sci.*, **42**, 145-150.

[10] Borovička, J.(1995) Television spectra of meteors. *Earth, Moon, and Planets*, **71**, 237-244.

[11] Borovička J., Zimnikoval P., Skvarka J., Rajchl J. and Spurny, P.(1996) The identification of nebular lines in the spectra of meteor trains. *Astron. Astrophys.*, **306**, 995-998.

[12] Borovička, J., Stork, R., and Bocek J.(1999) First results from video spectroscopy of 1998 Leonid meteors. *Meteoritics & Planetary Sci.*, **34**, 987-994.

[13] Bronshten, V. A. (Eds.)(1981) *Physics of Meteoric Phenomena*, 139-235, D. Reidel Publishing Company, Dordrecht, Holland.

[14] Caceci, M. S., and Cacheris, W. P.(1984) *Byte*, **340**.

[15] Chapman S.(1939) Nots on atmospheric sodium. *Astrophys. J.*, **90**, 309-316.

[16] Chapman S.(1959) *J. Geophys. Res.*, **64**, 2064-2065.

[17] Chu X., Liu A. Z., Papen G., Gardner C. S. Kelley, M., Drummond, J., Fugate, R.(2000) Lidar Observations of Elevated Temperatures in Bright Chemiluminescent Meteor Trails During the 1998 Leonid Shower. *Geophys. Res. Lett.*, **27(13)**, 1815.

[18] Ebizuka N., Iye M. and Sasaki T.(1998) Optically anisotropic crystalline grisms for astronomical spectrographs. *Appl. Opt.*, **37**, 1236-1242.

[19] Ebizuka N., Iye M., Sasaki T. and Wakaki M.(1998) Development of high dispersion grism and immersion gratings for spectrographs of Subaru telescope. *SPIE Conf. on Opt. Astron. Instrum.*, **3355**, 409-416.

[20] Fernndez, Y. R., Lisse, C. M., Ulrich K. H., Peschke, S. B., Weaver, H. A., A'Hearn, Michael F., Lamy, P. P., Livengood, T. A., Kostiuk, T.(2000) Physical Properties of the Nucleus of Comet 2P/Encke *Icarus*, **147(1)**, 145-160.

[21] Fujita, K., and Abe, T.(1997) SPRADIAN, Structured Package for Radiation Analysis: Theory and Application. *The Institute of Space and Astronautical Science Report*, **669**.

Halliday, I.(1958) Forbidden line of O I observed in meteor spectra. *ApJ*, **128**, 441-443.

[22] Gilmore, F. R., Laher, R. R., and Espy, P. J.(1992) Frank-Condon Factors, r-Centroids, Electronic Transition Moments, and Einstein Coefficients for Many Nitrogen and Oxygen Band System. *J. Phys. Chem. Ref. Data*, **21(5)**, 1005-1107.

[23] Greenberg, J. M.(2000) From Comets to Meteors *Earth, Moon and Planets*, **82-83**, 313-324.

[24] Grün, E., and Jessberger, E. K.(1990) Dust. *In Physics and Chemistry of Comets*(ed. W. F. Huebner), 113-176, Springer-Verlag, Heidelberg, Germany.

[25] Herzberg, G.(1950) *Molecular Spectra and Molecular Structure, Volume I - Spectra of Diatomic Molecules* Krieger, Publishing Company, Florida.

[26] Irwin, A. W.(1981) *ApJS*, **45**, 621.

[27] Ito, H., Ozaki, Y., Suzuki, K., Kondow, T., and Kuchitsu, K.(1991) Electronic transition moment for the B-X emission of CN. Analysis of dependence on the internuclear distance. *J. Chem. Phys.*, **94**, 5353.

[28] Halliday I.(1958) Forbidden line of O I observed in meteor spectra. *Astrophys. J.*, **128**, 441-443.

[29] Jenniskens P.(1996) Meteor stream activity. III. Measurement of the first in a new series of Leonid outburst. *Meteorit. Planet. Sci.*, **31**, 177-184.

[30] Jenniskens, P. and Butow, S. J.(1999) The 1998 Leonid multi-instrument aircraft campaign - an early review. *Meteoritics & Planetary Sci.*, **34**, 933-943.

[31] Jenniskens, P., Butow, S.J., Fonda, M.(2000a) The 1999 Leonid Multi-Instrument Aircraft Campaign - an early review. *Earth, Moon and Planets*, **82-83**, 1-26.

[32] Jenniskens, P., Crawford, C., Butow, S.J., Koop, M., Holman, D., Houston, J., Jobse, K., Kronk, G., Beatty, K., Nugent, D.(2000b) New hybrid visual and video meteor counting technique reveals Lorentz shaped comet dust trail cross section - implications for future Leonid storm encounters. *Earth, Moon and Planets*, **82-83**, 191-208.

[33] Jenniskens, P., Packan, D., Laux, C., Wilson, M., Boyd, I. D., Kruger,C. H., Popova, O., and Fonda, M.(2000c) Meteors: A Delivery Mechanism of Organic Matter to the Early Earth. *Earth, Moon and Planets*, **82-83**, 57-70.

[34] Jessberger, E. K., Christoforidis, A., Kissel, J.(1998) Aspects of the major element composition of Halley's dust *Nature*, **332**, 691-695.

[35] Kissel, J., and, Krueger, F. R.(1987) The Organic Component in Dust from Comet Halley as Measured by the PUMA Mass Spectrometer on Board VEGA 1. *Nature*, **326**, 755-760.

[36] Laux, C. O.(1993) Optical Diagnostics and Radiative Emission of Air Plasmas. *PhD thesis*, Stanford University.

[37] Martin W. C., Sugar J., Musgrove A., Wiese W. L. and Fuhr J. R.(1999) The NIST Atomic Spectra Database. *The National Institute of Standards and Technology (NIST)*

[38] McKinley D. W. R.(1961) Meteor Science and Engineering. McGraw-Hill, New York, USA.

[39] Millman, P.M.(1962) Photographic Meteor Spectra. *J. RAS. Canada*, **56**, 263-267.

[40] Millman, P.E., Cook A.F., and Hemenway C.L.(1971) Spectroscopy of Perseid meteors with an image orthicon. *Canadian J.Phys.*, **49**, 1365-1373.

[41] A multiplet table of astrophysical interest.(1945) *Contr. Princeton Univ. Obs.*, **20**, 146

[42] Mumma, M., J., Weissmann, P., R., and Stern, S., A.(1993) Comets and the origin of the solar system-Reading the Rosetta Stone. *Protostars and Planets III*(eds, Levy, E. H., and Lunine, J.,I.), 1177-1252, Univ. Arizona Press, Tucson, Arizona, USA.

[43] Murray, I.S., Beech, M., Taylor, M.J., Jenniskens, P., Hawkes, R.L.(2000) Comparisson of 1998 and 1999 Leonid light curve morphology and meteoroid structure. *Earth, Moon and Planets*, **82-83**, 351-368.

[44] Nagawasa K.(1978) Analysis of The Spectra of Leonid Meteors. *Ann. of Tokyo Astron. Obs.*, **16**, 157-187.

[45] Nelder, J.A. and Mead, R.(1965) A Simplex for function minimization. *The Computer J.*, **6**, 163-168.

[46] Olivero, J. J. andLongbothum, R. L.(1977) Empirical Fits to the Voigt Line Width: A Brief Review. *JQSRT*, **17**, 233-236.

[47] Park, C.,(1990) Nonequilibrium Hypersonic Aerothermodynamics. John Wiley & Sons, Inc.

[48] Rajchl J. and Peresty R.(1992) On persistent emission in all the long duration train BB1. *Astr. Inst. Czechosl. Acad. Sci.*, Preprint **138**, 1-5.

[49] Rajchl J., Bocek J., Ocenas D., Skvarka J., Zimnikoval P., Murayama H. and Ohtsuka, K.(1995) Results from several persistent train spectra intercompared. *Earth, Moon, and Planets*, **68**, 479-486.

[50] Richter E. S. and Sechrist C. F. Jr.(1979) A meteor ablation-cluster ion atmospheric sodium theory. *Geophys. Res. Lett.*, **6**, 183-186.

[51] Sykes, M.V. and Walker, R.G.(1992) Cometary Dust Trails 1. Survey. *ICARUS*, **95**, 180-210.

[52] Sunasaki, S., Yamazaki, J., Okuura, T., Takenouchi, K., Suzuki, H., and Nakamura, H.(1997) A Large Diameter I.I. CCD Camera for HD TV Use.(in Japanese) *ITE Technical Report*, **21(49)**, 7-12.

[53] Trowbridge C. C.(1907) Physical nature of meteor trains. *Astrophys. J.*, **26**, 95-116.

[54] Yamazaki, J., Majima, K., Yamaguchi, S., and Shirotake, K.(1998) Development of an Ultra-high-sensitivity HD TV I.I. Color Camera and Shooting Heavenly Bodies.(in Japanese). *ITE Technical Report*, **22(61)**, 35-40.

[55] Watanabe, J., Abe, S., Takanashi, M., Hashimoto, T., Iiyama, O., Ishibashi, Y., Morishige, K., and Yokogaw, S.(1999) HD TV observation of the strong activity of the Giacobinid meteor shower in 1998. *Geophysical Research Letters*, **26(8)**, 1117-1120.

[56] Watanabe J., Takahashi Y., Sasaki A., Abe, S., Kinoshita D., and Shiki S.(2000) TV Observation of the Leonid Meteor Shower in 1999: Secondary Peak over Japan. *Publ. of the Astronomical Society of Japan*, **52**, 21-24.

[57] Whipple, F. L.(1950) A Comet Model. I. The Acceleration of Comet Encke. *Astrophys. J.*, **111**, 375-394.

[58] Weissman, P. R., and Campins, H.(1993) Short-period comets. *Resources of Near-Earth Space*(eds. Lewis, J., Matthews, M. S., and Guerrieri, M. C.), 569-617, Univ. Arizona Press, Tucson, Arizona, USA.

[59] Yeomans D. K.(1981) Comet Tempel-Tuttle and the Leonid meteors. *Icarus*, **47**, 492-499.

[60] Zwitter, T., Mikuz, H., Munari, U., and Rejkuba, M.(1996) COMET C/1996 B2 (HYAKUTAKE). *IAU Circular* **6306**.